



Bournemouth University

Electroplated Composite Coatings with Incorporated
Nano Particles for Tribological Systems with the Focus
on Water Lubrication

Rizwan Sarwar Bajwa

A thesis submitted in partial fulfilment of the requirements of Bournemouth
University for the degree of Doctor of Philosophy

January 2016

NanoCorr, Energy & Modelling Research Group
Faculty of Science and Technology, Bournemouth University
In collaboration with
Schaeffler Technologies GmbH & Co. KG, Germany

Copyright Statement

This copy of the thesis has been supplied on condition that anyone who consults it is understood to recognise that its copyright rests according to the Bournemouth University – Industrial partner legal contract and due acknowledgement must always be made of the use of any material contained in, or derived from, this thesis with appropriate citation.

Abstract

Increasing demand of water-lubricated mechanical components or systems requires the development of novel materials with better wear or corrosion performance in the adjoining water environment. This applies to broad oceanic applications, for example, marine vessels, conventional power plants, tidal and wave energy systems and other water-lubricated industrial bearings. The current research project aims to evaluate the feasibility of the electrodeposited Ni-based nanocomposite coatings for water-lubricated tribological systems. The tribological behaviour of newly developed nanocomposite coatings is assessed under immersed water lubrication. For this reason test rig modification is deployed, to allow tribometer (TE92) to accommodate water lubrication facility to replicate water-lubricated contacts.

In this research tribological performance of electrodeposited nanocomposite coatings incorporating different nanoparticles, including Al_2O_3 , SiC and ZrO_2 are presented. Tribological performance experiments were conducted using modified ball-on-disc assembly with three ball system using TE92 Rotary Tribo-meter (Phoenix Tribology). The electrodeposition setup is installed for nanocomposite coatings. Different characterization tools including SEM, XRD, EDS and 3D surface profiling are used for nanocomposite coating investigations and to identify the optimized parameters for coatings in terms of tribological performance under water lubrication.

Overall, the addition of nanoparticles into a nickel matrix shows improvements in tribological properties than conventional pure nickel coatings. The specific wear rate is reduced almost 30% and corrosion resistance property enhanced nearly double in nickel composite of silicon carbide and alumina coatings respectively. All the coatings are mainly consisted of dispersive part of surface energy indicating covalent bonding between surface and liquids.

List of publications

Refereed Journal Papers

- 1) Bajwa RS., Khan Z., Bakolas V., Braun W. (2015) Water-lubricated nickel-based composite (Ni-Al₂O₃, Ni-SiC and Ni-ZrO₂) thin film coatings for industrial applications. *Acta Metallurgica Sinica (English Letters)*, 29 (1), 8-16.
- 2) Bajwa RS., Khan Z., Bakolas V., Braun W. (2015) Effect of bath ionic strength on adhesion and tribological properties of pure nickel and nickel composite coatings. *Journal of Adhesion Science and Technology*, 30 (6), 653-665.
- 3) Bajwa RS., Khan Z., H Nazir, Vivek Chacko, Adil Saeed. (2016) Wear and friction properties of electrodeposited Ni-based coatings subject to nano-enhanced lubricant and composite coating. *Acta Metallurgica Sinica (English Letters)*, DOI 10.1007/s40195-016-0470-6.
- 4) Bajwa RS., Khan Z., Bakolas V., Braun W. (2016) Tribological properties of Ni-based nanocomposites coatings reinforced with Al₂O₃, SiC, ZrO₂ and graphene platelets for marine applications. (*Under review*).
- 5) Khan Z., Pashaei P., Bajwa RS., Nazir MH., and Cakmak M. (2015) Fabrication and characterization of electrodeposited and magnetron sputtered thin films. *International Journal of Computational Methods and Experimental Measurements*, 3 (9), 165-174.

Conference Presentations with Refereed Published Abstract

- 1) Bajwa RS., Khan Z., Bakolas V., Braun W. (2015) An Experimental Investigation of Water Lubricated Electroplated Nanocomposite Coatings. Proceedings: 70th Annual Meeting of the Society of Tribologists and Lubrication Engineers, Dallas, USA.
- 2) Bajwa RS., Khan Z., Bakolas V., Braun W.. (2015) The Effect of Chemical Composition of Electrolyte on the Tribological Performance

of Electrodeposited Coatings. Proceedings: *70th Annual Meeting of the Society of Tribologists and Lubrication Engineers, Dallas, USA.*

- 3) Bajwa RS., Khan Z., Bakolas V., Braun W. (2015) Nickel-based composite nanocoatings for water-lubricated tribological systems. Proceedings: *20th International Conference on Wear of Materials (WOM), Toronto, Canada.*
- 4) Bajwa RS., Khan Z., Bakolas V., Braun W. (2014) Tribological performance of water lubricated electrodeposited nanocoatings in rolling contacts. Proceedings: *23rd Mission of Tribology Research, Institution of Mechanical Engineers (IMechE), London, UK.*
- 5) Bajwa RS., Khan Z., Bakolas V., Braun W. (2015) Electroplated nano-coatings for tribological systems in marine environments. (Accepted): *7th China-UK Tribology Symposium on "Tribology in Transportation Systems", Wuhan, China.*
- 6) Bajwa RS., Khan Z., Bakolas V., Braun W. (2015) Electroplated composite coatings with incorporated nano particles for tribological systems with the focus on water lubrication. Proceedings: *7th Annual Postgraduate Conference, Bournemouth University, UK.*
- 7) Bajwa RS., Khan Z., Bakolas V., Braun W. (2014) Electroplated composite coatings with incorporated nano particles for tribological systems with the focus on water lubrication. Proceedings: *6th Annual Postgraduate Conference, Bournemouth University, UK.*

Industrial Presentations without Refereed Written Publication

- 1) Bajwa RS. (18 Feb 2015). Electroplated composite coatings with incorporated nano particles for tribological systems with the focus on water lubrication. *Advanced Bearing Analysis, Schaeffler Technologies AG & Co. KG, Schweinfurt, Germany.*
- 2) Bajwa RS. (25 Feb 2015). Electroplated composite coatings with incorporated nano particles for tribological systems with the focus on water lubrication. *Coating Centre, Schaeffler Technologies, Head Quarter, Herzogenaurach, Germany.*

Table of Contents

Copyright Statement	i
Abstract	ii
List of publications	iii
Table of Contents	v
List of Figures	viii
List of Tables	xi
Nomenclature	xii
Acknowledgements	xiv
Chapter 1. Introduction	16
1.1. <i>Research background</i>	16
1.2. <i>Aims</i>	19
1.3. <i>Objectives</i>	19
1.4. <i>Novelty</i>	19
Chapter 2. Fundamentals and Literature Review	20
2.1. <i>An overview of electrodeposition techniques</i>	20
2.1.1. Types of electrodeposition techniques	22
2.1.2. Merits of PC/PRC over DC electrodeposition	24
2.1.3. Demerits of pulse current and pulse reverses current techniques.....	26
2.2. <i>Deep eutectic solvents (DESs) for water repellent composite coating</i>	26
2.2.1. Non-toxic/Low vapour pressure.....	27
2.2.2. Thermal stability	27
2.2.3. The wide potential windows.....	28
2.2.4. Water insensitive/ high solubility of metals	28
2.3. <i>Tribological contacts</i>	29
2.3.1. Wear mechanisms.....	29
2.3.2. Lubrication regime and lambda ratio	30
2.4. <i>Recent developments in nanocomposite coatings with focus on tribological performance</i>	32
2.5. <i>Summary of the literature review and research gaps</i>	38
Chapter 3. Experimental Methodology	43

3.1. <i>Electrodeposition of pure Ni and Ni-based composite coatings</i> ...	43
3.1.1. Coating development setup.....	43
3.1.2. Watts bath preparation	44
3.1.3. Substrate preparation.....	46
3.1.4. Pulse current electrodeposition parameter settings.....	46
3.1.5. Electrodeposition procedure.....	46
3.2. <i>Test rig setup for tribological testing</i>	47
3.2.1. Tribo-test conditions	48
3.2.2. Tribo-test procedure	50
3.2.3. Wear and friction coefficient evaluation.....	50
3.3. <i>Electrochemical corrosion tests</i>	51
3.4. <i>Wettability and surface energies test</i>	53
3.5. <i>Adhesion performance tests</i>	54
3.6. <i>Characterization tools and methods</i>	55
3.6.1. Sample preparations for characterizations	55
3.6.2. 3D surface profiler (Zygo NewView 5000).....	57
3.6.3. Optical microscopy (Olympus).....	58
3.6.4. Scanning electron microscopy /EDS	58
3.6.5. Micro and Nano-indentation tester	59
Chapter 4. Performance of nanocomposite coatings produced by various incorporated nanoparticles	61
4.1. <i>Characterisation of the coatings</i>	61
4.2. <i>Wear and corrosion results</i>	66
4.3. <i>Adhesion and wettability results</i>	70
4.4. <i>Conclusions</i>	75
Chapter 5. Performance of Ni and Ni-Al₂O₃ composite coatings produced by variable bath ionic strength	76
5.1. <i>Characterisation of the coatings</i>	76
5.2. <i>Tribological and corrosion results</i>	81
5.3. <i>Adhesion and wettability results</i>	84
5.4. <i>Conclusions</i>	89
Chapter 6. Conclusions and future work	90
6.1. <i>Conclusions</i>	90
6.2. <i>Recommendations for future work</i>	92
6.3. <i>Reference</i>	94
Appendix A	108

Appendix B	112
Appendix C	116
Appendix D	126

List of Figures

Figure 1 Schaeffler's coating systems and their areas of applications.....	18
Figure 2 Principle of nickel plating in nickel sulphate solution.....	21
Figure 3 A flowchart of chemical and electrochemical coating techniques.	22
Figure 4 Characterisation of lubrication regimes according to Stribeck curve...32	
Figure 5 Electrodeposition setup for nano-coatings manufacturing	44
Figure 6 Modified TE92 Rotatory tribometer with test specimen and schematic of loading configuration in magnified view.	48
Figure 7 Schematic demonstration of anodic polarization states.	52
Figure 8 Three-electrode configuration setup with coated specimen as working electrode at bottom.....	53
Figure 9 Scratch test configuration setup with dimensions of coated specimen.	55
Figure 10 Coated sample cutting and preparation procedure to conduct different investigations	56
Figure 11 Three-dimensional surface profiling machine (ZYGO NewView 5000)	57
Figure 12 Leitz Metallux 3 optical microscopy with magnification in range of 100X-1000X.....	58
Figure 13 Scanning electron microscopy for microstructure and EDS analyses (JEOL JSM-6010PLUS/LV).	59
Figure 14 Hardness and elastic modulus measuring machines (a) Nano- indentation (CSM) (b) Micro-indentation (LECO).....	60
Figure 15 Surface morphologies of different electrodeposited coatings under scanning electron microscopy, (a) Pure Ni (b) Ni/Al ₂ O ₃ (c) Ni/SiC and (d) Ni/ZrO ₂ (Bajwa, R. S. et al., 2015b)	62
Figure 16 Surface roughness of different electrodeposited coatings (Bajwa, R. S. et al., 2015b).....	63

Figure 17 The display of incorporated particle distributions within the nickel matrix for different nanocomposites through SEM, (a) Ni/Al ₂ O ₃ (b) Ni/SiC and (c) Ni/ZrO ₂ (Bajwa, R. S. et al., 2015b).....	65
Figure 18 The mechanical properties of different electrodeposited coatings (Bajwa, R. S. et al., 2015b).....	65
Figure 19 XRD pattern of different electrodeposited coatings(Bajwa, R. S. et al., 2015b).....	66
Figure 20 The comparison of wear rates for different electrodeposited coatings subject to water lubrication (Bajwa, R. S. et al., 2015b).	67
Figure 21 Surface failure examinations for different electrodeposited coatings by using SEM (Bajwa, R. S. et al., 2015b).....	68
Figure 22 Potentiodynamic polarization curves for different electrodeposited coatings (Bajwa, R. S. et al., 2015b).....	69
Figure 23 The variations of critical loads for different electrodeposited coatings (Bajwa, R. S. et al., 2015b).....	71
Figure 24 Kinds of electrodeposited coating failure subject to various incorporated nanoparticles after scratch test according to DIN EN 1071-3.....	72
Figure 25 The variations of water contact angle and surface energy for different electrodeposited coatings (Bajwa, R. S. et al., 2015b).	74
Figure 26 Wetting envelopes for different electrodeposited coatings.....	74
Figure 27 Surface morphology of coatings produced by different types of electrolyte (Bajwa, R. S. et al., 2015a).....	78
Figure 28 The effect of ionic concentration of solution on surface roughness of different electrodeposited coatings (Bajwa, R. S. et al., 2015a).....	79
Figure 29 The variation of mechanical properties for coatings electrodeposited from different ionic strength of electrolyte (Bajwa, R. S. et al., 2015a).....	79

Figure 30 The demonstration of incorporated particle distributions in coatings electrodeposited from different ionic strength of electrolyte (Bajwa, R. S. et al., 2015a).....	80
Figure 31 The variations of wear resistance and mean-steady friction coefficient properties for coatings electrodeposited from different ionic concentration of solution (Bajwa, R. S. et al., 2015a).	82
Figure 32 Corrosion resistance behaviour of coatings electrodeposited from different ionic concentrations of solution (Bajwa, R. S. et al., 2015a).	83
Figure 33 The variation of critical load values for coatings electroplated from different ionic concentrations of solution (Bajwa, R. S. et al., 2015a).	85
Figure 34 Kinds of electrodeposited coating failure subject to various ionic concentrations after scratch test according to DIN EN 1071-3.	86
Figure 35 The variations of water contact angle and surface energy for coatings electroplated from different ionic concentrations of solution (Bajwa, R. S. et al., 2015a).....	87
Figure 36 Wetting envelopes for electrodeposited coatings produced from the different ionic strength of plating baths.	88

List of Tables

Table 1 A summary of the tribological properties of some nanoparticles-filled metal nanocomposites.....	35
Table 2 A summary of electrodeposition of nanocomposite coating with focus on tribological improvements	39
Table 3 A summary of configuration parameters effect on coefficient of friction and wear.	41
Table 4 Chemical components of the substrate material (Bajwa, R. S. et al., 2015a).	44
Table 5 Composition of electrolytes with various ionic concentrations (Bajwa, R. S. et al., 2015a).....	45
Table 6 List of pulse parameters used for surface area 0.72dm^2 of the cathode.....	46
Table 7 Known physical properties for calculation of lubrication regime	49

Nomenclature

B_{hc}	High ionic concentration bath
B_{mc}	Medium ionic concentration bath
B_{lc}	Low ionic concentration bath
E_r	Equivalent young's modulus
E_{corr}	Free corrosion potential or circuit opening potential
E_{pit}	Pitting initiation potential
E_t	Tranpassivation potential
G	Materials parameter
H_{min}	Dimensionless parameter for minimum film thickness
h_{min}	Minimum lubricant film thickness
I_A	Average current density
i_{pass}	Passive current density
k	Ellipticity parameter
L_c	Critical load value at which first failure observed
P	Normal force
R_{qb}	r.m.s roughness of ball
R_{qc}	r.m.s roughness of coated disc
R_x	Equivalent curvature in X-direction
R_y	Equivalent curvature in Y-direction

T_{OFF}	Pulse OFF time
T_{ON}	Pulse ON time
U	Speed parameter
v	Entraining surface velocity [m/s]
W	Load parameter
η_0	Lubricant dynamic viscosity
λ	Lubricant film thickness to composite r.m.s roughness ratio
ξ	Pressure-viscosity coefficient

Acknowledgements

I would like to express the deepest appreciation to my PhD supervisor Dr Zulfiqar Khan for his continuous invaluable support, guidance and bring new ideas. His friendly nature coupled with his enthusiasm and inspiration was a great source of encouragement and confidence and will count to influence my future career as well.

I would like to thank my industrial supervisors Dr Vasilios Bakolas and Dr Wolfgang Braun for their fruitful advices during regular project discussion meetings. A special thanks goes to Dr Wolfgang Braun for his research support and hospitality during my time at the Schaeffler Technologies Research Center – The Germany.

My appreciation also goes to technical staff at the Bournemouth University research laboratory, Brian Wright and Will D Lambert for their help in this project.

I would like to acknowledge the Schaeffler Technologies GmbH & Co. KG – Germany and Bournemouth University – United Kingdom for financial and in-kind support of this project.

Acquire the knowledge and impart it to the people

- *The Prophet Mohammad (s.a.w)* -

This dissertation is dedicated

To my parents (Pillars of Stability) & brothers

To my wife HINA NAWAZ

To my children MARYAM SARWAR BAJWA

&

MUHAMMAD SHAHEER BAJWA

Chapter 1. Introduction

1.1. Research background

Surfaces of materials or components have limited lives due to mechanical interactions of components within the system or chemical/electrochemical influences of the operating environment. These changes may damage the functionality and in some worse cases cause catastrophic breakdown of the system which might lead to hazardous effects for human and the environment. For example, surface in contact with chemicals and exposure to humid atmosphere cause to surface change due to chemical or electrochemical corrosion, tribological or wear damage (Kanani, N., 2004). In order to overcome these challenges various coating technologies have been used such as evaporation, painting, thermal spraying and metalising including electroless or electroplating coating.

Increasing demand of water-lubricated mechanical components or systems requires the development of novel materials with better tribological performance in the presence of the water environment. This applies to a wide range of marine applications such as marine vessels, conventional power plants, tidal and wave energy systems and other water-lubricated industrial bearings.

One common requirement of protective coatings for mechanical component/systems is significant surface hardness to withstand subject to high loads and to provide a certain wear resistance properties. In the case of water lubrication an additional requirement is a high corrosion resistance. The absence of cracks may enhance the corrosion resistance. The incorporation of nano particles is another instrument to influence the surface properties, especially the friction and wear resistance. Due to the process it is possible to form nano crystalline metals and also to incorporate different particles. For all kinds of coatings it is a great challenge to remain adhered to the substrate for longer lifetime because of the high stresses on the interface

layer. So the adhesion strength of the coating is important, especially for industrial applications.

Recently, protecting coatings produced by electrodeposition technique have gained attraction due to superior economic approach and control over a wide range of pulse settings and deposition process parameters. By using optimal values of these parameters, it is possible to produce more complex geometries of electrodeposited coating as compared to line-of-sight deposition methods such as PVD and CVD. Extensive work has been completed to evaluate the feasibility of electroplated coating for various industrial applications.

However, it is necessary to study the tribological performance of the electrodeposited composite coating incorporating nanoparticles for application in water lubricated contacts. Therefore, this research is looking into the tribological performance of nanocomposite coatings with special focus on water lubricated rolling contact. This applied research will provide fundamental design solutions for electroplated nanocomposite coatings with nano-enhanced wear and corrosion resistance efficiencies for water lubricated tribological component or systems.

This research project is conducted in collaboration with industrial partner Schaeffler Technologies GmbH & Co. KG, Germany. In this project, Schaeffler provided access to their laboratories to conduct several experiments, including corrosion tests, wettability and mechanical testing. The Schaeffler Group with its product brands INA, FAG and LuK is a leading manufacturer of high-quality rolling bearings, plain bearings, linear guidance systems, and engine components for mechanical engineering, aerospace and the automotive industry worldwide. An overview of various kinds of coating supported products with different industrial applications produced by Schaeffler Group is shown in Figure 1. These coatings are categorized according to four main functions, namely; (1) anti-corrosion, (2) anti-wear and friction protection, (3) current insulation and (4) surfaces exposed to high tribo-mechanical stresses.

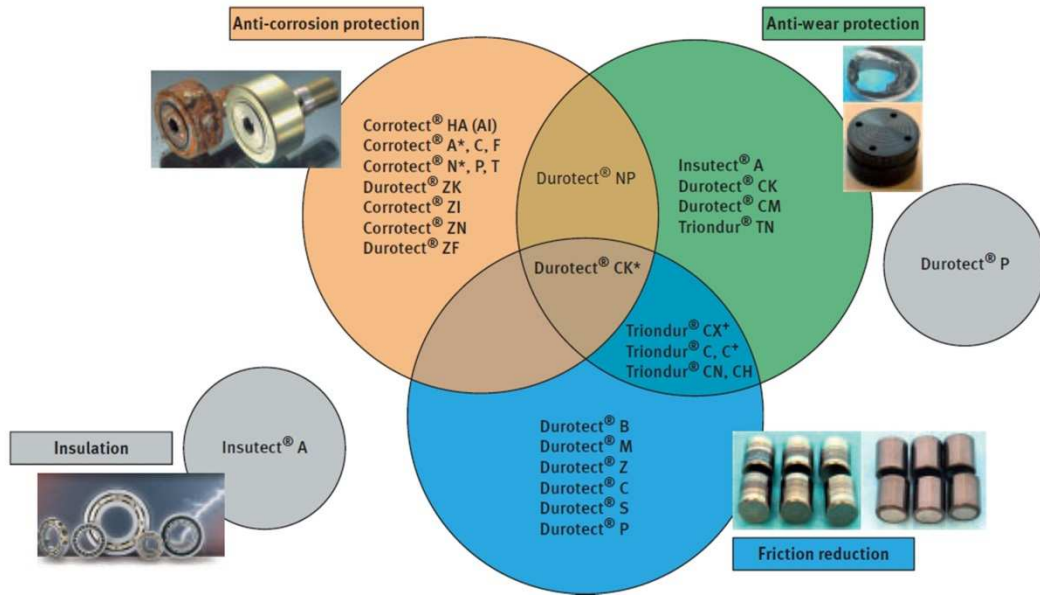


Figure 1 Schaeffler's coating systems and their areas of applications.

During the last decade, extensive work have been completed in the field of electroplating coating techniques especially with a focus on wear and corrosion resistant coatings, self-lubricating systems and dispersion-strengthened coatings (Gyftou, P. et al., 2008; Lee, C., 2012; Musiani, M., 2000; Su, F. et al., 2013a). As reported, electrochemical composite coating investigations started from the beginning of 20th century as researchers started investigating the effect of electrochemical co-deposition of Cu-graphite as a self-lubricating agent in the car engine since 1928 and sand particles with nickel matrix were used for anti-slip coating purposes (Gomes, A. et al., 2011; Hovestad, A. and Janssen, L., 1995).

Electroplating is a versatile technique for co-deposition of nanoparticles of metals, metal oxides, carbides, borides, and polymers with a metal or alloy matrix such as nickel, copper and chromium. In recent years nano-composite coating of metals and alloys have been of great interest due to peculiar behaviour and novel properties of nanomaterials, typically with their sizes below 100nm (Khazrayie, M. and Aghdam, A., 2010; Langdon, T. G., 2009). Numerous studies have been reported on composite coating containing inert particles of micro and nano size with metal matrix using electrodeposition techniques which include Al₂O₃, ZrO₂, TiO₂, SiC, Si₃N₄, Fe₂O₃, and CeO₂.

The results from these studies are summarised in Table 2 and 3 in section 2.4.

1.2. Aims

This research aims to study the potential of the electrodeposited Ni-based composite coatings incorporating nanoparticles to improve the tribological performance of water-lubricated tribological systems.

1.3. Objectives

The research objectives for current research are as follows,

- Investigate and understand the tribological properties of electrodeposited composite coating incorporating various nanoparticles subject to water lubricated contact.
- Test rig modification is needed in TE92 rotary tribometer to assess the tribological properties of newly developed electrodeposited coatings subject to water lubricated contact.
- Identify the optimal parameters for the production of nickel based nanocomposites coatings and corresponding chemical compositions with nano-enhanced tribological, mechanical and wettability properties.

1.4. Novelty

The novelty of research in this thesis is to evaluate the tribological performance of electrodeposited nanocomposite coatings incorporating various nanoparticles under water lubrication by using a modified version of rolling contact tribometer. To identify the optimal formulations for the production of nickel based nanocomposites and corresponding chemical compositions with nano-enhanced tribological, mechanical and wettability properties. This research will provide novel design solutions for selecting suitable electroplated nickel composite coatings for tribological applications in harsh water-lubricated contacts.

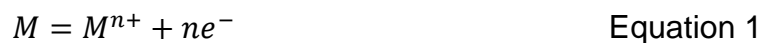
Chapter 2. Fundamentals and Literature Review

2.1. An overview of electrodeposition techniques

Aqueous electrolytes also known as electrolyte baths are metal salts (of metal to be deposited) which ionize when dissolved in suitable ionizing solution such as water to form electrically charged anions and cations.

In addition to metal salts some additives, chemicals such as acids and salts or buffers are commonly used in order to promote conduction, optimizing the coating properties and to keep pH constant, as these parameters play an important role in the preferred properties of finished coated products.

For example, when nickel sulphate NiSO_4 (metal salt) is dissolved in water, it ionizes into Ni^{2+} and SO_4^{2-} ions. In the presence of an external power supply, the Ni^{2+} gets started releasing at anode due to the oxidation. These Ni^{2+} are attracted by negative SO_4^{2-} ions to form nickel sulphate. At the same time some electron transfer to positively charged Ni^{2+} ions to form free metallic nickel atoms which deposit themselves on the cathode. In this way the oxidation and reduction process continue at anode and cathode, respectively, to maintain the electrolyte charge more or less uniform. In general anode-solution interface oxidation and cathode-solution interface reduction follows equation 1 and 2 respectively.



Where M , M^{n+} and ne^{-} are atom in the metal surface, ion in solution and electron(s) in metal respectively.

Figure 2 illustrating the basic principle of electroplating methodology for plating of nickel in a solution of nickel sulphate.

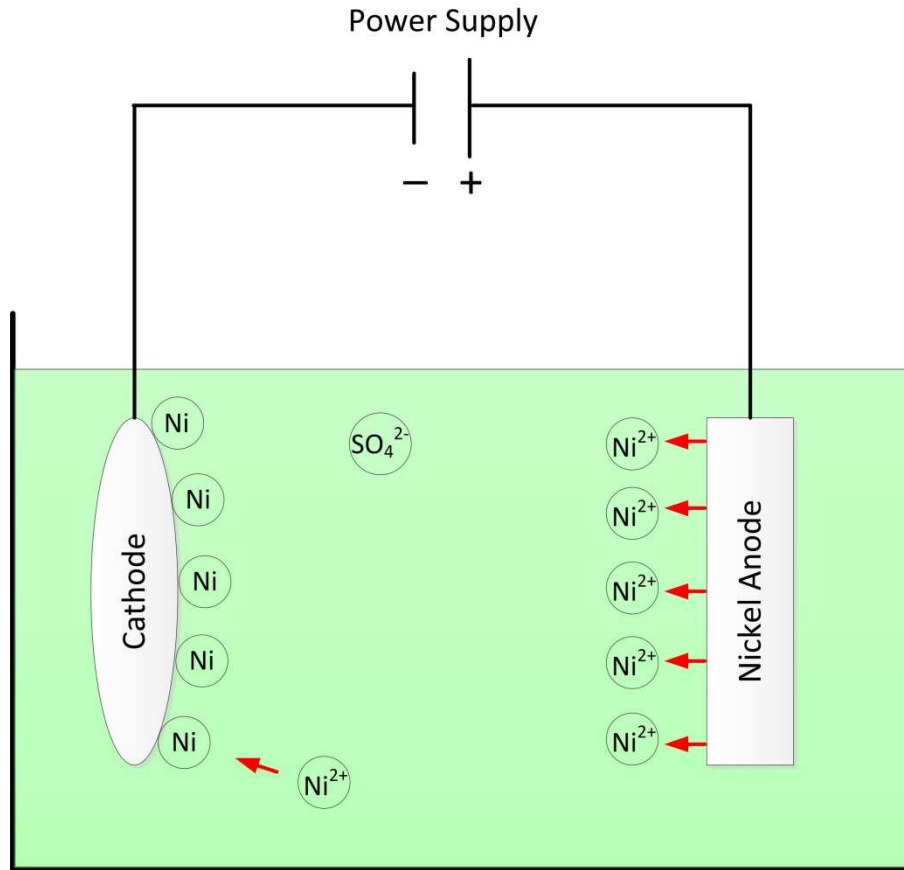


Figure 2 Principle of nickel plating in nickel sulphate solution.

In addition to metal salts and additives to promote conduction there will be a source to start metal deposition process which is as an external source of applied voltage in case of electrodeposition or electroplating technique and strong reducing agent in case of electroless or chemical deposition technique. Third type of deposition technique is Laser-induced or Laser-enhanced deposition based on laser technology and applied to either above two deposition techniques to accelerate metal deposition rate (Horio, K. et al., 1991; Morgenstern, T. and Schultze, J., 1997). The flow chart of chemical and electrochemical coating techniques is shown in Figure 3.

In this discussion, electroplating technique with various processes such as direct current (DC) and pulse current (PC) and pulse reversed current (PRC) processes are studied. Moreover, the effect of electrodeposition conditions is also discussed.

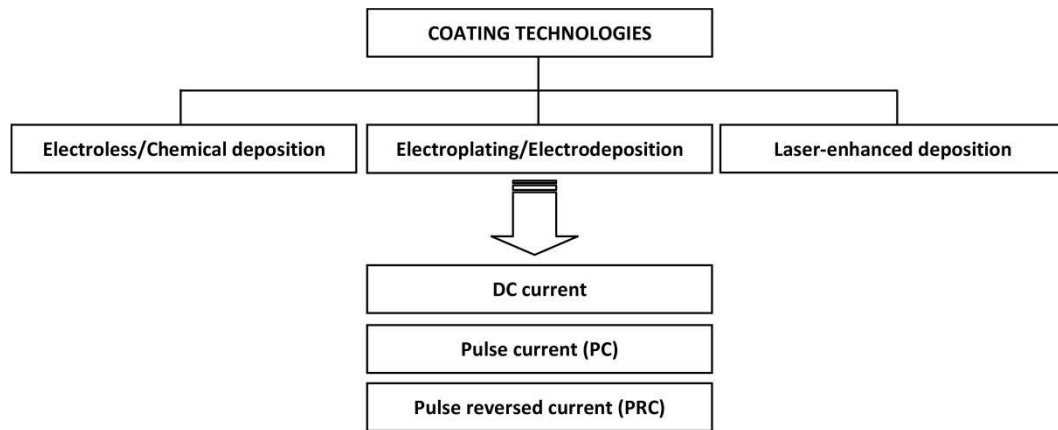


Figure 3 A flowchart of chemical and electrochemical coating techniques.

2.1.1. Types of electrodeposition techniques

2.1.1.1. Direct current electrodeposition

Conventional direct current electrodeposition methodology is an economical approach which does not include the additional cost of sophisticated controlled pulse supply system. Simple rectifiers or batteries are used as a direct current supply to start the deposition process at the cathode (of metal to be deposited) as discussed above. Nevertheless, there is only one parameter (current density) to adjust in order to optimise the morphological and physical properties of coating (Lou, H. H. and Huang, Y., 2005). Secondly, due to non-uniform current distribution (higher at sharp edges and lower at recessed areas of the cathode) cause non-symmetric thickness layers of the depositing materials, geometrical shape and current densities are modified to overcome such issues. Also, due to direct current supply in DC electroplating there is not a homogenous distribution of ions in the bath which create more depleted area with high current density and less depleted areas with low current densities. Consequently, such uneven distribution of ions affects the morphological properties of the coating (Kelly, J. et al., 2000). As current flow is a continuous phenomenon in the direct current electrodeposition process the duty cycle is 100% and average current density is equal to peak current density.

2.1.1.2. Pulse current (PC) and pulse reverse current (PRC) electrodeposition

During the last decades, the rapid advancements in the field of electronics bring great flexibility in regulating the variable parameters of the applied current waveform. These parameters play an important role in controlling the various characteristics such as morphological structure of metals or alloy as well as the composition of particles incorporated in composite coating even at the atomic scale. PC and PRC electrodeposition techniques are basic sources for recent development in the field of nano-tribology for enhancement of tribological properties in the field of nanotechnology.

The pulse current refers to applied current waveform with one direction. To characterise the pulse current the following parameters are considered:

- Cathodic peak current density (I_p)
- Cathodic pulse length or pulse ON time (T_{ON})
- Interval between the pulses or pulse OFF time (T_{OFF})

Using these parameters the duty cycle (γ) and frequency can be defined by Eq. 3 and Eq. 4 as (Beattie, S. and Dahn, J., 2003; Chandrasekar, M. and Pushpavanam, M., 2008),

$$Duty\ cycle = \frac{T_{ON}}{T_{ON}+T_{OFF}} \quad \text{Equation 3}$$

Duty cycle is defined as the portion of each cycle during which current is ON.

$$Frequency = \frac{1}{T_{ON}+T_{OFF}} \quad \text{Equation 4}$$

Average current density (I_A) is defined by following equation (Chandrasekar, M. and Pushpavanam, M., 2008; Puipe, J. C. and Ibl, N., 1980).

$$(I_A) = Peak\ current \times Duty\ cycle \quad \text{Equation 5}$$

The current density is defined by Eq.6 as peak current divided by the surface area to be electroplated.

$$Current\ density\ A = \frac{Peak\ current\ A}{Surface\ area\ /dm^2} \quad \text{Equation 6}$$

The pulse reverse current refers to applied current waveform bipolar direction where anodic and cathodic pulses are mixed through sophisticated regulating pulse generator as shown in Figure 4(c). In order to characterize pulse reverse current following parameters are considered,

- Anode pulse (reverse) time T_{AA}
- Cathode pulse (forward) time T_C
- Anode current density I_{AA}
- Cathode current density I_C
- Average current density \bar{I}_A
- The cycle time T

For pulse reverse current the average current density (\bar{I}_A) and duty cycle (γ') followed as (Grimmett, D. L. et al., 1993),

$$\bar{I}_A = \frac{I_C T_C - I_{AA} T_{CC}}{T_{AA} + T_C} \quad \text{Equation 7}$$

$$\text{duty cycle } (\gamma') = \frac{T_C}{T_{AA} - T_C} \quad \text{Where } T_{AA} = T_C \quad \text{Equation 8}$$

2.1.2. Merits of PC/PRC over DC electrodeposition

2.1.2.1. Additional parameters

PC/PRC offers additional current parameters by means of which output current can be periodically altered, which is an advantage in enhancing the deposition rate and quality of deposited coating as well as the needs for additives also significantly reduced. For example, current OFF time T_{OFF} in (PC) or and (PRC) significantly discharge the double layer which is a barrier for penetration of ions at cathode (Borkar, T. and Harimkar, S. P., 2011). Secondly, continuous direct current is applied in DC electrodeposition which creates an uneven distribution of ions with more and less current density area in the electrolyte which affect the quality of the coating. Whereas, in PC and PRC, the T_{OFF} significantly enhance the quality of the coating by increasing the ions distribution in electroplating solution (Chandrasekar, M. and Pushpavanam, M., 2008). Balasubramanian studied the influences of current duty cycle and frequency on the electroplated copper thickness and

plating current efficiency over stainless steel and demonstrated good adhesion of copper with maximum current efficiency and deposited thickness with duty cycle of 80% and frequency of 50Hz (Balasubramanian, A. et al., 2009).

2.1.2.2. Mechanical and tribological properties

Compared with DC electrodeposition method, the PC and PRC can yield significant improvements in mechanical and tribological properties in deposited coating. It is reported that nanocrystalline Cu electrodeposition using PC method provided greater hardness, reduced friction coefficient and higher wear resistance in comparison to DC electrodeposition. Furthermore, PC deposited coating is more electrochemical stable in comparison to DC deposition (Ogihara, H. et al., 2012; Tao, S. and Li, D., 2006). With the revolution in the field of nanotechnology, nano-tribology research using PC/PRC in comparison to DC electrodeposition techniques has attracted great interest due to its remarkable improvements in coating tribological properties such as wear resistant, friction and corrosion resistance and mechanical properties (Huang, S. et al., 2011; Landolt, D. and Marlot, A., 2003; Lee, C., 2012; Low, C. et al., 2006; Mishra, R. et al., 2004; Tao, S. and Li, D., 2006; Thuvander, M. et al., 2001; Zhou, Q. et al., 2009).

2.1.2.3. Structure and morphological properties

The independent control over different parameters of PC/PRC techniques can deliver significant improvement in micro-nano structures and morphological properties of the deposited coating of metals, alloys and nanoparticles composites which is not possible with DC techniques (Kelly, J. et al., 2001; Marlot, A. et al., 2002; Nakanishi, T. et al., 2001).

Researchers have investigated comparative studies of direct current and pulse current electrodeposition techniques with a focus to overcome porosity problems and have proposed PC/PRC techniques to achieve lower porosity (Balasubramanian, A. et al., 2009; Barcena, J. et al., 2008; Liu, Z. et al., 2011; Ramanauskas, R. et al., 2008). Porosity linked to the quality of the deposited coating as well as tribological properties such as corrosion, with increasing porosity can provide a safe way to various unwanted ions to

penetrate through the pores which may increase pitting corrosion behaviour of the underlying substrate (Liu, Z. et al., 2010; Notter, I. and Gabe, D., 1992; Zhou, Q. et al., 2009). It was reported that the formation of hydrogen bubbles during the electroplating process resulting into the porosity around the microstructure grains boundaries of the coatings (Nakahara, S. et al., 1976). Zhengwei Liu et al. explained the relationship between porosity and pulse plating conditions (Liu, Z. et al., 2010). It was concluded that the lower porosity can be achieved under high pulse frequency and lower current density conditions.

2.1.3. Demerits of pulse current and pulse reverses current techniques

The demerits of PC/PRC techniques are not as significant as its benefits over DC deposition techniques. As Potentiostats/Galvanostats systems for pulse generation are highly sophisticated designs which allow independent control over different parameters of the waveform due to which its cost is greater than simple DC unit. Furthermore the complex procedures of PC/PRC techniques required proper planning about different parameters ahead to retrieve improvements in results (Chandrasekar, M. and Pushpavanam, M., 2008).

2.2. Deep eutectic solvents (DESs) for water repellent composite coating

Electrodeposition coating technique with aqueous solution electrolytes is a versatile approach for wide range of composite materials incorporating micro to nano sized particles with improved tribological properties as reported above. However issues relating high metals solubility and instability of colloidal dispersion rose while using water sensitive materials for example the composites coatings incorporating water repellent materials such as Polytetrafluoroethylene (PTFE) and deposition on water sensitive substrates such as aluminium, consequently the coating will result in reduced content ratio of particles as well as increased surface roughness in final deposited coating (Abbott, A., 2011; Armand, M. et al., 2009; Changdong, G. et al., 2012). To overcome these issues with water repellent material in aqueous

baths several strategies have been adopted during the last decade such as using ultrasonic stirrer for stabilising the distribution of particles or use of non-ionic/cationic wetting agent.

Most recently the deep eutectic solvents approach invented by Abbott and co-workers to improve surface morphologies with better metals solubility and stability due to less surface energy of DESs electrolyte than water and water insensitive behaviour (Abbott, A. P. et al., 2004). Deep eutectic solvents (DESs) based ionic liquids are most commonly Choline chloride based liquids using ethylene glycol (EG or Ethaline) as the hydrogen bond donor is an advantageous media for metals electrodeposition in comparison to conventional electrolytes with the following advantages.

2.2.1. Non-toxic/Low vapour pressure

Traditional electroplating or Electrodeposition process based on cyanic or phosphate electrolytes such as poisoning baths are toxic, quite corrosive and hazardous for the environment. However, DES solvents are environment friendly and considered as a suitable alternative for many poisonous electrolytes (El Abedin, S. Z. et al., 2007; Gu, C. et al., 2012). Extreme low vapour pressure of ionic liquid based solvents around (10^{-11} – 10^{-10} mbar) is an advantage to prevent releasing of harmful vapours into the atmosphere (El Abedin, S. Z. et al., 2007; Liu, Z. et al., 2012). In comparison to ionic liquids the deep eutectic solvents are easy to prepare and cost effective with high purity and can be efficiently recycled upon excessive dilution in water (Abbott, A. P. et al., 2004; Gu, C. et al., 2012). As deep eutectic solvents are a mixture of already known chemicals so they don't need to be registered with REACH as new entities which is an advantage for commercial application (Abbott, A., 2011).

2.2.2. Thermal stability

The low vapour pressure of ionic liquid based solvents has significantly improved the thermal stability of electrodeposition baths as compared with common aqueous solutions and can be used in a temperature range of 300-400°C (Bonhote, P. et al., 1996; Zein El Abedin, S. et al., 2012). Electroplating of Ta which is not possible to be deposited from an aqueous solution has been electrodeposited using a eutectic combination of LiF–NaF–KF and K_2TaF_7 at

temperatures between 650 and 850°C (Zein El Abedin, S. et al., 2005). Electrodeposition electrolytes at such a high temperature, cause to increase expected loss in current efficiencies, corrosion rate and similar technical and economic issues, considering these problems. Abedin and co-workers reported that Tantalum can be electroplated at temperature of 200°C with composition of TaF_5 and 1-butyl-1-methyl-pyrrolidinium bis (tri-fluoromethylsulfonyl) imide as a mixture of ionic liquid (Zein El Abedin, S. et al., 2005).

2.2.3. *The wide potential windows*

The electrochemical potential window is a significant parameter of electrodeposition technique which defines the electrochemical stability of solvents at certain potential range at which the depositing electrode oxidized or reduced. The electrochemical potential windows for electrodeposition of metals and alloys in water based electrolytes is about up to 1.2 V (Fomin, A., 2010). On the other hand majority of the deep eutectic based solvents have potential window up to 3V and some ionic liquids are reported to have to 6V capability (Zein El Abedin, S. et al., 2004). The wide potential range of ionic liquid based solvent give access for electrodeposition of elements which are not possible with aqueous or organic electrolytes (El Abedin, S. Z. et al., 2007).

2.2.4. *Water insensitive/ high solubility of metals*

Unlike the room-temperature ionic liquids, the DES based solutions are easy to prepare with low cost and high purity as well as these solvents are nonreactive with water which is an advantage to quality coatings. Water insensitive property DES based solutions is an important factor towards quality coating in term of several advantages over conventional electrolytes for example, (1) significantly reduced hydrogen embrittlement (gaseous hydrogen produced during water electrolysis) from coating substrates (Haerens, K. et al., 2009), (2) better distributions/dispersion of metals/alloys and micro/nano sizes particles of water repellent materials (e.g. PTFE or Teflon) (Changdong, G. et al., 2012), (3) Electrodeposition of metals over

substrate which are sensitive to water (Abbott, A. P. et al., 2008; Liu, Y.-S. and Pan, G.-B., 2011).

2.3. Tribological contacts

Tribology is the science and technology of interacting surfaces in relative motion. The tribological interacting surfaces subject to dry or lubricated contact may result into loss of material from bodies in contact. The removal of materials from tribological interacting surfaces is known as “wear”. The wear failure can occur in various ways depending on contact situation, sliding, rolling and impact. The force producing relative motion between two solid bodies in contact is known as “friction force”. The ratio between friction force and applied normal is defined as coefficient of friction and is a dimensionless property. Friction is not a material property, but a system parameter which may affect by the surrounding environment. The surrounding environment includes the lubrication, humidity and wear debris, resulting from different type of wear mechanism. For example, under lubricated contact, the bodies in contact can be separated by a thin lubrication film depending applied load, sliding/rolling speed and viscosity of the lubricant. This thin lubrication film may contribute to the lower wear and friction behaviour. The thickness of separation film is used to identify that what type of lubrication regime exists between the contact. Therefore, the term tribology encompasses the study of wear, friction and lubrication.

Tribology aims to understand/improve the friction and wear properties of materials/surfaces for the specific application case. The wear and friction properties of the wide ranging engineering component can be enhanced by employing protective coatings. The lubricants are used for several purposes, to minimize the friction and wear, to remove wear debris from contact areas and as an anti-corrosive agent when used in the form of grease lubrication.

2.3.1. Wear mechanisms

A number of different wear mechanisms have been defined in the literature. However, the following four wear mechanisms are generally recognized as the main types of wear behaviour (Burwell, J. T., 1957),

- Adhesive wear
- Abrasive wear
- Fatigue wear
- Corrosive wear

The adhesive wear occurs as a result of micro-joints between the contacting asperities of counter bodies in relative motion. The transfer of material from one surface and the addition of it to counter surface is defined as scuffing or galling.

The abrasive wear occurs when one material is harder than that of counter body material. The abrasive wear can be occurs as a result of two-body abrasive wear or three-body abrasive wear. In two-body contact the abrasive wear is caused by the surface asperities of hard material. While, in three-body contact the abrasive wear is caused by the hard particle trapped within rubbing surfaces. One of the types of abrasive wear is micro-ploughing in which material of softer material is shifted to the sides of worn wear groove.

The fatigue wear occurs under cyclic loading when the applied load exceeded the fatigue strength limit of the material. The repeated loading may lead to the formation and propagation of micro-cracks on/below the surface. The material delamination occurs when the micro-cracks get connected to each other and resulting in the material separation.

The degradation of materials as a result of accelerated corrosion between rubbing surfaces is called corrosive wear. The corrosive wear is combined effect of wear and corrosion and also called tribocorrosion. The fundamental cause of corrosive wear is the chemical reaction between the worn surfaces and corrosive media.

2.3.2. Lubrication regime and lambda ratio

Under lubricated tribo-test conditions the rubbing surfaces can be separated by a thin lubrication film. The thickness of separation film is used to identify that what type of lubrication regime exists between the contact. The minimum film thickness between surfaces in contact is calculated by using (Hamrock,

B. J. and Dowson, D., 1981) Elasto-hydrodynamic lubrication (EHL) equation with known physical properties.

$$H_{\min} = 3.63U^{0.68}G^{0.49}W^{-0.073}(1 - e^{-0.68k}) \quad \text{Equation 9}$$

Where H_{\min} , U , G , W and k are dimensionless parameters for dimensionless minimum film thickness, speed, materials, load and ellipticity properties respectively and defined as,

$$U = \frac{\eta_0 u}{E_r R_x}$$

$$G = \xi E_r$$

$$W = \left(\frac{P}{E_r R_x^2} \right)$$

$$k = \left(\frac{R_x}{R_y} \right)^{\frac{2}{\pi}}$$

Where η_0 , u , E_r , ξ , P , R_x and R_y are viscosity, average surface velocity, reduced elastic modulus, pressure viscosity, load, effective radius in x direction and effective radius in y direction respectively. The reduced modulus of elasticity is calculated as,

$$\frac{1}{E^*} = \frac{1}{2} \left(\frac{1 - \nu_1^2}{E_1} + \frac{1 - \nu_2^2}{E_2} \right)$$

Where E_1, E_2, ν_1 and ν_2 are the Young's modulus and poisson ratios of contacting bodies respectively.

The actual minimum film thickness is product of dimensionless minimum film thickness and effective radius of ball which is defined as,

$$h_{\min} = H_{\min} R_x \quad \text{Equation 10}$$

The lambda (λ) ratio or specific film thickness ratio is define as the ratio of measured minimum lubrication film thickness between the surfaces in contacts to r.m.s roughness of bodies in contact (Hamrock, B. J. et al., 2004). The three lubrication regimes are distinguished based on the value of lambda (λ) in the Stribeck curve and are shown in Figure 4. These values are approximated as $\lambda > 3$ for (elastohydrodynamic lubrication, $1 < \lambda < 3$ for partial or mixed lubrication and $\lambda < 1$ for boundary lubrication.

$$\lambda = \frac{h_{\min}}{\sqrt{R_{qb}^2 + R_{qd}^2}} \quad \text{Equation 11}$$

Where R_{qb}^2 and R_{qd}^2 are the r.m.s roughness values of balls and coated disc respectively.

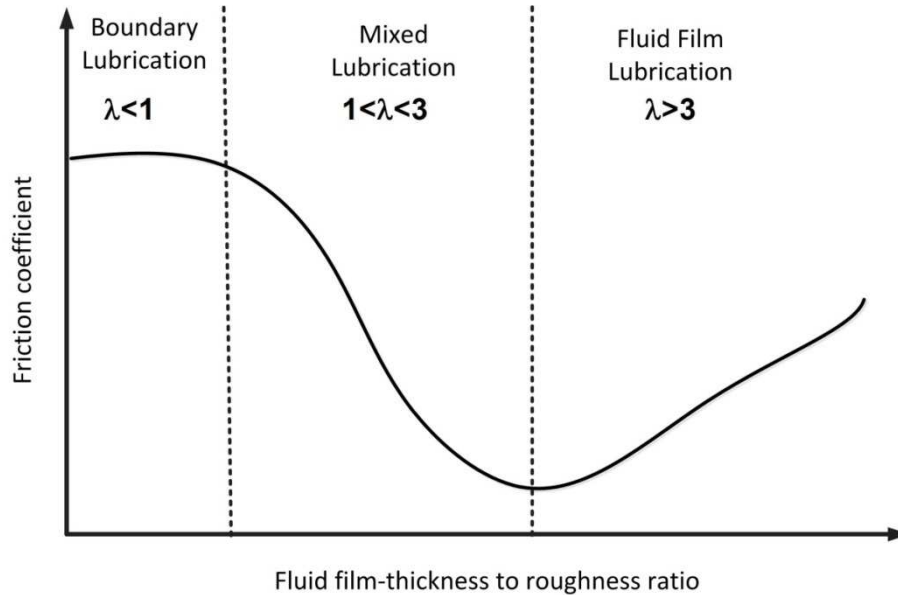


Figure 4 Characterisation of lubrication regimes according to Stribeck curve.

2.4. Recent developments in nanocomposite coatings with focus on tribological performance

Table 1 presents a summary of tribological properties of electrodeposited composite coatings incorporating various metal nanoparticles with Ni matrix. It shows improved tribological performance in all kinds of composites using metal nanoparticles as filler in Ni matrix. The effect of electrodeposition conditions for direct current (DC), pulse current (PC) and pulse reverse current (PRC) for pure nickel and Ni-based composite on sliding wear behaviour are investigated by Borkar and Harimkar (Borkar, T. and Harimkar, S. P., 2011). It was demonstrated that for all pulse conditions the nickel composite coatings showed enhanced wear resistance than pure nickel coatings. Furthermore particles enforcement improved with pulse current (PC) and pulse reverse current (PRC) conditions when compared to direct current (DC) and Ni-Al₂O₃ exhibited better wear resistant properties when compared to Ni-silicon carbide and Ni-zirconium oxide. The influence of

current density on wear resistance performance of nickel and nickel composite of TiO_2 was investigated by Denny and Andreas (Denny, T. and Andreas, B., 2008). It was concluded that the wear resistance of Ni- TiO_2 composite enhanced with decreasing current density which increased the hardness and refined the nanocrystalline grain size.

The deposition pulse frequency was identified as a dominant factor to optimize the grain size, microhardness and corrosion resistance properties of Ni-W coatings (Argañaraz, M. et al., 2011). Abdel Aal et al, determined the optimum electrodeposition parameters and concentration (41 wt.%) of incorporated nanoparticles of aluminium nitride (1-40-150nm) into Ni matrix for improved tribological performance in term of wear resistance, corrosion resistance and coefficient of friction (Aal, A. A. et al., 2006). Tribo-tests were conducted subject to room temperature under a load of 500 g and sliding speed of 70 rpm. It was demonstrated that the composite coatings of Ni-AlN significantly enhanced the tribological performance in comparison to nickel coatings. The wear and friction behaviour of electroplated Ni- Si_3N_4 with focus of ionic liquid lubrication under ball on disc sliding rig studied by Yanqiu Xia et al. (Xia, Y. et al., 2007). It was presented that the tribological properties of co-deposit coatings were excellent under ionic lubrication. The friction and wear tests were conducted under a load of 10 N and sliding speed of 0.055 m s^{-1} .

Gül and co-workers studied the influence of current density on the tribological performance of Ni-alumina co-deposited by using direct current and PC methods (Gül, H. et al., 2009; Gül, H. et al., 2014). It was concluded that the co-deposit composite coatings manufactured by PC technique resulted into an increased percentage of incorporated particles and also with enhanced particle distribution within the matrix. It was found that the wear rate of coatings produced by using DC technique was reduced with increasing current density. On the other hand, no significant influence of current density was observed in coatings produced by using PC technique.

An optimum value for immersed particles (Gül, H. et al., 2012) and sodium dodecylsulfate (SDS) (Kartal, M. et al., 2015) into electrodepositing electrolyte has been reported in literature as 20 gram per litre and 0.10 gram

per litre respectively in order to achieve better mechanical and tribological properties of electroplated Ni-silicon carbide and Ni-tungsten carbide composite coating.

Beltowska-Lehman et al (Beltowska-Lehman, E. et al., 2015) investigated the effect of ultrasonic treatment on Ni-ZrO₂ composite coatings. It was established that the composite coatings Ni-W/ZrO₂ showed the uniform distribution and a greater content of particles subject to lower ultrasonic treatment. It was the reason for the enhanced mechanical properties of developed coatings. The corrosion resistance behaviour of nickel alumina composite coatings as a function of incorporated nano-alumina particles was investigated by Zhou et al (Zhou, Q. et al., 2009). It was proved that the integration of nano-alumina particles increases the corrosion resistance, reducing the porosity of the coatings and also increases the abrasion resistance. It was because of the better dispersion of nano-sized particles with respect to the micro-sized particles. The effect of depositing pulse frequency on the wear behaviour of nanocomposite coatings under sliding contact was studied by Chen et al. (Chen, L. et al., 2006). It was indicated that the volume fraction of alumina particles in coatings increased with the increase of pulse frequency and the wear behaviour of coating depend on reinforcement content of the particles into coating rather pulse frequency. It was confirmed that the wear properties of electrodeposited coatings as a function of changing pulse frequencies act significantly dissimilar subject to dry and oil lubricated situations.

Earlier, researchers have studied the influences of chemical composition strength (ionic concentration) of electrolyte on surface morphologies of coatings produced by electroplating method (Beltowska-Lehman, E. et al., 2011). It was established that the lower ionic strength of electrolyte results into good particle distribution within the nickel matrix, also the refined microstructure of deposited pure nickel and nickel co-deposit of alumina nanoparticles. The volume of electroplating bath also contribute to the characteristics of deposit coating as researchers reported in the literature (Oloruntoba, D. et al., 2010). It was observed that the coating deposition time is significantly reduced at higher volume of electrolyte.

Table 1 A summary of the tribological properties of some nanoparticles-filled metal nanocomposites.

Matrix/nanoparticles	Filler Size (nm)	Method	Change of H	Change of COF	Wear resistance	Corrosion resistance	Reference
Ni/Al ₂ O ₃	50-150	DC,PC	~450	~0.2 – 0.25	↑	↑	(Borkar, T. and Harimkar, S. P., 2011; Zhou, Q. et al., 2009)
Ni/SiC	50	PC	~650	~0.29 – 0.34	↑	↑	(Vaezi, M. et al., 2008; Wielage, B. et al., 2008)
Ni/ZrO ₂	100	PC	~434-446	-	↑	↑	(Benea, L., 2009; Kumar, K. A. et al., 2012)
Ni/TiO ₂	21	DC	~400-450	~0.66 – 0.75	↑	↑	(Denny, T. and

							Andreas, B., 2008; Lampke, T. et al., 2006; Wang, Y. et al., 2014)
Ni/W	60-150	PC	~650-850	~0.30 – 0.40	↑	↑	(Argañaraz, M. et al., 2011; Surender, M. et al., 2004b)
Ni/AlN	40-150	DC	~650	~0.012 – 0.016	↑	↑	(Aal, A. A. et al., 2006)
Ni/Si ₃ N ₄	100	DC	~484	~0.04 – 0.06	↑	-	(Xia, Y. et al., 2007)
Ni/CeO ₂	40	DC,PC	~360-400	~0.48 – 0.52	↑	↑	(Aruna, S. et al., 2006; Xue, Y.-J. et al., 2006; Xue, Y.-J. et al., 2010)

Chapter 2 Fundamentals and Literature Review

Ni/Fe ₂ O ₃	<100	DC	~300-320	~0.25 – 0.30	↑	↑	(Haq, I. U. et al., 2013)
Ni/SnO ₂	<100	DC	~450-480	~0.22 – 0.35	↑	-	(Khan, T. I., 2011)

Table 2 provides a summary of recent research papers related to electrodeposited nanocomposite coatings with different process method used to examine the friction, wear and corrosion properties of coatings. The key investigations demonstrate that the results are quite dependent to the experimental condition of both electrodeposition parameters and configuration parameters of tribo test methods used. Table 3 demonstrates a summary of the key results of the investigation related to effect of configuration parameters such as testing method, sliding velocity, contact frequency, contact area, temperature and coating material on wear and friction coefficient properties.

2.5. Summary of the literature review and research gaps

The tribological performance of nickel composite nanocoating has been extensively studied by various researchers in dry and oil lubricated sliding contacts. However, the tribological performance of nickel nanocomposite coatings under rolling contact with focus on water lubricated environment is left obscure. Earlier investigations were conducted based on pin-on-disc or ball-on-disc sliding wear test condition under dry or oil lubricated environment.

Tribological performance of electrodeposited coatings in the presence of water lubrication may considerably differ from dry or oil lubricated contacts. Water-lubrication film between tribologically interacting surfaces may alter the friction, wear and corrosion properties of electrodeposited coatings. The incorporation of nanoparticles, the wettability behaviour and chemical composition of electroplating solution are some parameters which may unpredictable tribo-properties of the coatings. Further study is necessary to investigate the tribology of nano-enhanced electroplated coatings subject to water lubrication contacts.

Therefore, in the current study, a modified ball-on-disk assembly with three ball system by using a Rotary Tribo-meter (Phoenix Tribology) was designed to simulate industrial water-lubricated rolling contact. These coatings were studied in terms of tribological and mechanical properties, coatings-substrate interface adhesion strength, wettability behaviour and surface free energies.

Table 2 A summary of electrodeposition of nanocomposite coating with focus on tribological improvements

Coating process		Tribo test method	Composite materials	Investigations	Reference
DC, PRC	PC,	Ball-on-disk	Co-W (15-70nm)	<ul style="list-style-type: none"> • COF • Hardness • Wear 	(Su, F. et al., 2013b)
DC, PRC	PC,	Ball-on-disk	Co (10-50nm)	<ul style="list-style-type: none"> • COF • Hardness • Wear 	(Su, F. et al., 2013b)
DC		Ball-on-disk	PTFE particles (2 μ m)	<ul style="list-style-type: none"> • Wettability • Corrosion resistance • Wear 	(Changdong, G. et al., 2012)
DC		Electrochemical measurements	Ni-Co	<ul style="list-style-type: none"> • Corrosion resistance 	(You, Y. et al., 2012)
DC, PRC	PC,	Ball-on-disk	Co-W (20-50nm)	<ul style="list-style-type: none"> • COF • Hardness • Volume fraction 	(Su, F.-H. and Huang, P., 2012)
DC		Ball-on-disk	SiC (50 nm) , Al ₂ O ₃ (50 nm)	<ul style="list-style-type: none"> • Hardness • Wear • COF 	(Abbott, A. P. et al., 2012)
DC, PRC	PC,	Electrochemical measurements	10-25 nm Ni grains	<ul style="list-style-type: none"> • Wettability • Corrosion resistance 	(Gu, C. and Tu, J., 2011)
PC		Ring on Disk	Ni-W/ Al ₂ O ₃ , Al ₂ O ₃ (80nm)	<ul style="list-style-type: none"> • Wear • COF • Hardness 	(Hou, K.-H. and Chen, Y.-C., 2011)
DC, PRC	PC,	Ball-on-Disc	Al ₂ O ₃ (150 nm), SiC (30-60 nm), ZrO ₂ (200 nm)	<ul style="list-style-type: none"> • Wear • COF • Hardness • Volume fraction • Coating thickness 	(Borkar, T. and Harimkar, S. P., 2011)
PC		Pin-on-disc	Ni-CNT, CNT (30-50 nm)	<ul style="list-style-type: none"> • Wear • Hardness • Wear resistance 	(Borkar, T. and Harimkar, S., 2011)
DC		Ring on disk	Ni-W alloy (1.5-8.7 nm)	<ul style="list-style-type: none"> • Wear • COF • Hardness • Heat treatment effect • Deposition rate 	(Hou, K.-H. et al., 2010)

PC, DC	Electrochemical	Ni-Cu, grain size (18-31nm)	<ul style="list-style-type: none"> • Hardness • Deposition morphology • Corrosion resistance 	(Agarwal, M. et al., 2010)
DC	Pin on disk	Ni-Al ₂ O ₃ (50nm)	<ul style="list-style-type: none"> • Adhesive strength • Volume fraction • Hardness • Wear 	(Saha, R. et al., 2010)
PC	Ring on disk	Ni-P-SiC, (300nm)	<ul style="list-style-type: none"> • Wear • COF • Micro hardness 	(Hou, K. H. et al., 2008)
DC	Electrochemical Measurements	Ni-Al ₂ O ₃ (13nm)	<ul style="list-style-type: none"> • Corrosion resistance. 	(Ciubotariu, A. C. et al., 2008)
DC, PC	Vickers micro-hardness	Ni/nano-SiC(20nm)	<ul style="list-style-type: none"> • Hardness • Volume fraction 	(Gyftou, P. et al., 2008)
DC, PRC	PC, Vickers micro-hardness	Ni-Al ₂ O ₃ (13nm)	<ul style="list-style-type: none"> • Parameters effects • Volume fraction • Hardness 	(Thiemig, D. et al., 2007)
DC, PC	Ring on disk	Ni-P-SiC, (300 nm)	<ul style="list-style-type: none"> • Wear • COF • Micro hardness • Volume fraction 	(Hou, K.-H. et al., 2006)
DC, PC	Ring on disk	Ni-P	<ul style="list-style-type: none"> • Internal stress • Wear • COF • Micro hardness 	(Hou, K.-H. et al., 2007)
DC	Ring on disk	Ni-Co/Si ₃ N ₄ (20nm)	<ul style="list-style-type: none"> • COF • Micro hardness 	(Shi, L. et al., 2005)
PC	Ball-on-flat	Ni-WC	<ul style="list-style-type: none"> • COF • Hardness • Wear 	(Surender, M. et al., 2004a)
DC	Ring on disk	Ni-SiC(293 nm)	<ul style="list-style-type: none"> • Wear • COF • Hardness • Volume fraction 	(Hou, K. et al., 2002)

Table 3 A summary of configuration parameters effect on coefficient of friction and wear.

Tribo Tester	Specimens	Experimental Conditions	Key Results	Investigations	Reference
ring-on-disc pin-on-disc	<ul style="list-style-type: none"> • (CuSn) alloy • Aluminum (Al99.6) • Steel (rings and disc) 	<ul style="list-style-type: none"> • 1000 rpm • 100–180 °C • lubricated 	<ul style="list-style-type: none"> • As compared to PoD the RoD method is a better approach for bench testing of journal bearing application due to following benefits. • A uniform lubrication conditions • Demonstrates a better way of heat flow from the contact points. • A better simulation of load bearing capacity of the component/systems. 	<ul style="list-style-type: none"> • Effect of testing method 	(Pondicherry, K. S. et al., 2013)
ball-on-disc	<ul style="list-style-type: none"> • Multi-layered DLC • AISI 52100 steel ball 	<ul style="list-style-type: none"> • Dry • 16–20 C° • SV 0.06-0.5 	<ul style="list-style-type: none"> • Increasing sliding velocity and normal load contribute to reduction in COF. • The wear rates reduced with increasing normal load. The wear rate increases up to certain value of increasing sliding velocity and then started decreasing with further increase in velocity. 	<ul style="list-style-type: none"> • Effect of sliding velocity 	(Kim, D.-W. and Kim, K.-W., 2012)
ball-on-disc	<ul style="list-style-type: none"> • 7475aluminum alloy • H11 steel ball 	<ul style="list-style-type: none"> • 300–450 °C • Dry 	<ul style="list-style-type: none"> • The coefficient of friction and deformation significantly increased with an increase in the testing temperature. 	<ul style="list-style-type: none"> • Effect of temperature 	(Wang, L. et al., 2010)
ball-on-disc	<ul style="list-style-type: none"> • PTFE coating • GCr15-bearing steel ball 	<ul style="list-style-type: none"> • Air • Vacuum 	<ul style="list-style-type: none"> • There was no significant influence of surrounding environment on friction coefficient .The increasing normal load contributed to the reduction in COF. • The wear resistance behavior of PTFE type 	<ul style="list-style-type: none"> • Effect of load and surrounding Envir. 	(Yuan, X.-D. and Yang, X.-J.,

			coating decreases subject to vacuumed condition. However, the behavior was reverse when normal load was increased above 6N.		2010)
ball-on-disc	<ul style="list-style-type: none"> AlCrN , TiAlN coating Si3N4 balls 	<ul style="list-style-type: none"> RH 50–60% Dry 318 rpm 	<ul style="list-style-type: none"> The AlCrN show better wear and coefficient of friction behaviour than that of TiAlN. The experimental results show s that the AlCrN is good candidate to achieve better oxidation and spalling resistance properties of the coatings. Also these coatings proved better in terms of removing wear debris at contact interface. 	<ul style="list-style-type: none"> Effect of coated material 	(Mo, J. et al., 2007)
ball-on-disc	<ul style="list-style-type: none"> Steel AISI 1045 Corundum balls 	<ul style="list-style-type: none"> 50% RH Dry 0.64 and 16 Hz 	<ul style="list-style-type: none"> In addition to sliding velocity and normal load the wear rate also depends on contact frequency. It was proven that the contact frequency provides information about wear mode also under constant sliding speed and applied load conditions. The oxidational and adhesive type wear mechanism was observed above 9 Hz and bellow 4 Hz respectively. 	<ul style="list-style-type: none"> Effect of contact frequency 	(Navas , C. et al., 2006)
ball-on-disc	<ul style="list-style-type: none"> MoS2 Steel balls 	<ul style="list-style-type: none"> Room temperature Dry 	<ul style="list-style-type: none"> The Wear rate and average COF of coatings reduced with increasing counter ball diameters. However, influences from ball size vanished when increased above 6.35 mm. 	<ul style="list-style-type: none"> Effect of contact area/ball size 	(Jiang, J. et al., 2000)

Chapter 3. Experimental Methodology

3.1. Electrodeposition of pure Ni and Ni-based composite coatings

3.1.1. Coating development setup

Electrodeposition experiments are performed by using a conventional electroplating technique with two electrode system placed parallel vertically in a beaker containing 1L of electrolyte solution. The electrodeposition experimental setup used for small scale coating development in this research is shown in Figure 5.

Pure nickel (99.99% Ni, supplier: Wieland Edelmetalle GmbH) rectangular plates (100mm x 50mm) are used as an anode with surface area 2dm^2 , see appendixes A for calculations. The cathode specimen is a steel substrate (dimensions; 80mm diameter and 8.20mm thick) for coating deposition over a surface area of 0.70 dm^2 . The steel substrate is remained constant for all types of coatings. The chemical constituent of substrate material is provided in Table 4. Polyvinyl chloride (PVC) is used to seal the areas which are not required to be plated. Prior to coating development process the surface conditioning is conducted by mechanically polishing the substrate and surface cleaning in liquids under ultrasonic treatment. The pH of the electroplating solution is maintained between 4.0 and 4.5 by adding NaOH or diluted H_2SO_4 and noted by using the Tecpel pH meter. Pulse plating is carried out using MicroStar DPR: 20-15-30 model supplied by Dynatronix (USA). The pulse current conditions such as plating time and pulse on/off time settings can be controlled through the MicroStar Pulse interface.

Table 4 Chemical components of the substrate material (Bajwa, R. S. et al., 2015a).

Materials	C (wt. %)	Si (wt. %)	Mn (wt. %)	S (wt. %)	P (wt. %)
Mild steel (230M07)	0.14	0.27	0.91	0.25	0.02



Figure 5 Electrodeposition setup for nano-coatings manufacturing

3.1.2. Watts bath preparation

3.1.2.1. Watts bath preparation for electrodeposition of pure Ni and co-deposition of Ni-Al₂O₃, Ni-SiC and Ni-ZrO₂ coatings

For standard Watts bath preparation the chemical constituent are consisted of NiSO₄ 6H₂O (265 g/L), NiCl₂ 6H₂O (48 g/L) and H₃BO₃ (31 g/L) and supplied by Fisher Scientific. For deposition of nanocomposite coatings the nano-sized (~50nm 99.9%) particles of alumina oxide, silicon carbide and zirconium oxides ZrO₂ are provided by Io-Li-Tec GmbH & Co. KG. For better suspension of nanoparticles, the electrolyte solution was continuously

ultrasonically stirred (Sonic system P100) during the plating process of coating deposition.

3.1.2.2. Watts bath preparation with various ionic strength of electrolyte solution

The laboratory procedure for the preparation of Watts's bath is same as discussed above in section 3.1.2.1. However, during this current study, six electrolytes solutions with three distinct strengths are prepared (i.e. High concentration (B_{hc}), moderate concentration (B_{mc}) and light concentration (B_{lc})). The Ni and Ni-alumina coatings are developed from these baths in order to study the influence of different ionic strength on the tribological performance of these coatings. The chemical constituents of these dissimilar electrolytes are given in Table 5.

Table 5 Composition of electrolytes with various ionic concentrations (Bajwa, R. S. et al., 2015a).

Chemical constituent (gram per liter)				
Bath No.	Nickel sulphate	Nickel chloride	Boric acid	Nano-alumina
High concentration (B_{hc})				
1	331	60	38	-
2	331	60	38	20
Moderate concentration (B_{mc})				
3	265	48	31	-
4	265	48	31	20
Light concentration (B_{lc})				
5	200	48	31	-
6	200	48	31	20

3.1.3. Substrate preparation

Prior to deposition the steel disc was mechanically polished on one side and sealed with Polyvinyl chloride PVC on the other side. The polishing is applied to achieve substrate roughness bellow (R_a) $0.1\mu\text{m}$ to get better coating-substrate interface adhesion. The pre deposition process includes a sequence of surface conditioning using deionised water, acetone and etching in 25% acidic solution.

3.1.4. Pulse current electrodeposition parameter settings

The deposition pulse current conditions are controlled through the MicroStar Pulse interface. All types of coatings carried out under constant pulse current parameters, as given in Table 6.

Table 6 List of pulse parameters used for surface area 0.72dm^2 of the cathode

Pulse parameters				
Current density (A/dm^2)	$T_{\text{ON}}/T_{\text{OFF}}$ (mS)	Duty cycle (%)	Frequency (Hz)	Peak current (A)
3	20/80	20	10	2.10

3.1.5. Electrodeposition procedure

- 1) Pour the prepared electrolyte bath in the bathtub and let it stir for about 1 hour for homogeneous mixing of composition compartments.
- 2) Hang the pure nickel anode to one wall and steel disc as cathode to be plated to the opposite wall.
- 3) The negative terminal of the Dynatronix power supply (-) was connected to the substrate.

- 4) The positive terminal of the Dynatronix power supply (+) is connected to the nickel sheet.
- 5) In case of nanocomposite coatings submerge the horn of ultrasonic wave machine inside the electrolyte and make sure it should not touch either anode or cathode.
- 6) Select the desired plating pulse configuration setting in the Dynatronix power supply ProntPanel+ interface software to start the plating process.

3.2. Test rig setup for tribological testing

The Phoenix Tribology TE92 rotatory tribometer allow to accommodate various other test rig combinations including pin-on-disc and four balls systems. High Speed Microprocessor Rotary Tribometer (HSMRT) is modified to accommodate ball-on-disc assembly with the water lubrication ability. The calibration of tribometer was conducted by a technical engineer from the TE92 supplier and calibration certificate for TE92 Microprocessor Controlled Rotary Tribometer is enclosed in appendix C. The ball-on-disk tribometer contained an upper sample (coated) and three lower counter 100Cr6 steel balls, equally spaced at 120°. A close up of the modified version of HSMRT to mimic industrial applications subject to water-lubricated rolling contacts is shown in Figure 6. The electrodeposited specimen disc (80mm diameter and 8.20mm thick) is mounted with a shaft hub located at the outer diameter of spindle of TE92 HS produces rotation and transmits the load on balls rolling in the fixed disk at the base of the chamber. The test specimen and counter body located within the test chamber are fully immersed in water during testing.

The successful commissioning of modified version of HSMRT provide an opportunity to conduct tribo tests for electrodeposited coatings subject to rolling contact under water or oil lubrication. Furthermore, the electrodeposited specimen disc with 80mm diameter can provide three different wear tracks for tribo-test repeatability purpose. The wear track radius on the coated specimen can be controlled by changing the ball holder race with different radius of 33mm, 28mm and 23mm.

The test conditions speed and contact pressure are controlled through programmable user interface COMPEND-2011.

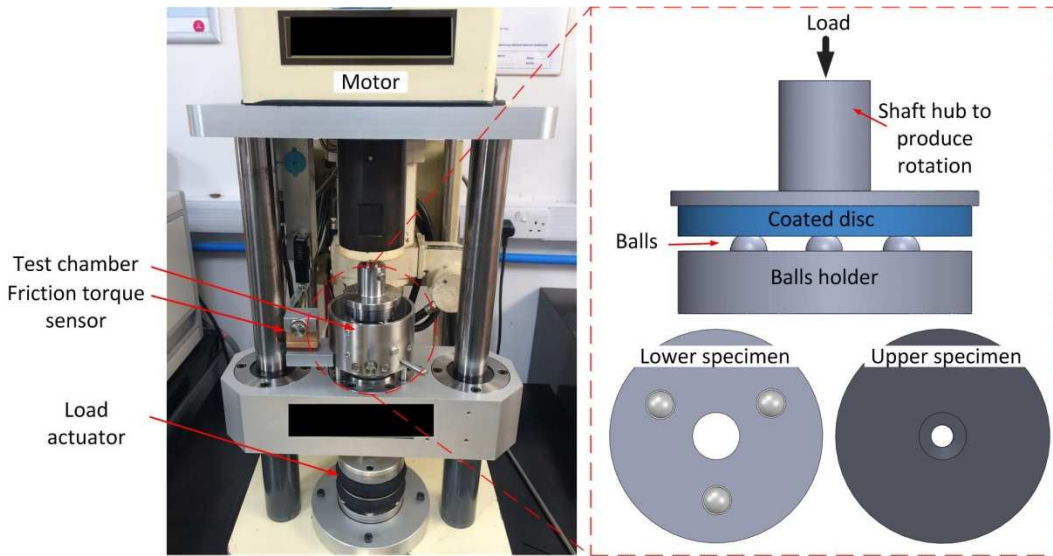


Figure 6 Modified TE92 Rotatory tribometer with test specimen and schematic of loading configuration in magnified view.

3.2.1. *Tribo-test conditions*

All tribo tests are conducted under immersed distilled water lubrication to assess the tribological properties of newly developed coatings subject to water-lubricated contacts. The test conditions were kept constant as 1m/sec speed, 45N of applied load and a test duration of 30 min. The resulting Hertzian contact pressure (Johnson, K., 1974) can be predictable to 1.75 GPa. The elastic modulus and poisson's ratio of steel balls are 210 GPa and 0.30 respectively and assumed values for coated specimens as 230 GPa and 0.28 (Lille, H. and Koo, J., 2005). The tribological experiments are repeated at least three times in order to reduce the uncertainty in the experimental data.

Tribo-test conditions were chosen to simulate boundary lubrication. Hamrock and Dowson formula for minimum film thickness and specific film thickness ratio can be used to evaluate the type of lubrication regime by using known physical properties in Table 7.

Table 7 Known physical properties for calculation of lubrication regime

Known properties		SI Units
η_0	1.08×10^{-3}	Ns/m ²
ξ	4.6×10^{-10}	m ² /N
u	1	m/s
R_x	4.76×10^{-3}	m
E_r	2.30×10^{11}	N/m ²
P	45	N
k	1	
R_{qb}	5.1×10^{-8}	m
R_{qd}	3.1×10^{-8}	m

According to equation (9), the dimensionless minimum film thickness is,

$$H_{\min} = 3.63(9.83193E - 13)^{0.68}(106.15)^{0.49}(8.60638E - 06)^{-0.073}(1 - e^{-0.68k})$$

$$= 2.82197E - 07$$

According to equation (10), the actual minimum film thickness is,

$$h_{\min} = (2.82197E - 07)(4.76E - 3) = 1.34326E - 09 \text{ m}$$

The specific film thickness ratio (λ) or lambda ratio can be calculated by using equation (11),

$$\lambda = \frac{(1.34326E - 09)}{\sqrt{5.1E - 08^2 + 3.1E - 08^2}} = 0.022$$

The calculated value of λ (0.022) depicts that the tribological tests were conducted within boundary lubrication regime range.

3.2.2. Tribo-test procedure

- 1) The test specimens and fixing screws were ultrasonically cleaned in order to get rid of any contaminant traces on the surfaces.
- 2) After surface cleaning, the surface roughness of coated specimens were evaluated by using three-dimensional white light interferometry at three different points.
- 3) The coated specimen was mounted with a shaft hub located at the outer diameter of spindle of TE92 HS produces rotation. The counter three steel balls were placed in the fixed disk (bearing race) at the base of the chamber which allows free rotation of balls.
- 4) The test chamber with a capacity of 500ml was fully immersed with distilled water. The test chamber was cleaned with acetone after fresh water was used prior to each test.
- 5) The tribo-test parameters were pre-defined in tribometer software COMPEND-2011 which also runs the test. The resulting output data was automatically stored in the excel data file and was used for friction coefficient analyses.
- 6) After completion of tribo test, the specimens were carefully removed from the tribo assembly without touching worn tracks and ultrasonically cleaned with acetone.

All specimens were labelled and stored in antistatic grip seal shielding bag to avoid any environmental influences.

3.2.3. Wear and friction coefficient evaluation

The cross-sectional areas of worn surfaces on the disc during wear testing are considered by means of a 3D surface analysis profilometry (ZYGO). The wear volume of worn surfaces are calculated from $V=AL$, where A and L are the worn track cross-sectional area in mm^2 and length of the worn track in mm respectively. The specific wear rate (mm^3/Nm) is equal to V (mm^3) divided by Load (N) x rolling distance S (m).

HS Rotary Tribo-meter (TE92) can only measure the torque which was converted to friction force at a track radius appeared at coated specimen. The coefficient of friction was calculated from equation, friction force divided by normal load.

3.3. Electrochemical corrosion tests

The initiation and propagation of destructive attack on metals and alloys by chemical or electrochemical process with its environment is called corrosion. Most metals and alloys when placed in corrosive medium a spontaneous corrosion current initiates and suddenly corrosion current drops and intact area behaves passively. Resulting in a passive film, it is non-porous and provides protective corrosion resistant surface of working material. However, subject to certain harsh environments, this anti-corrosive film can be affected by localized corrosion incubation points. These localized failure points referred to as pitting corrosion which results in the deterioration of passive film and the base structure with the increasing reaction time.

Corrosion is an electrochemical process involving oxidation and reduction phenomena which can be measured through electrochemical measurement instruments. Electrochemical corrosion measurement is a standard method to measure natural reactions between surface and electrolyte in contact. Also, oxidation and reduction reactions can be controlled through external applied voltage. The stimulation of oxidation or reduction reactions at metal–solution interface through regulating free corrosion potential or open circuit potential (E_{corr}) is called polarization. An increasing in E_{corr} towards positive direction will accelerate the oxidation and a decrease in the E_{corr} towards negative direction will accelerate the reduction. The resulting currents are called anodic and cathodic currents for oxidation and reduction respectively (Kelly, R. G. et al., 2002).

The anodic polarization curve measures the passivity and pitting performance of metal or alloys under examination. In this technique a potential is applied towards a positive direction starting from open circuit potential (E_{corr}) until oxidation of electrolyte or sharply increase in current occurs. A typical resulting anodic polarization curve plots current density vs

potential and shown in Figure 7. The passivity of metals subject to specific metal-solution system can be characterized by decreasing current density with increasing potential. The longer the passive region in anodic direction higher the passive film strength and the lower the current density the higher is the degree of passivation. In anodic polarization plot the pitting potential can be described by the anodic potential at which larger current observed. The pitting potential tendencies of metals or alloys can also be estimated from point of intersection by extrapolating of potential and current intersect (Spies, H., 2014).

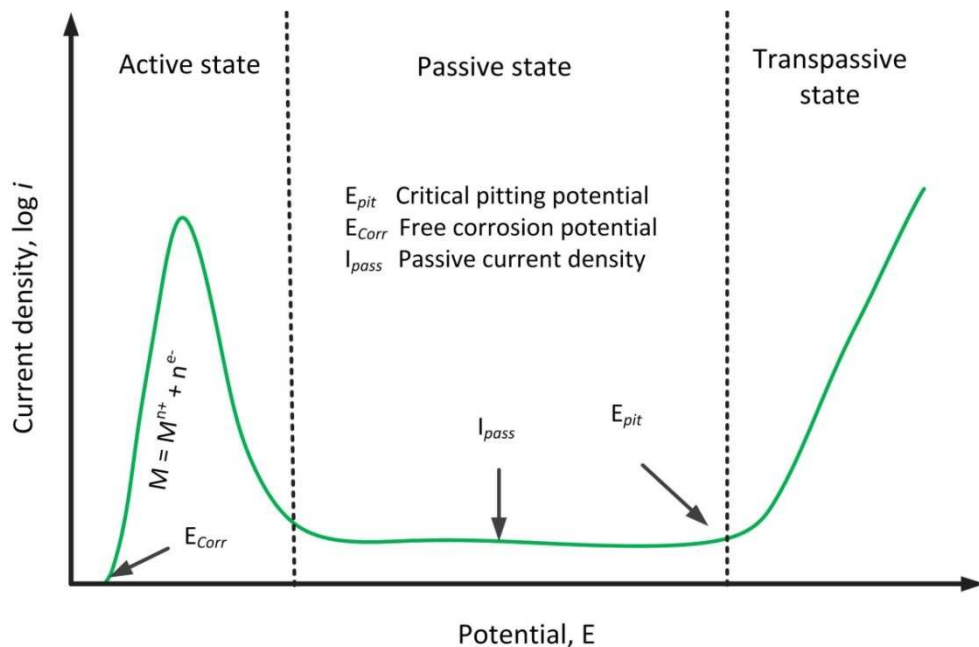


Figure 7 Schematic demonstration of anodic polarization states.

The experimental setup used for electrochemical corrosion measurements in this research is shown in Figure 8. The electrochemical corrosion measurements are conducted by using a conventional three-electrode bench testing system (Gamry instruments). A platinum wire and Ag+/AgCl electrode are used as counter electrode and a reference electrode respectively. The working electrode is the electroplated specimen, placed at the bottom in direct contact with 3.5 wt. % NaCl solution at a temperature of 20°C. Prior to starting the test the opening circuit potential (OCP) was stabilized and experiment was conducted on scanning rate of 0.001 V/s. The

corrosion behaviour of each coating is examined through potentiodynamic anodic polarization curves. The specimen preparation procedure for conducting the corrosion test is provided in section 3.6.1.

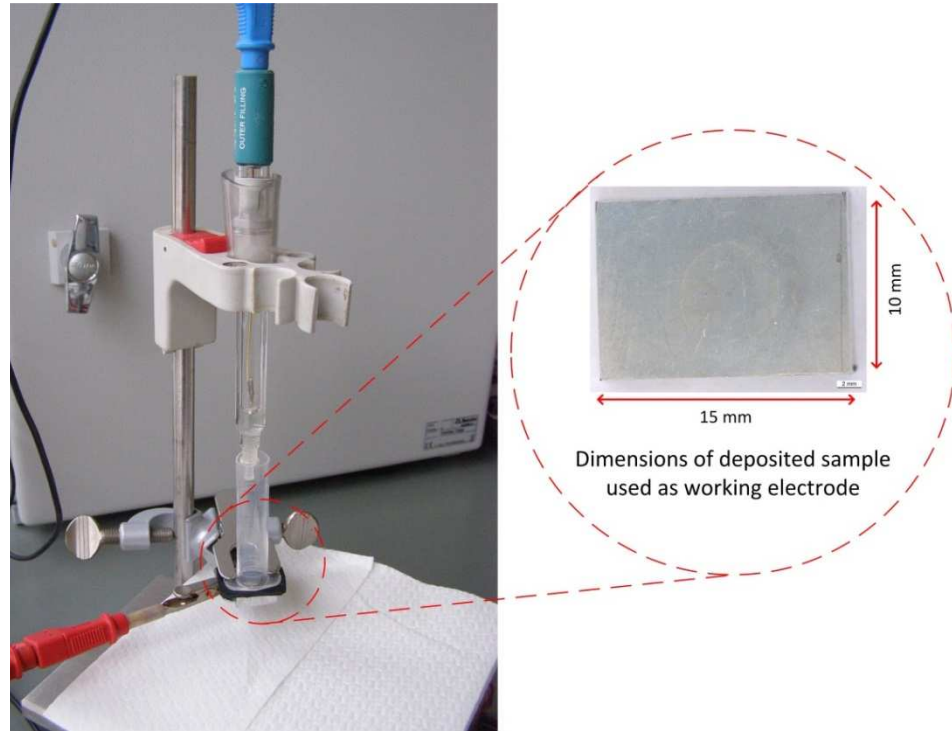


Figure 8 Three-electrode configuration setup with coated specimen as working electrode at bottom.

3.4. Wettability and surface energies test

The wettability and surface energies tests were conducted to understand the lubricity behaviour of electrodeposited coatings with different type lubricants. The surface energy or surface tension of electrodeposited nickel and nickel nanocomposite coatings are examined by using Drop Shape Analyser DSA 100 (KRÜSS GmbH) based on Owens and Wendt (OWRK) technique (Owens, D. K. and Wendt, R., 1969). The reference liquids used in the contact angle measurement (CAM) and surface energy (SE) experiments are the H_2O and CH_2I_2 with known surface energies. In order to reduce the uncertainty in the results, three to four droplets are made on each coated specimen for CAM and SE. The experimental method for study of surface energy or surface tension of solid surfaces through contact angle measurement technique is discussed in the literature elsewhere

(Lugscheider, E. and Bobzin, K., 2001). The specimen preparation procedure for conducting surface wettability behaviour study is provided in section 3.6.1.

3.5. Adhesion performance tests

The adhesion enactment of newly developed coatings is studied by using DIN EN 1071-3 standard method based on the scratch testing technique. The specimen preparation procedure for conducting the scratch test is provided in section 3.6.1. The scratch experiments are conducted with the help of the CSM machine consisted of Rockwell C diamond with tip radius of 200 μ m and testing setup shown in Figure 9. The scratch test standard parameters are as follows,

- Load: 0 to 100 N
- Scratch length: 10 mm
- Test time: 60 seconds

Optical microscopic examinations are conducted on 200X magnifications to investigate the critical load value (L_c) at which the first failure mode was witnessed.

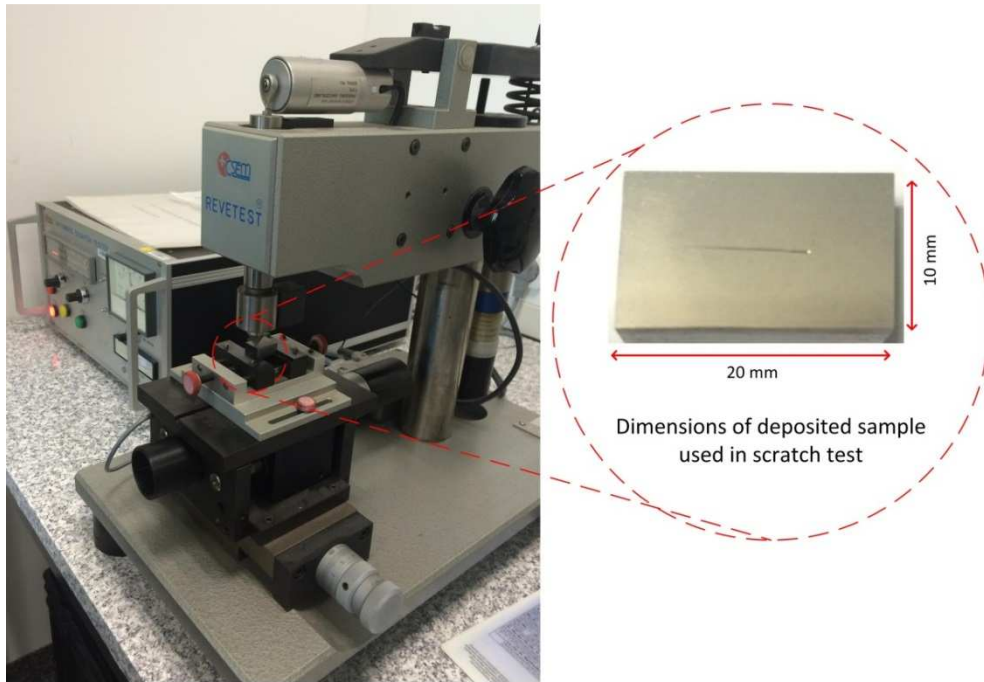


Figure 9 Scratch test configuration setup with dimensions of coated specimen.

3.6. Characterization tools and methods

The surface morphology and mechanical properties of newly developed electrodeposited coatings are examined by using advanced characterization methods such as, X-ray diffraction (XRD) analysis, scanning electron microscopy (SEM), 3D white light interferometry and micro nano indentation techniques. These techniques are discussed in this section.

3.6.1. *Sample preparations for characterizations*

Each type of electrodeposited sample is cut into sub samples using a precision cutting machine (ATM brilliant 220) in order to conduct different investigations. The coated sample cutting procedure and preparation can be seen in Figure 10. Following investigation are conducted by using different segments of actual specimen,

- SEM/EDS
- XRD
- Hardness and elastic modulus
- Scratch testing

Chapter 3. Experimental Methodology

- Corrosion testing
- Wettability and surface energies testing

The coated specimens are embedded by using an ATM OPAL 460 apparatus to study coating-substrate interface adhesion. The top surface of the embedded sample is grounded and mechanical polished under, the lubrication of polycrystalline diamond particles.



Figure 10 Coated sample cutting and preparation procedure to conduct different investigations

3.6.2. 3D surface profiler (Zygo NewView 5000)

The 3D surface profiling is conducted by using Zygo NewView 5000 Model (shown in Figure 11) for surface mapping and to quantify the amount of wear of worn surfaces of the coatings. The measured roughness parameters are R_a (arithmetic mean of roughness) and R_z (sum of peak height and depth) are used for surface mapping. The ZYGO white light interferometry is a non-destructive technique for surface characterisation of without special specimen preparation.



Figure 11 Three-dimensional surface profiling machine (ZYGO NewView 5000)

3.6.3. Optical microscopy (Olympus)

Leitz Metallux 3 optical microscopy is used for coatings failure inspection after scratch tests (as shown in Figure 12). The coated thickness and coating-substrate interface adhesion are also examined by Metallux 3. This microscopy can conduct examinations in a range of 100x-1000x magnification with 10x-100x objectives.



Figure 12 Leitz Metallux 3 optical microscopy with magnification in range of 100X-1000X.

3.6.4. Scanning electron microscopy /EDS

The microstructure and surface morphology examinations of newly developed coatings are conducted by using a scanning electron microscope (as shown in Figure 13). The embedded samples of electrodeposited coatings for coating-substrate interface analysis are also used for SEM analysis. These embedded specimens are used for the examination of reinforced nanoparticles distributions within the matrix. The Energy

Dispersive X-ray spectroscopy (EDS) an additional functionality of SEM is used to determine weight percentage of incorporating particles in the composite coatings. The standard surface conditioning requirements of specimens prior to putting in the SEM analysis were followed.



Figure 13 Scanning electron microscopy for microstructure and EDS analyses (JEOL JSM-6010PLUS/LV).

3.6.5. Micro and Nano-indentation tester

The mechanical properties of newly developed coats are measured with nano-Indentation (CSM) (Figure 14a) and micro-indentation (LECO) (Figure 14b) testers. Nanoindenter is a suitable tester to reduce the influence of substrate material on the resulting mechanical properties of coated materials by controlling the load and depth penetration capability. For comparison purpose tests are conducted both micro and nano indentation machines. To avoid the influences of surface roughness peaks on the hardness or elastic modulus properties of the coating under examination, all the samples are

mechanically polished to develop smooth surfaces to decrease uncertainty in the retrieving data points. This is because in uneven topology the localized stress developing through contact between the roughness peak and the applied load can cause into relatively deeper and small applied load. The principle of instrumented indentation testing is described in appendix B.

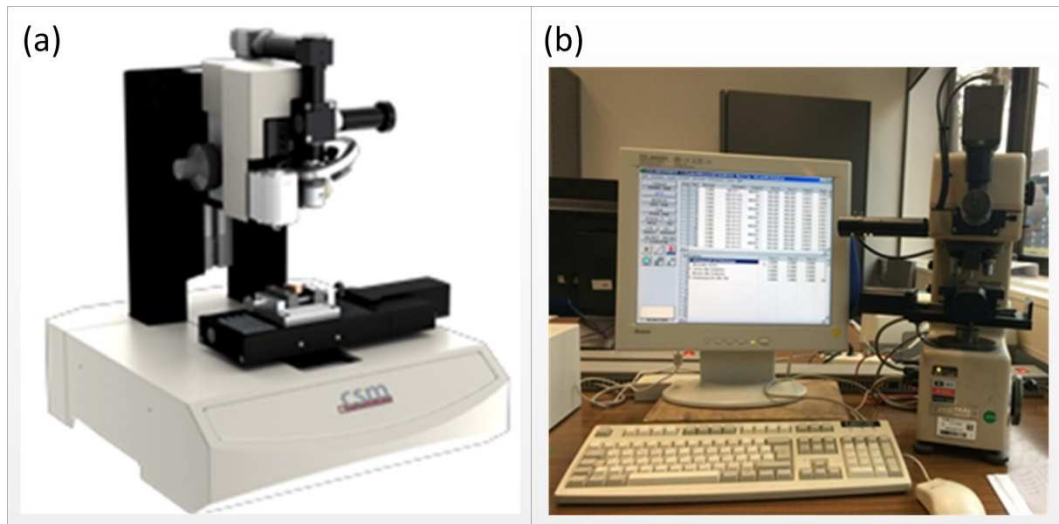


Figure 14 Hardness and elastic modulus measuring machines (a) Nano-indentation (CSM) (b) Micro-indentation (LECO).

Chapter 4. Performance of nanocomposite coatings produced by various incorporated nanoparticles

As discussed in section (2.4) of chapter 2, extensive studies have appeared to examine the wear, friction and corrosion performance of nano-composite coatings embedded with nanoparticles into nickel as a matrix. These electrodeposited nanocomposite coatings have demonstrated improvements to enhance wear, friction or corrosion properties with wide-ranging engineering applications. The aim of the study included in this chapter is to assess the practicability of electroplated pure nickel and Ni-based composite coatings for water-lubricated tribological components/systems. Following properties of newly developed coatings are investigated,

- Wear-resistance
- Corrosion-resistance
- Adhesion strength
- Wettability and surface tension

4.1. Characterisation of the coatings

The pure Ni and Ni composite coatings are produced by using the pulse electroplating method displays shiny grey look, surface evenness and well adhered to the substrate. Figure 15 shows the SEM surface images of pulse electrodeposited pure nickel and nickel co-deposition of nanoparticles (i.e. Alumina, silicon carbide and zirconium).

As can be seen from SEM micrographs in Figure 15, all the coatings demonstrate compacted fine grain microstructure. However, the nickel composite of SiC nano-sized particle revealed bigger grain size when compared to the remainder. This has also contributed to increased roughness parameters R_a and R_z of Ni-SiC coating with values 0.21 μm and 1.38 μm respectively. The variation in roughness parameters for all coatings is provided in Figure 16. Although, the Ni-ZrO₂ composite coating shows fine compact grain size, but the roughness parameters are close to that of Ni-SiC coatings. The reason for this behaviour can be attributed to the existence of

Chapter 4. Performance of nanocomposite coatings produced by various incorporated nanoparticles

agglomerated bigger particles on the surface. Also, porous structure is observed in Ni/ZrO₂ under magnified view of surface images which may also contribute to increased roughness parameters with R_a and R_z values of 0.20 μm and 2.2 μm respectively. In case of Ni-Al₂O₃ composite coating the minimum surface roughness are achieved with R_a of 0.05 μm and R_z of 0.63 μm . This is also understood from finer smooth surface morphology of Ni-Al₂O₃ coating as can be seen in Figure 15b. After that, the pure nickel with R_a of 0.08 μm and R_z of 0.73 μm . The distribution of reinforced nanoparticles within the nickel matrix can be seen from the cross-sectional images as presented in Figure 17. The thickness of composite coatings was controlled by constant electrodeposition time. However, in comparison the thickness of Ni/ZrO₂ composite is less than that of Ni/Al₂O₃ and Ni/SiC composites. This is because the heavier zirconia nanoparticles resulting in the poor suspension of nanoparticles in the electrolyte consequently the thickness is reduced.

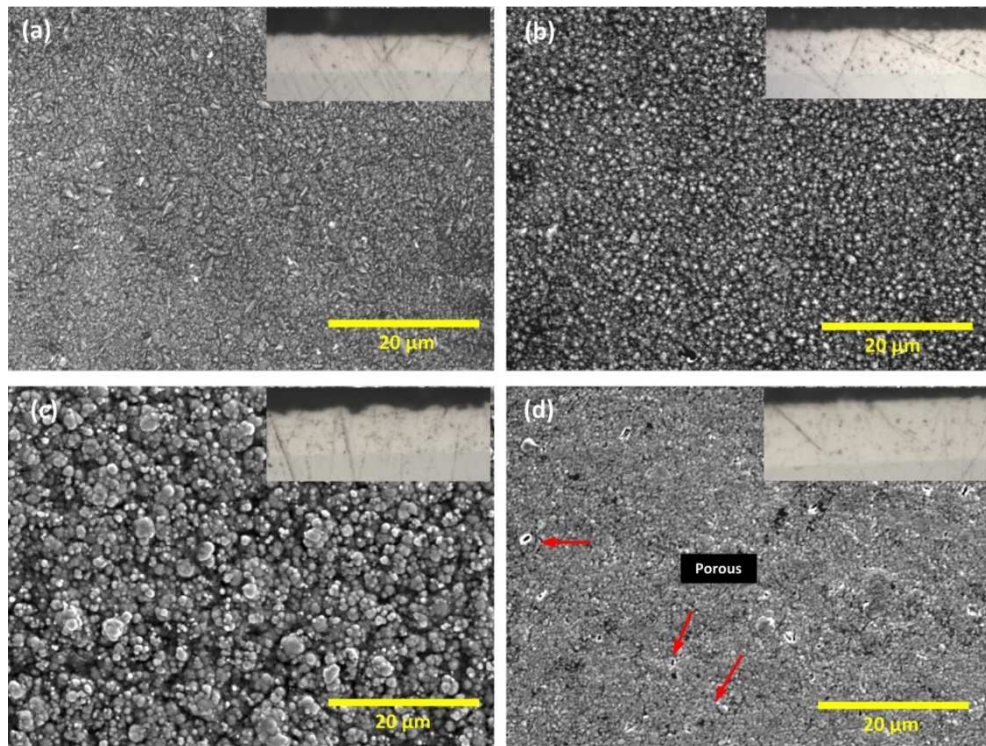


Figure 15 Surface morphologies of different electrodeposited coatings under scanning electron microscopy, (a) Pure Ni (b) Ni/Al₂O₃ (c) Ni/SiC and (d) Ni/ZrO₂ (Bajwa, R. S. et al., 2015b)

Chapter 4. Performance of nanocomposite coatings produced by various incorporated nanoparticles

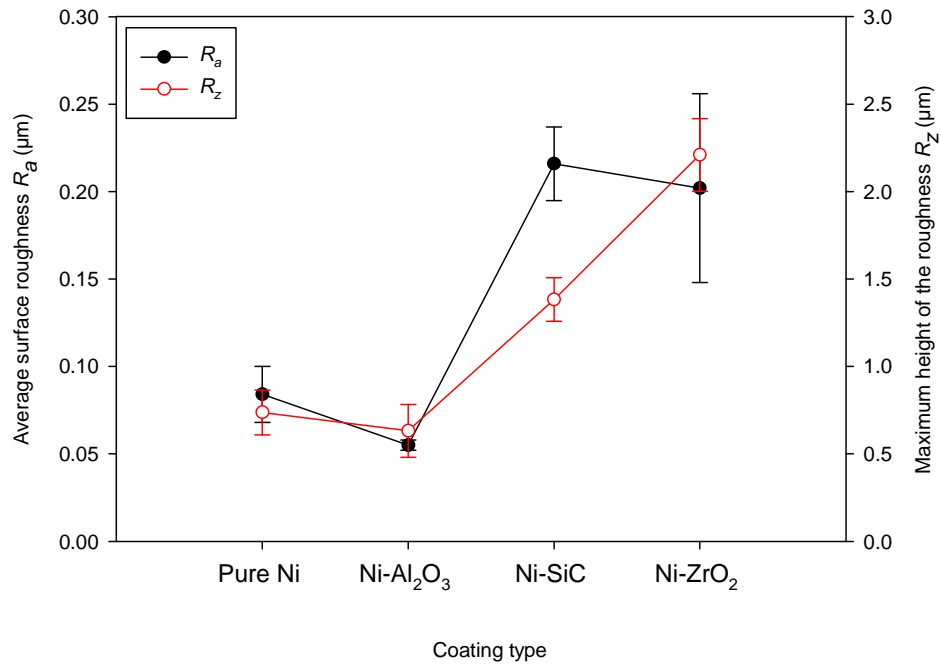


Figure 16 Surface roughness of different electrodeposited coatings (Bajwa, R. S. et al., 2015b).

The calculated reinforcement content of incorporating particles is ranging between 2.5–3 weight percentages as measured by using energy-dispersive spectroscopy. The influence of different type of incorporating nanoparticles (i.e. nano–alumina, nano–silicon–carbide and nano–zirconium) on the hardness and elastic modulus properties of nickel composite coatings with reference to a pure nickel coating are presented in Figure 18. In contrast to previous outcomes in the literature no significant change is observed in the hardness property of newly developed coatings. Previously it was concluded that the reinforced hard ceramic particles contributed to enhanced hardness of co-deposit electroplated coating. This contradiction is perhaps due to dissimilar percentages of incorporated hard particles in the nickel matrix, in earlier study the reinforcement content of nanoparticles were ranges between 8-12 weight % (Borkar, T. and Harimkar, S. P., 2011). Although, this is well-known that strengthening effects of incorporating hard particles result into to increasing the mechanical properties of composite coatings. Alternatively, it has been reported that the plasticity index ratio or hardness to

Chapter 4. Performance of nanocomposite coatings produced by various incorporated nanoparticles

elastic modulus ratio (H/E) is also an essential parameter to predict the properties of coatings/materials (Beltowska-Lehman, E. et al., 2015). Similarly, as shown in Figure 18 the hardness of nickel alumina composite with value 375_{HV} and nickel–zirconia 405_{HV} are less than that of pure nickel which can be due to the reduced H/E ratio of composite coatings. In case of nickel–silicon–carbide composite the H/E ratio is the maximum value which predicts the better wear resistance performance of this coating. Previously, it was established that the plasticity index ratio is also an effect parameter to simulate the wear resistant behaviour of materials (Leyland, A. and Matthews, A., 2000). In comparison a higher standard deviations were observed in the hardness values of Ni/SiC and Ni/ZrO₂ composite which is relate of high roughness values of these composites. This is because the roughness peak coming in contact to indenter can result in a greater depth of indent at relatively lower load due to increased localized stress at the point of contact.

Figure 19 shows the X-ray diffraction results for pulse electrodeposited Ni and nickel-based composite (nano–alumina, nickel–silicon–carbide and nickel–zirconia) coatings. The typical peaks of 111 and 200 patterns of nickel are observed in this work as also informed by numerous scholars about electrodeposited nickel coatings (Beltowska-Lehman, E. et al., 2015; Gül, H. et al., 2012; Gül, H. et al., 2014). Regarding variations in orientations, the reflection of 311 patterns appeared intense in case of nano–alumina. Whereas, the reflection of 002 appeared not as much of the rest of the coatings. In case of nickel–silicon–carbide coating the reflection of 022 patterns appeared noticeably intense. Note that the diffraction patterns for incorporated nano-sized particles are not visible because of insignificant loaded content of particles contained by the composite coatings (Borkar, T. and Harimkar, S. P., 2011). The XRD pattern is used to calculate the crystalline size of electrodeposited coating and measured as (nm); 39, 33, 34 and 30 for Ni, alumina, silicon carbide and zirconium composite coating respectively. To some extent, the grain size of the nickel coating decreased with incorporation of nanoparticles which is in agreement with previous results (Benea, L. et al., 2015; Gül, H. et al., 2009; Kartal, M. et al., 2015).

Chapter 4. Performance of nanocomposite coatings produced by various incorporated nanoparticles

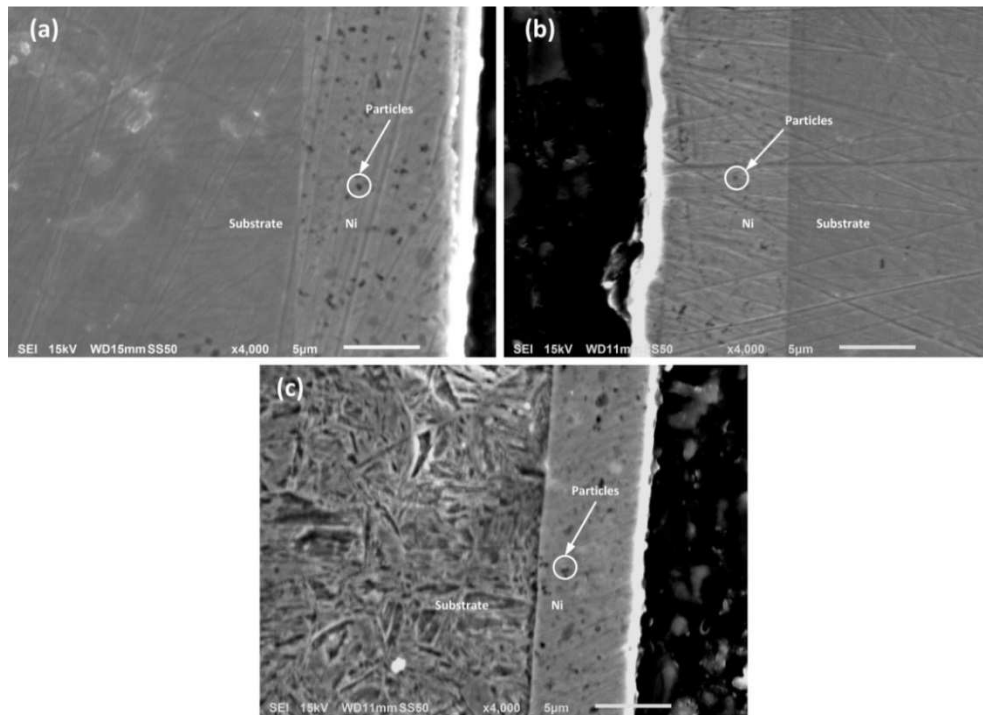


Figure 17 The display of incorporated particle distributions within the nickel matrix for different nanocomposites through SEM, (a) Ni/Al₂O₃ (b) Ni/SiC and (c) Ni/ZrO₂ (Bajwa, R. S. et al., 2015b).

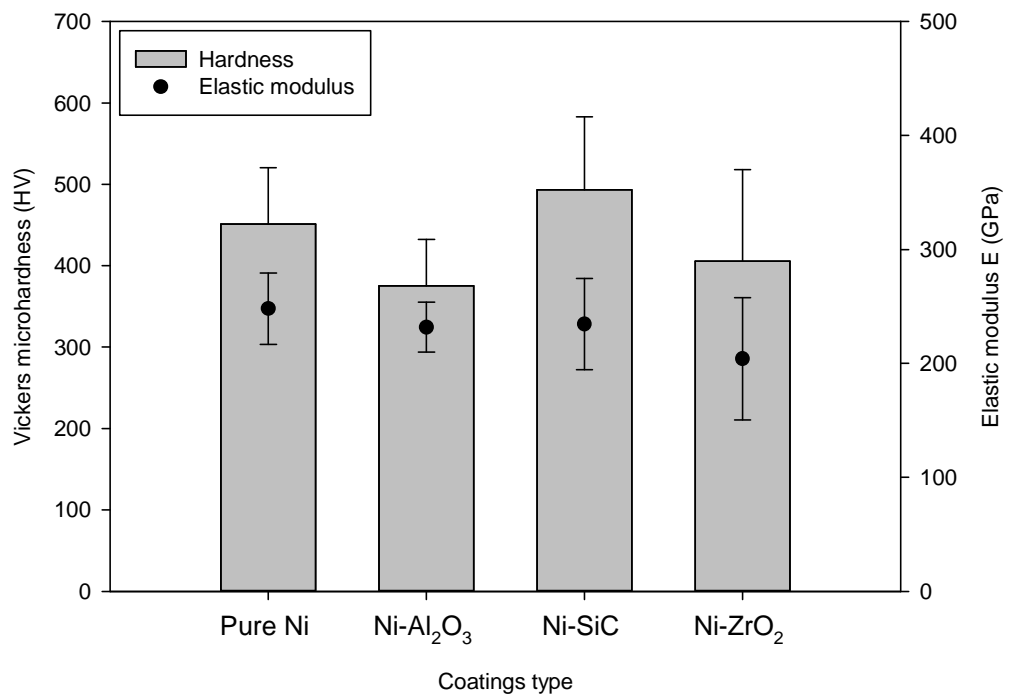


Figure 18 The mechanical properties of different electrodeposited coatings (Bajwa, R. S. et al., 2015b).

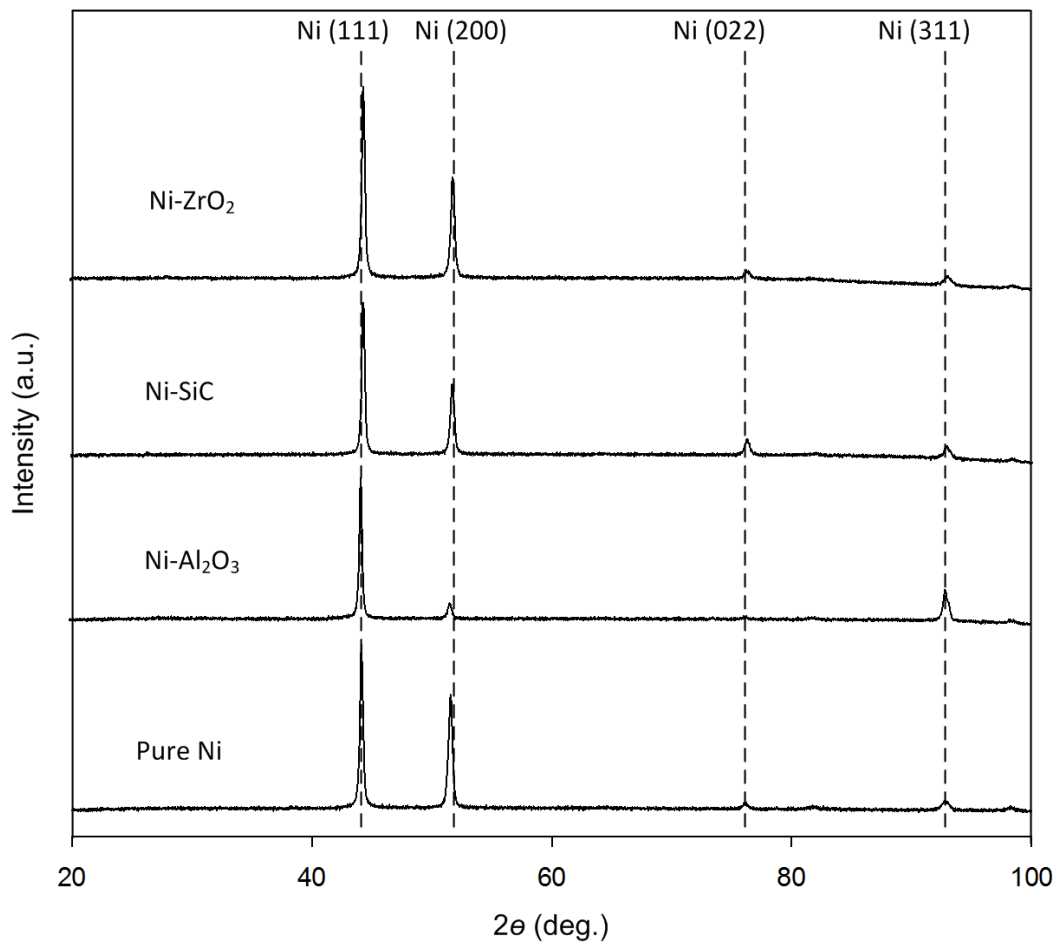


Figure 19 XRD pattern of different electrodeposited coatings(Bajwa, R. S. et al., 2015b).

4.2. Wear and corrosion results

The wear resistance assessment experiments were conducted by using a ball-on-disc assembly subject to water lubrication. Figure 20 shows the comparison of wear properties of Ni and Ni composite incorporating different nanoparticles. The nickel composite of silicon carbide shows the minimum wear which can be because of the maximum plasticity index ratio as discussed above in section 4.1. Although, the nickel alumina composite exhibits the high wear rate than that of nickel SiC composite however, the difference is not much significant. Likewise, there is not much difference in the wear rates of pure nickel and nickel zirconium coatings.

Chapter 4. Performance of nanocomposite coatings produced by various incorporated nanoparticles

Overall, the wear rate behaviour of pure nickel is reduced almost 25 to 30% with the addition of nanoparticles, except in case of nano-zirconium particles. This may be because of manufacturing defects resulting into porous structure and occurrence of agglomerated particles on the surface of nickel zirconia coatings. Consequently, the hardness has reduced and roughness of the surface has increased as mentioned in section 4.1. The three-dimensional surface profiling of worn surfaces during wear tests revealed two body abrasive wear and plastic deformation in all electrodeposited coatings. However, the harsh plastic deformation behaviour of Ni coating is considerably reduced with the addition of reinforced nano-sized particles, except in case of nickel zirconium.

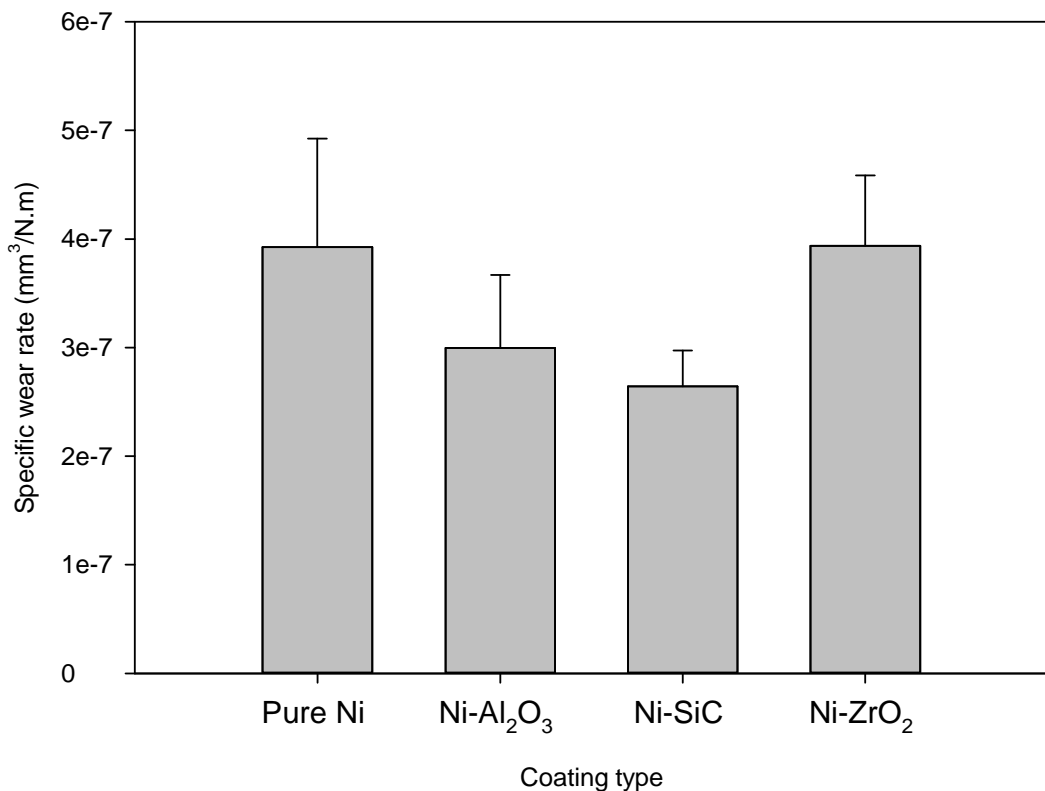


Figure 20 The comparison of wear rates for different electrodeposited coatings subject to water lubrication (Bajwa, R. S. et al., 2015b).

Chapter 4. Performance of nanocomposite coatings produced by various incorporated nanoparticles

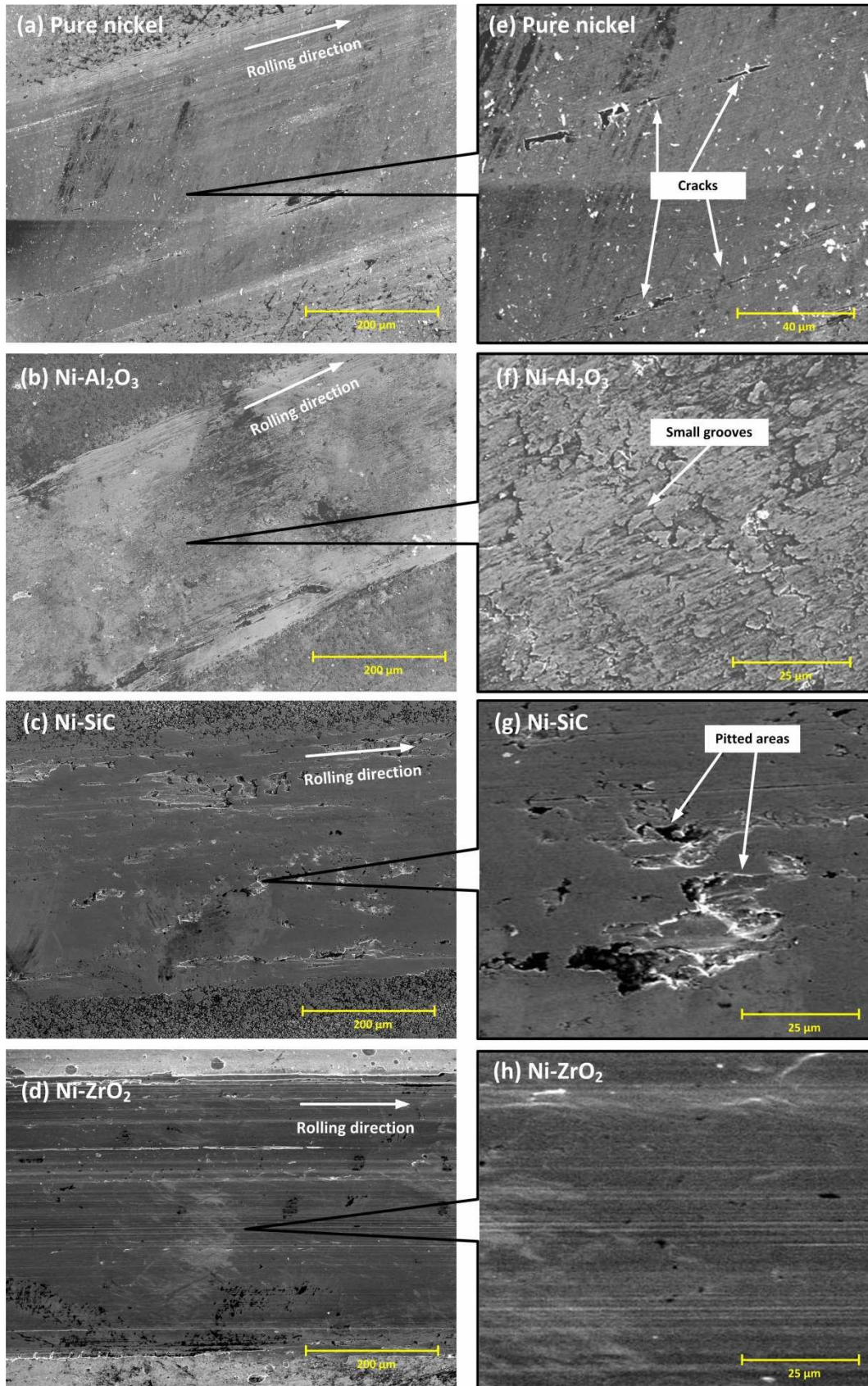


Figure 21 Surface failure examinations for different electrodeposited coatings by using SEM (Bajwa, R. S. et al., 2015b).

Chapter 4. Performance of nanocomposite coatings produced by various incorporated nanoparticles

Figure 21 show the surface examination by using scanning electron microscopy of worn wear tracks after wear experiments with magnified images in Figure 21e-h. As shown in Figure 21e and h, the Ni and Ni zirconium have similar worn surface morphologies with smooth surfaces under severe plastic deformation. Whereas, in case of nickel alumina and nickel silicon carbide two types of surface failure mechanisms are seen, namely; microploughing and adhesive wear respectively. These surface failure mechanisms may attribute to the three body abrasion wear during pulling out of incorporated nanoparticles in wear tests (Cui, G. et al., 2013).

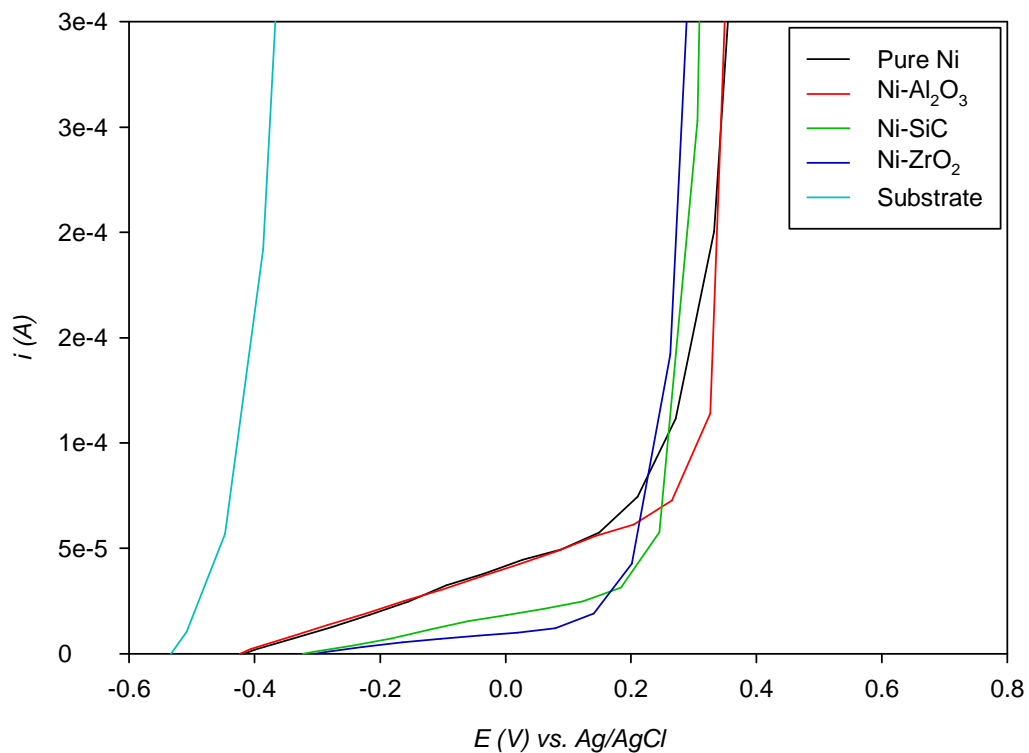


Figure 22 Potentiodynamic polarization curves for different electrodeposited coatings (Bajwa, R. S. et al., 2015b).

The influence of incorporated nanoparticles on the corrosion resistance behaviour of electrodeposited coating investigated by using electrochemical testing method and the potentiodynamic results are shown in Figure 22. As

expected the corrosion resistance property of steel substrate has significantly enhanced with deposit of protective coating. In comparison between Ni and composite coating, it can be seen that corrosion resistant potential of Ni is lower than that of nickel alumina composite which validates the previous results (Feng, Q. et al., 2008; Ramesh, C. et al., 2013). It is interesting to note that the nickel composite of SiC and ZrO₂ exhibits the less corrosion resistant potential than the pure nickel which contradict the previous investigations. This contradiction is because of the significantly higher surface roughness of these composite coatings in comparison to pure nickel as described in Figure 16. Due to the high surface roughness the peak valleys on the coating surface can cause for rapid diffusion of destructive electrolyte on the way to the substrate to boost up pitting corrosion failure. This behaviour can be overcome by increasing the coated thickness of coating and surface polishing of the coatings to reduce surface roughness. The influence of coating thickness on the corrosion resistance potential of coating is described in chapter 6 in detail.

4.3. Adhesion and wettability results

The adhesion strength of the coating to the substrate is an important factor before considering for application in industry. Therefore the adhesion force of newly developed coating are investigated and compared with the required adhesion force of 30 N for wide ranging industrial applications (refer by Schaeffler). The adhesion strength result in terms of critical load values (L_c) experimentally calculated by using the standard scratch test method is shown in Figure 23. The newly developed pure nickel and nickel based composite of nanoparticles demonstrated the adhesion force above the required value for engineering applications with exception of nickel zirconium specimen. The nickel alumina composite presented the maximum adhesion force of 79 N followed by pure nickel, Ni-SiC and nickel zirconium with a minimum value of 28 N. The adhesion of these electrodeposited coatings can further improve by inducing intermediate plating of favourable coating subject to the substrate material.

Chapter 4. Performance of nanocomposite coatings produced by various incorporated nanoparticles

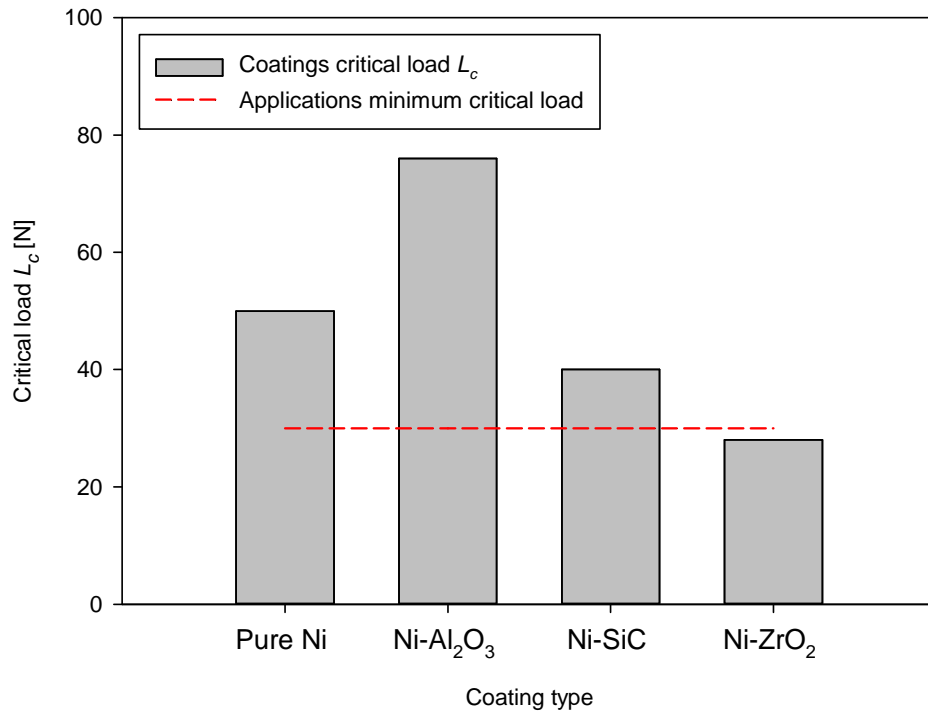


Figure 23 The variations of critical loads for different electrodeposited coatings (Bajwa, R. S. et al., 2015b).

The worn track developed by the scratch tests is further examined by using optical microscopy to understand the failure mechanism of these coatings and surface images are shown in Figure 24. For each specimen the microscopic images are taken at starting, central and ending point of developed scratch. There is a visible accumulation of wear debris at the ending point of scratch in case of Ni and nickel alumina composite. This accumulation of coating indicates the poor adhesion of the coating to the counter body material. In case of nickel SiC and nickel ZrO₂, no accumulation of coating material is observed.

Chapter 4. Performance of nanocomposite coatings produced by various incorporated nanoparticles

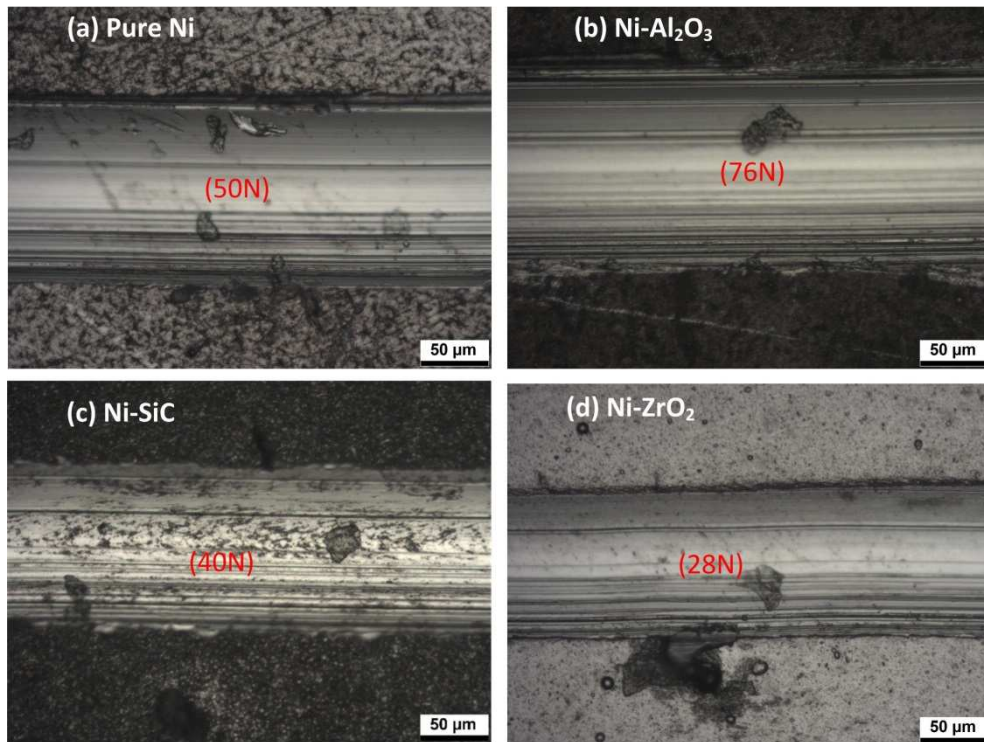


Figure 24 Kinds of electrodeposited coating failure subject to various incorporated nanoparticles after scratch test according to DIN EN 1071-3.

The contact angle measurement subject to water and surface energy results of electrodeposited coatings are presented in Figure 25. The surface free energy properties of coatings are presented in terms of polar and dispersive parts. As can be seen from Figure 25 the coatings are mainly consisted of dispersive part of surface energy which is an indication of covalent bonding between surface and liquids. The dispersive and polar component of coatings, produced from electrodeposition technique ranging from 29–36 mN/m and from 2–16 mN/m respectively. There are not considerable influences introduced by the nanoparticles addition to the nickel matrix except in case of nickel alumina composite. The polar component of the surface energy in case of nickel alumina is reduced significantly in comparison to rest of the coat. Consequently, the water contact angle of nickel alumina is considerably higher than the rest of the coating. This is because the decreasing polar component of surface energy contribute to the higher hydrophobic behaviour of the surface (Grishke, M. et al., 1998). The lower polar share and corresponding surface energy of nickel alumina with

Chapter 4. Performance of nanocomposite coatings produced by various incorporated nanoparticles

the best comparative adhesion is contradicting the previous findings in the literature (Lugscheider, E. and Bobzin, K., 2001). The reason for this contradiction can be due to the coating manufacturing method as those coatings were produced by PVD method. Based on surface energies measurement data, the wetting envelopes are also developed for each coating and shown in Figure 26. Wetting envelop provides the information about suitable combination of surface material and counter lubricating liquid to achieve desired wettability behaviour. The wettability behaviour depends on the types of application such as good hydrophobicity is needed for water repellent applications and good hydrophilicity is needed for better oil lubrication effects. The hydrophobicity is physical property of molecules which dislike/repel water and prefer to make cluster together. On the other hand, hydrophilicity is physical property of molecules which like to attract or dissolve in water. For example water on hydrophilic surface will exhibit low contact angle and on hydrophobic surface will exhibit a high contact angle.

Chapter 4. Performance of nanocomposite coatings produced by various incorporated nanoparticles

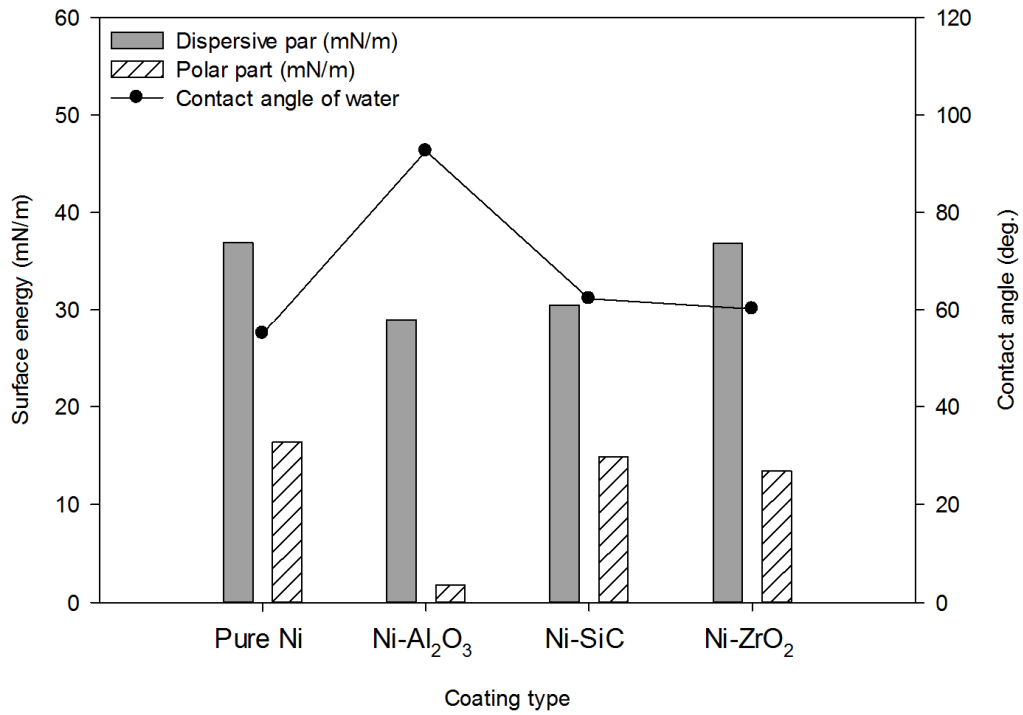


Figure 25 The variations of water contact angle and surface energy for different electrodeposited coatings (Bajwa, R. S. et al., 2015b).

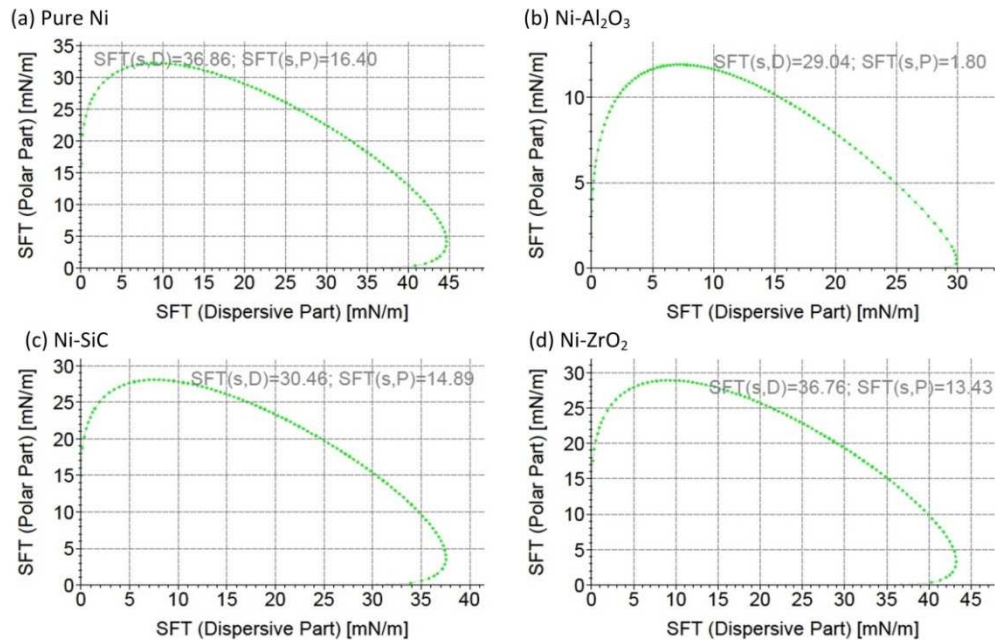


Figure 26 Wetting envelopes for different electrodeposited coatings.

4.4. Conclusions

The aim of this study was to investigate the tribological performance of electroplated Ni-based coatings incorporating nanoparticles. Experimental results showed that the incorporation of nanoparticles significantly enhanced the wear and corrosion properties. The wear rate of nickel composite coating embedded with silicon carbide nanoparticles reduced almost 30% than a pure Ni coating. The better wear resistance behaviour was also predicted from the higher plasticity index ratio (H/E) of Ni/SiC composite coatings. Regarding corrosion resistance, the nickel composite of Al₂O₃ nanoparticles showed the maximum corrosion resistance potential of 0.37V. The corrosion resistance potential of pure Ni was measured as 0.22 V. It was found that the corrosion resistance behaviour can be significantly influenced by the surface roughness. The maximum surface roughness of nickel composite of silicon carbide (0.21µm) resulted in the lower corrosion resistance behaviour. The effect of incorporating particles in the changing phase orientation of composite coating was insignificant. All the coatings showed the typical high peaks for (111) and (200) crystal planes of Ni. However, the (311) reflection grows more intense in case of Ni/Al₂O₃. Whereas, the (002) grows relatively less intense in the same coating. The adhesion tests demonstrated that all the exhibit good coating-substrate adhesion except Ni/ZrO₂. The Ni/Al₂O₃ coating showed the maximum adhesion force of 79 N which meets the industrial minimum (at least 30 N) requirement for coating adhesion strength.

Overall, nickel composite of alumina presented the best tribological and corrosion properties. Therefore, in the next chapter only Ni/Al₂O₃ composite coating is considered in which the effect of ionic concentration on coating performance is evaluated.

Chapter 5. Performance of Ni and Ni-Al₂O₃ composite coatings produced by variable bath ionic strength

The pulse current or pulse reverses current electrodeposition method allow a liberty to control various current parameters such as pulse on/off time, frequency, current density and duty cycle, etc. These parameters play an important role in optimisation of coating properties in terms of wear, corrosion and mechanical properties. Numerous experimental findings in the field of electrodeposited coatings are either contradictory or very difficult to relate because of the variety of pulse and process parameters (Golchin, A. et al., 2013; Gomes, A. et al., 2011; Hovestad, A. and Janssen, L., 1995).

During the last decade, many experimental investigations have been reporting on the optimisation of these parameters with focus to various industrial objectives. Nevertheless, the influences of ionic concentration in the electroplating solution on the wear, corrosion, adhesion and wettability have not investigated previously. Therefore, in this work different electrolytes are prepared with an intention to explore the influence of this parameter over above mentioned properties.

5.1. Characterisation of the coatings

The influence of various ionic concentrations on the microstructure morphology of Ni and nickel based composite of nano alumina coating is shown in Figure 27. Bared surface images of steel substrate have also included for comparison purpose in Figure 27d and h. These coatings are produced under the constant pulse and process parameters of electrodeposition technique. The electrolytes are named as high concentration (B_{hc}), moderate concentration (B_{mc}) and light concentration (B_{lc}). As evident from Figure 27, there is no significant influence of B_{hc} and B_{mc} is seen over changing coating surface morphologies. This conclusion is valid for Ni as well as for co-deposits. On the other hand, the coating

Chapter 5. Performance of Ni and Ni-Al₂O₃ composite coatings produced by variable bath ionic strength

developed by using B_{lc} type chemical solution exhibit relatively increased microstructure features and also spherical agglomerated particles are visible. These agglomerated particles also contributed to relatively more rough surfaces of these coatings, particularly in the nickel–alumina composite coating as shown in Figure 28. The higher standard deviation of roughness parameters in composite coating, produced from B_{lc} type bath is also due to agglomerated particles on the surface.

Interestingly, the similar effect of bath solution is observed with respect to their hardness and elastic modulus properties as shown in Figure 29. The hardness of coatings, produced from B_{hc} and B_{mc} type solution varies between 250 to 451 HV in pure and composite coatings. The hardness values for coatings produced from B_{lc} solution changes from 200 to 515 HV without and with nanoparticle incorporation respectively. The maximum hardness values for composite (515 HV) and pure nickel (451 HV) are achieved from B_{mc} and B_{lc} respectively. Note that, to avoid the influences of surface roughness peaks on the hardness or elastic modulus properties of the coating under examination, all the samples are mechanically polished to develop smooth surfaces to decrease uncertainty in the retrieving data points. This is because in uneven topology the localized stress developing through contact between the roughness peak and the applied load can cause into relatively deeper and small applied load.

Chapter 5. Performance of Ni and Ni-Al₂O₃ composite coatings produced by variable bath ionic strength

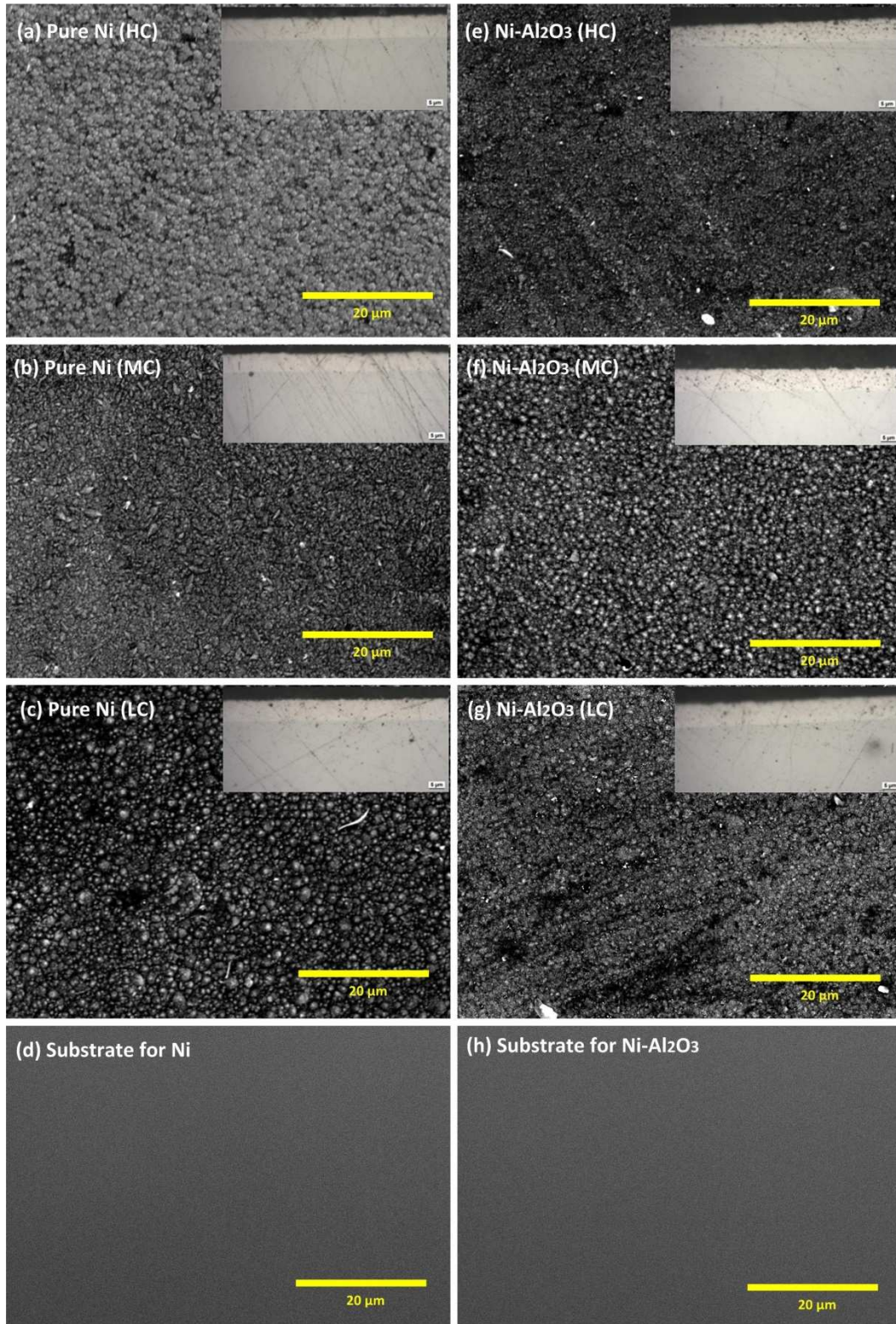


Figure 27 Surface morphology of coatings produced by different types of electrolyte (Bajwa, R. S. et al., 2015a).

Chapter 5. Performance of Ni and Ni-Al₂O₃ composite coatings produced by variable bath ionic strength

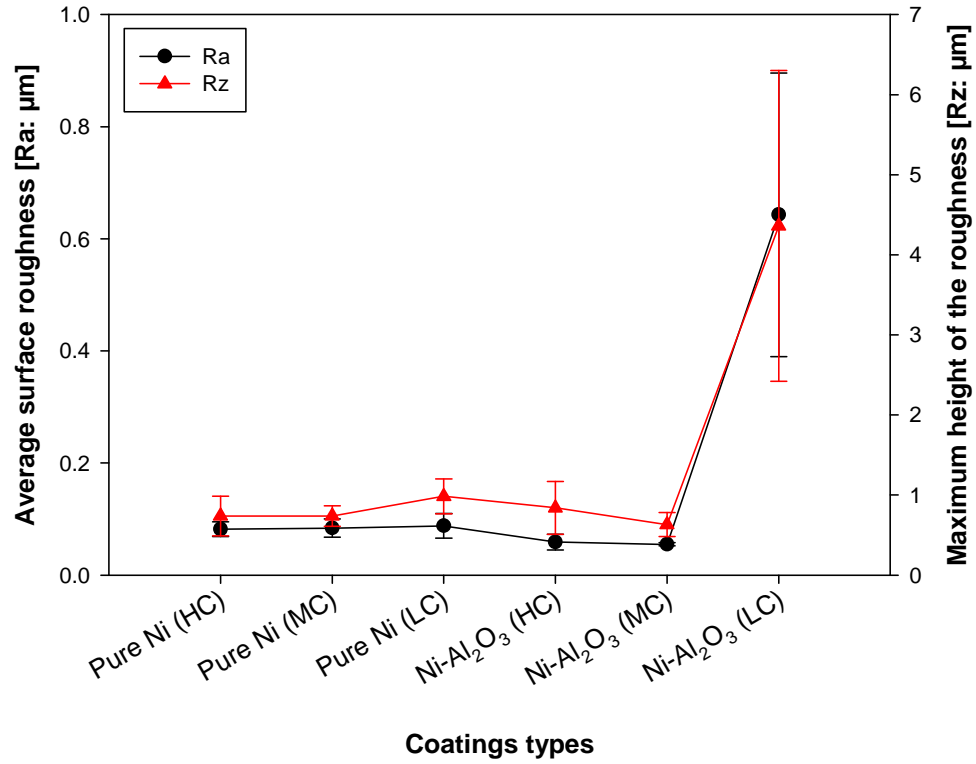


Figure 28 The effect of ionic concentration of solution on surface roughness of different electrodeposited coatings (Bajwa, R. S. et al., 2015a).

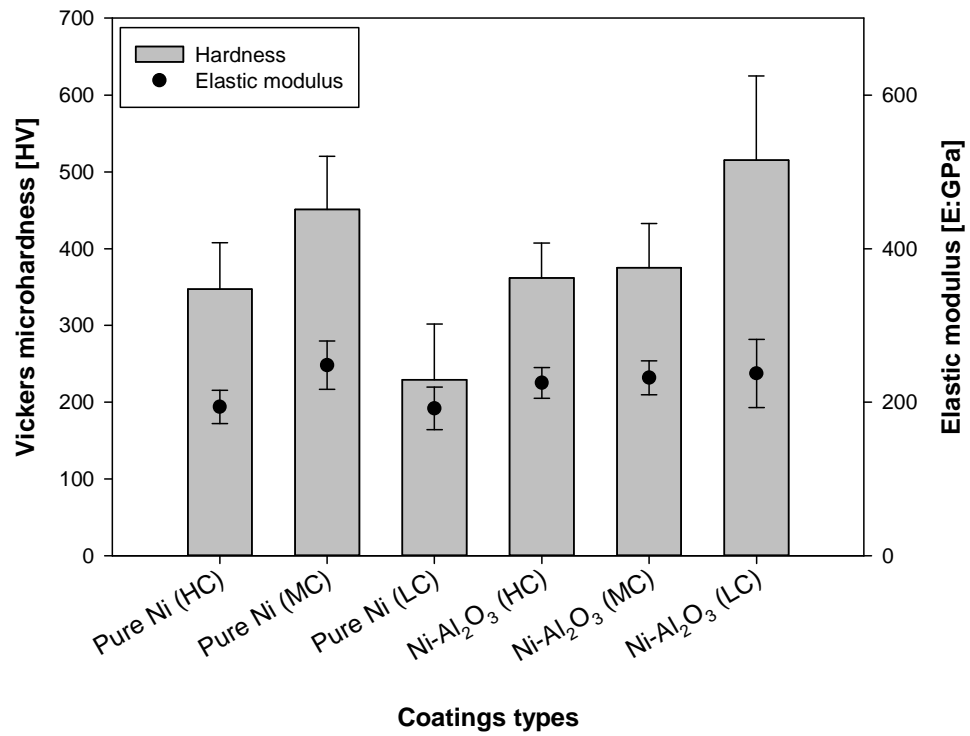


Figure 29 The variation of mechanical properties for coatings electrodeposited from different ionic strength of electrolyte (Bajwa, R. S. et al., 2015a).

Chapter 5. Performance of Ni and Ni-Al₂O₃ composite coatings produced by variable bath ionic strength

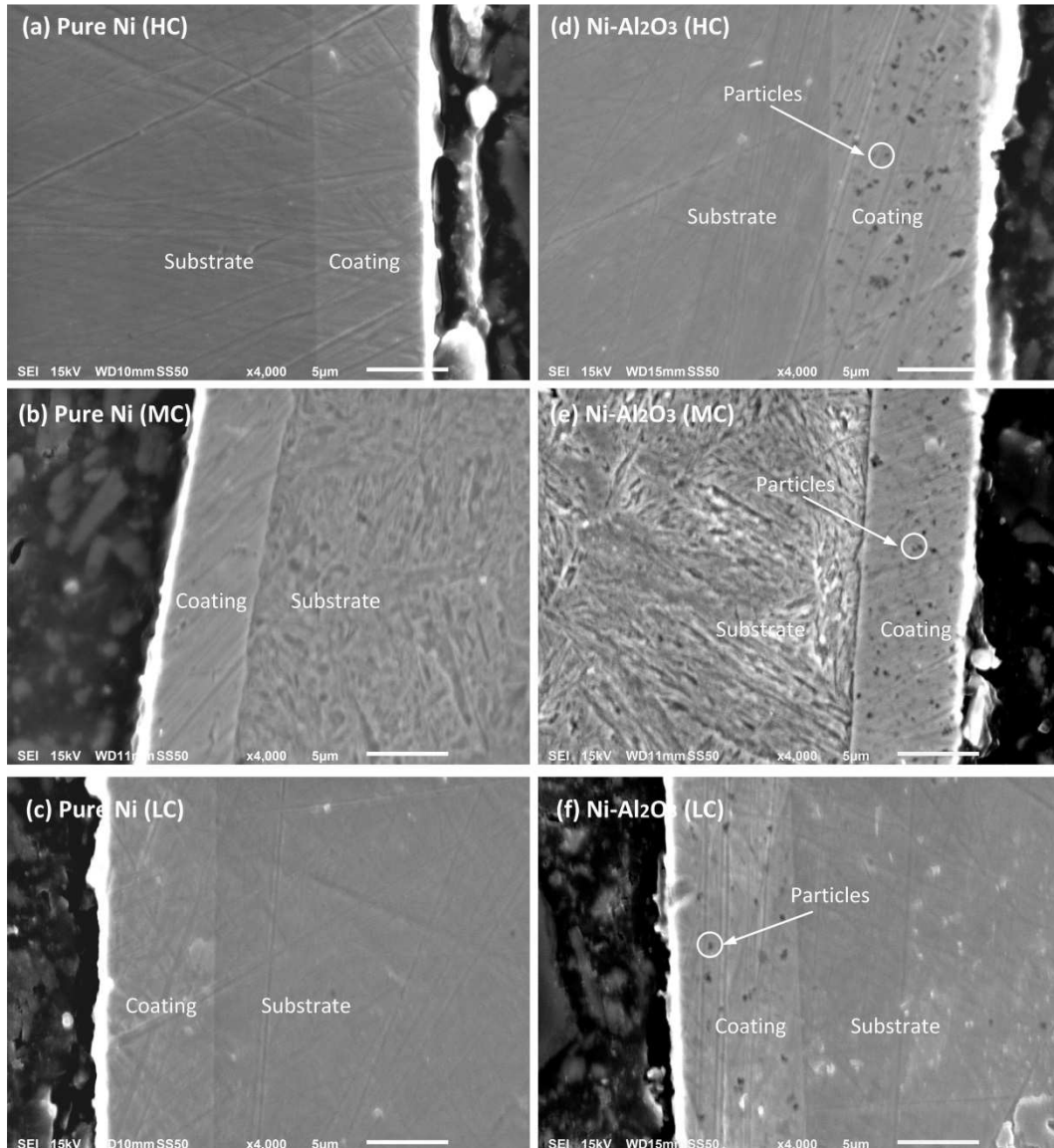


Figure 30 The demonstration of incorporated particle distributions in coatings electrodeposited from different ionic strength of electrolyte (Bajwa, R. S. et al., 2015a).

The typical globular form microstructure is visible under SEM for nickel and composite coatings produced by using electrodeposition method. These surface morphologies are in agreement with the previous experimental results about nickel based electroplated coatings (Jegan, A. and Venkatesan, R., 2013; Jung, A. et al., 2009; Thiemig, D. and Bund, A., 2009; Thiemig, D. et al., 2007). In comparison to Ni deposit the co-deposits display relatively more compact microstructure. This is because of incorporation of particles

which are contributing to cathodic polarization mechanism. The distribution of reinforced nanoparticles within the nickel matrix subject to different electroplating solutions can be seen from the cross-sectional images as shown in Figure 30. There is not considerable influence of depositing solution's ionic concentration over nanoparticles distribution and uniformly distributed in the matrix. However, in case of coating which are plated from B_{lc} solution slightly differ in terms of relatively lower content of agglomerated particle. Possibility, this behaviour also contributed to the maximum value of hardness of Ni-Al₂O₃ (B_{lc}) composite coating.

5.2. Tribological and corrosion results

This is well established that the wear properties of the coatings enhanced with the reinforcement of nano-sized particles as reported by numerous scholars and in agreement with the current study as shown in Figure 31 (Borkar, T. and Harimkar, S. P., 2011; Wang, S.-C. and Wei, W.-C. J., 2003; Wielage, B. et al., 2008). When comparing the wear rate of pure Ni coatings, the wear rate of coating deposit from B_{mc} reduced half of B_{lc} type and 25 % than B_{hc} type coatings. The maximum hardness value and bigger plasticity index of B_{mc} type coating can be attributed to the enhanced wear resistance property (Wang, Q. et al., 2013). When comparing the wear rate of composite coatings, the wear rate of coating deposited from B_{hc} and B_{lc} type solutions show similar wear property as shown in Figure 31. Whereas, the wear rate of B_{mc} type coating is almost double than that of B_{hc} and B_{lc} type coatings. Therefore, in order to achieve better wear resistance performance in pure nickel coating the B_{mc} is a favourable candidate. For composite coatings, both B_{hc} and B_{lc} are favourable candidates to get better wear resistance results.

As shown in Figure 31, the strengthening influence of reinforced nano-sized particles has also contributed to reduce the mean-steady friction coefficient values as compared to pure nickel coatings. Previously, it was found that increasing percentage of particle to composite significantly decrease the coefficient of friction (Borkar, T. and Harimkar, S. P., 2011; Fan, H., 2010). Nevertheless, there is no significant effect of depositing solution's ionic

Chapter 5. Performance of Ni and Ni-Al₂O₃ composite coatings produced by variable bath ionic strength

concentration on changing the coefficient of friction value in both nickel and nickel composite coatings is observed here.

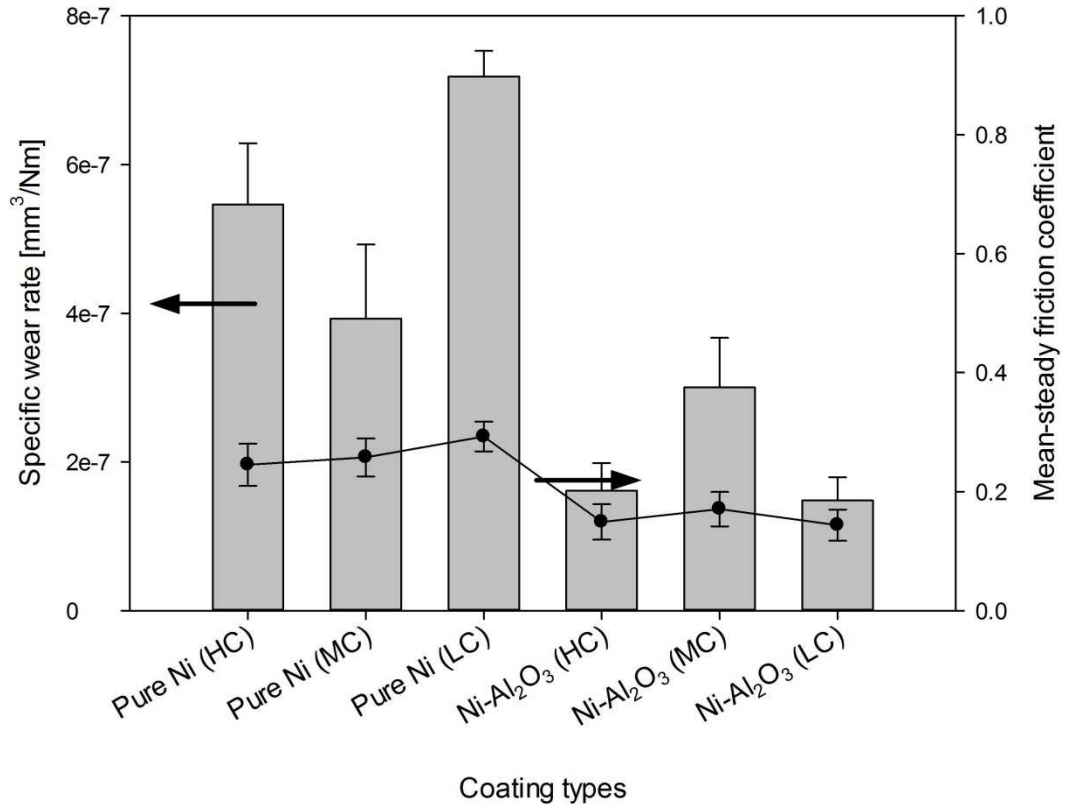


Figure 31 The variations of wear resistance and mean-steady friction coefficient properties for coatings electrodeposited from different ionic concentration of solution (Bajwa, R. S. et al., 2015a).

The corrosion resistance of the electrodeposited coating subject to different ionic strength calculated from potentiodynamic polarization curves. The experimental results for electrochemical corrosion behaviour are shown in Figure 32 in terms of potentiodynamic polarization curves. Overall, with all forms of solution the nanocomposite show improvement in the corrosion resistance when compared to pure Ni deposit. Similar effect of reinforcement of nano sized relating corrosion resistance was reported in the literature (Feng, Q. et al., 2008). When comparing the influence of ionic power of electrodepositing solution, the B_{mc} show the maximum corrosion resistance

Chapter 5. Performance of Ni and Ni-Al₂O₃ composite coatings produced by variable bath ionic strength

potential in pure nickel as well as in nanocomposite coating. When considering performance of these coating both in terms of wear and corrosion properties, the favourable electrolyte is B_{mc}. Nevertheless, this conclusion is applicable only for the electrodeposited pure nickel without nanoparticles into the matrix. In case of nickel alumina nanocomposite coating the favourable solution is B_{mc} for corrosion resistance and B_{hc} and B_{lc} solutions are suitable for better wear resistance properties.

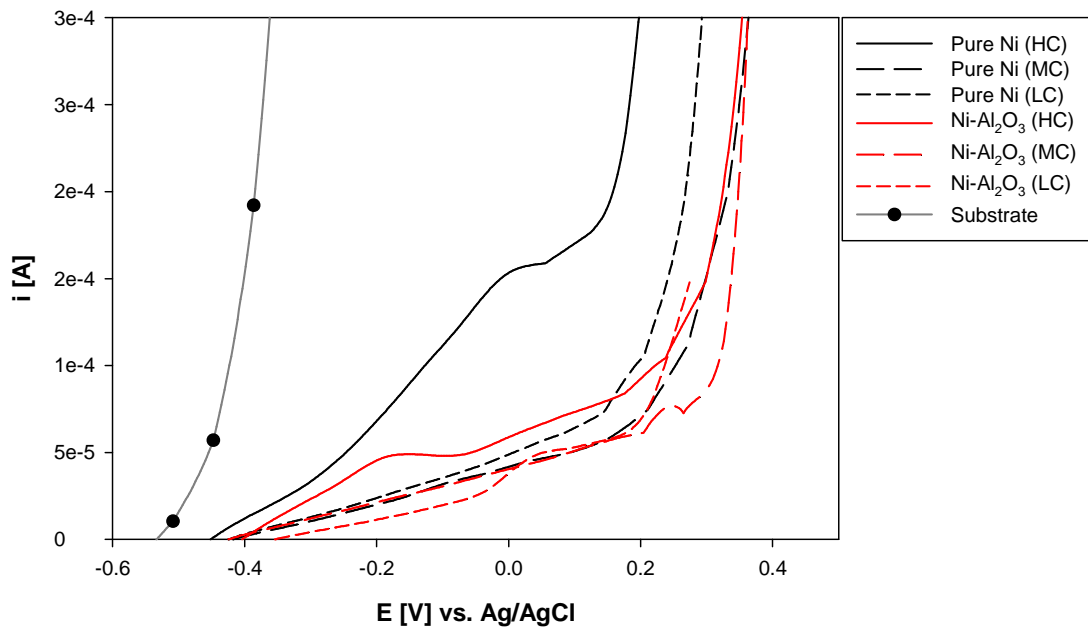


Figure 32 Corrosion resistance behaviour of coatings electrodeposited from different ionic concentrations of solution (Bajwa, R. S. et al., 2015a).

On the other hand, the corrosion resistance of B_{lc} type coating can be further enhanced by introducing surface polishing to reduce the surface roughness. This may be the peak valleys of surface roughness can also cause for rapid diffusion of harsh electrolyte on the way to the substrate to boost up the pitting corrosion failure.

5.3. Adhesion and wettability results

The adhesion of the coating to the substrate is an essential factor before taking into account for applications. For that reason the adhesion of newly developed coating is evaluated and compared with the required adhesion force of 30 N for wide ranging industrial applications. The adhesion strength result in terms of critical load values (L_c) is shown in Figure 33. The newly developed coatings subject to different plating solutions confirmed the adhesion force above the necessary value for industrial applications with exception of pure nickel (B_{hc}). When comparing pure nickel coatings, the Ni (B_{mc}) display the best adhesion force of 50 N followed by Ni (B_{lc}) with a value of 44 N and Ni (B_{hc}) with a minimum value of 20 N. When comparing nanocomposite coatings, all types of coatings exhibit the relatively higher adhesion than pure nickel with values; 60 N/(B_{hc}), 76 N/(B_{mc}) and 80 N/(B_{lc}). The use of favourable intermediate coating can further enhance the current adhesion results of these coatings. The surface failure mechanisms of worn tracks for all coatings are studied by using optical microscopy and micrograph images are shown in Figure 34. These images are taken at three different points of worn tracks that are starting, central and ending areas of the wear scar. Regardless of depositing solution ionic strength of pure nickel coatings, there is a visible accumulation of coated material at the ending point of the scratch. Additionally, severe delamination is visible in Ni (B_{hc}) type coatings. On the other hand, in nanocomposite coatings regardless of solution ionic strength coated materials is not accumulated at the wear scar's ending point. As discussed above in section (4.3) such transfer of materials related to the coating and counter body adhesion/wettability properties.

The contact angle measurement and surface energy results subject to different ionic concentration of the electroplated coating are shown Figure 35. The surface free energy properties of coatings are presented in terms of polar and dispersive parts. Regardless of depositing solution ionic strength all the coatings are mainly consisted of dispersive part of surface energy indicating covalent bonding between surface and liquids. The dispersive and polar component of coatings produced from electrodeposition technique is ranging from 29–39 mN/m and from 2–18 mN/m respectively. There were not

Chapter 5. Performance of Ni and Ni-Al₂O₃ composite coatings produced by variable bath ionic strength

considerable influences introduced by solution ionic strength in both pure nickel and nanocomposite coatings. However, the surface energy value of nickel alumina is reduced significantly. Consequently, the water contact angle of nickel alumina is considerably higher than the rest of the coat. Perhaps, the higher contact angle of Ni-Al₂O₃ (B_{mc}) has also contributed to increased wear rate.

Wetting envelopes for pure nickel and nickel nanocomposite coatings electrodeposited from variant solution are presented in Figure 36. These wetting envelopes are helpful in practical application for deciding appropriate lubricant for specific combinations of materials and area of application.

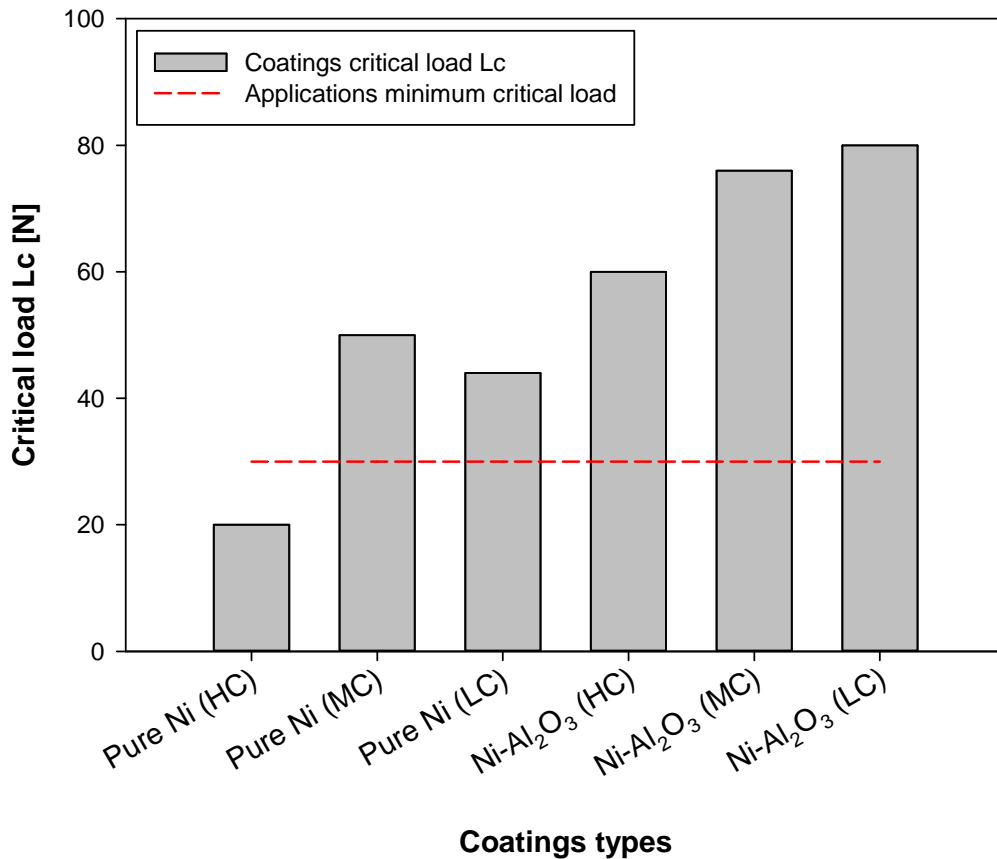


Figure 33 The variation of critical load values for coatings electrodeposited from different ionic concentrations of solution (Bajwa, R. S. et al., 2015a).

Chapter 5. Performance of Ni and Ni-Al₂O₃ composite coatings produced by variable bath ionic strength

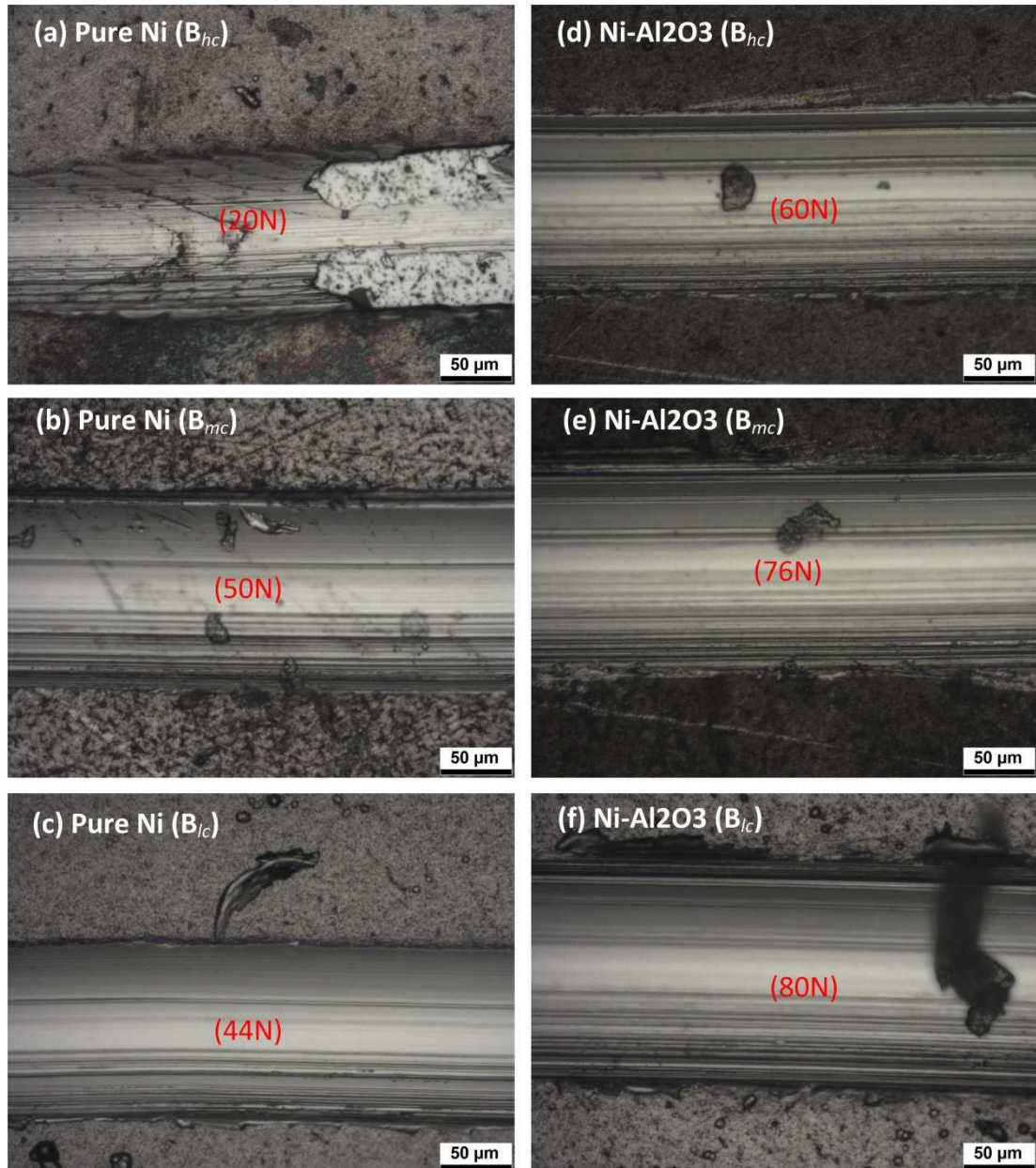


Figure 34 Kinds of electrodeposited coating failure subject to various ionic concentrations after scratch test according to DIN EN 1071-3.

Chapter 5. Performance of Ni and Ni-Al₂O₃ composite coatings produced by variable bath ionic strength

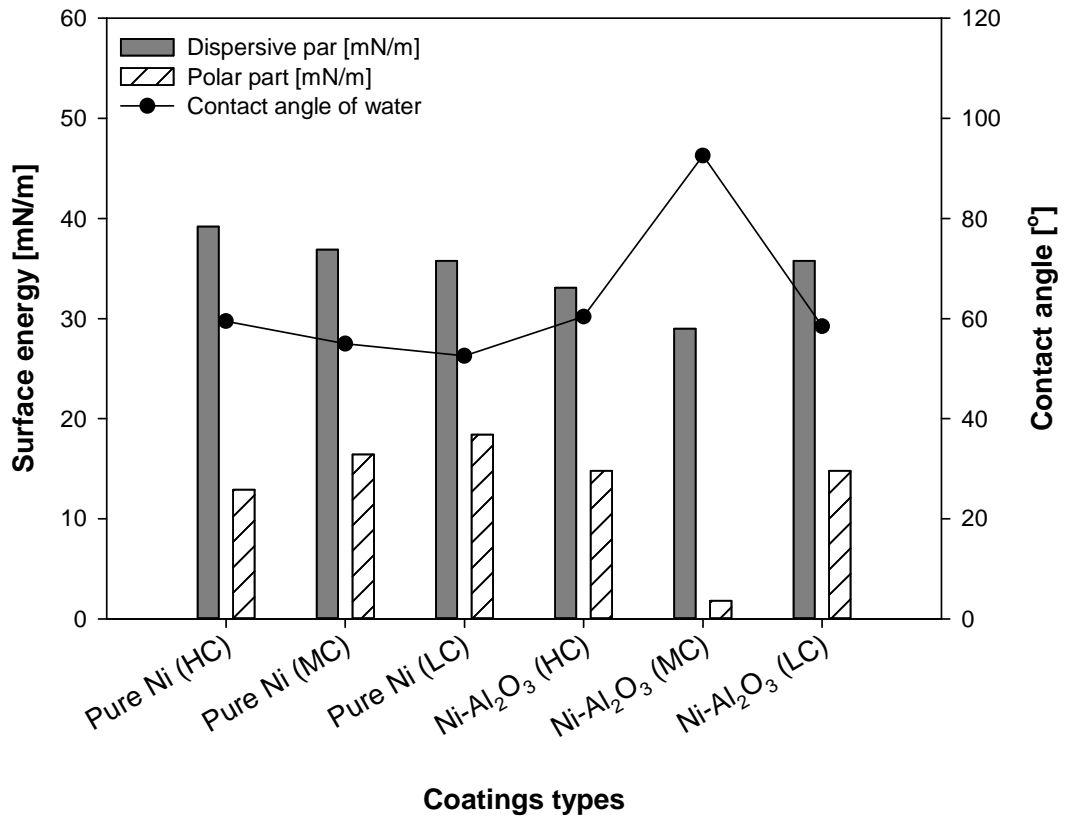
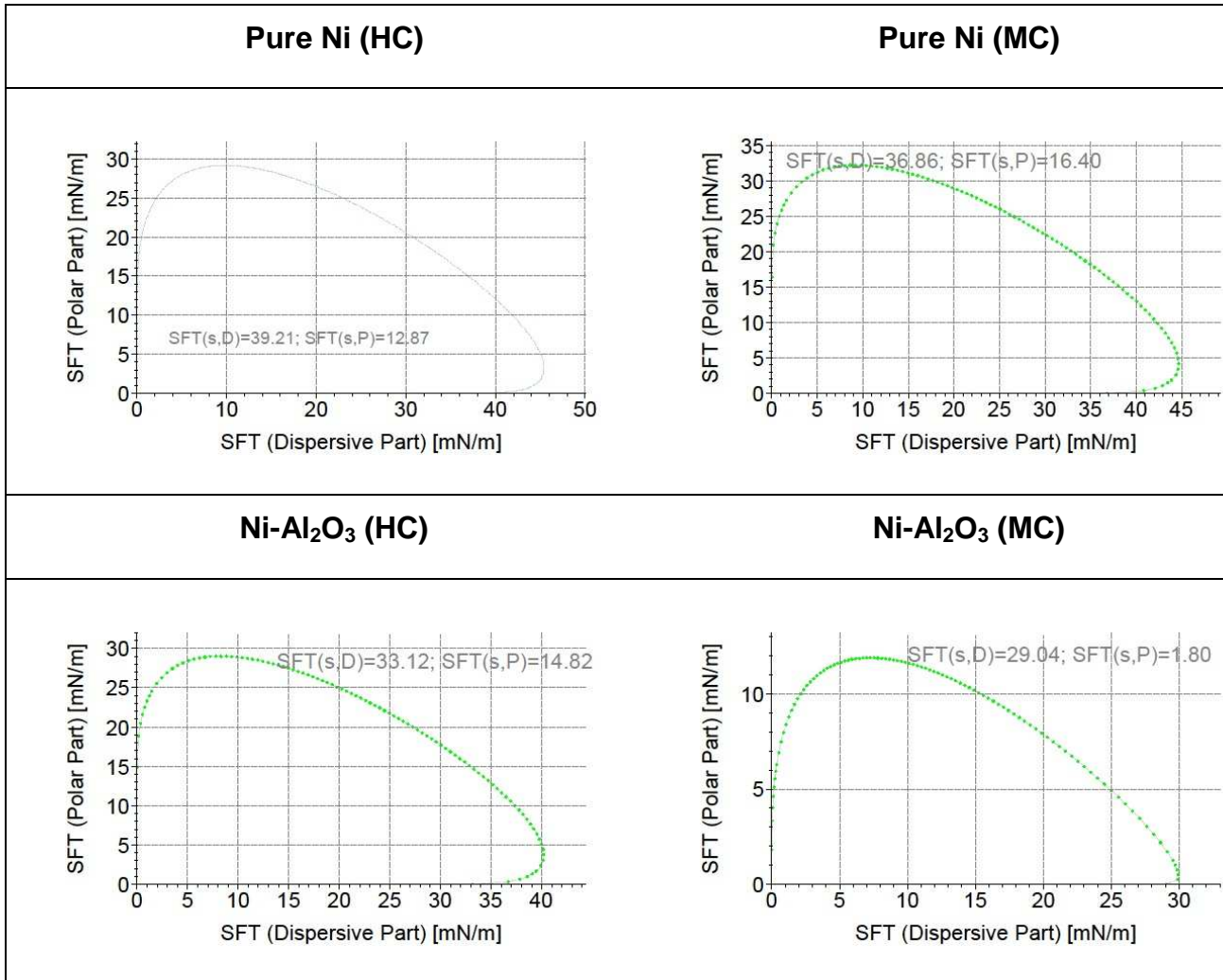


Figure 35 The variations of water contact angle and surface energy for coatings electroplated from different ionic concentrations of solution (Bajwa, R. S. et al., 2015a).

Chapter 5. Performance of Ni and Ni-Al₂O₃ composite coatings produced by variable bath ionic strength

Figure 36 Wetting envelopes for electrodeposited coatings produced from the different ionic strength of plating baths.



5.4. Conclusions

The aim of this study was to investigate the influences of ionic concentration in the electroplating solution on the wear, corrosion, adhesion and wettability properties of manufactured coatings. The surface morphology of electrodeposited Ni and Ni-alumina composite coatings was not much influenced by ionic strength. However, coatings developed by using B_{lc} solution contributed to the agglomeration of Ni particles on the surface, resulting in increased surface roughness. The maximum hardness value of 515HV was achieved for Ni-Al₂O₃ composite coatings by using electrolyte of lower concentration (B_{lc}). It was concluded that the adsorption of nano-sized particles on the substrate surface contributed to the cathodic polarization phenomenon and resulting into compact morphology of the deposited coating. Regarding nanoparticles distribution in the nickel matrix, it was found that the B_{lc} type electrolyte can present the best homogenous distribution. The wear rate of Ni coatings (B_{mc}) reduced almost 30% and 50% than that of B_{hc} and B_{lc} type Ni coatings. Whereas, in composite coatings the wear rate of B_{hc} and B_{lc} was nearly similar and 50% less than B_{mc} type composite. Likewise, a significant reduction in mean friction coefficient from (0.12-0.17) to (0.27-0.31) was observed in composite coatings than pure pure nickel coating, respectively.

Corrosion tests showed that the maximum corrosion resistance potential was always achieved with B_{mc} type electrolyte, both in pure Ni and Ni-alumina composite coatings. The cross-sectional examinations showed that all the coatings are well adhered to the substrate without an interface delamination or cracks. The effect of ionic concentration on the surface wettability of electrodeposited was found insignificant. However, the Ni-alumina composite deposited from B_{mc} type electrolyte showed the maximum contact angle of 92°. Whereas, for the rest of the coatings the contact angle was ranging between 52-60°. It was believed the high contact angle of Ni-Al₂O₃ (B_{mc}) resulting into lower wettability and consequently the higher wear rate.

Chapter 6. Conclusions and future work

6.1. Conclusions

In this research work, an extensive tribological and corrosion study has been carried out to evaluate the feasibility of newly developed Ni-based coatings for bearing applications. The tribological performance of electrodeposited coating was investigated for the first time subject to water-lubrication conditions. The main conclusions of current work can be summarized as below.

Electrodeposition of high quality Ni-based nanocomposite coatings:

The surface morphology and microstructure studies of newly developed coatings indicated the effect of embedded nano-sized particles on the surface finishing, crystal orientation and mechanical properties. The resulting coating exhibits, increased hardness, surface evenness, refined grain structure and well adhered to the substrate. Regarding the influence of various ionic concentrations on the microstructure morphology of Ni and nickel composite of alumina nanoparticles, no significant influence of B_{hc} and B_{mc} was seen. Whereas, the B_{lc} type chemical solution contributed to increased grain size and creation of spherical agglomerated particles at the surface of coatings.

Tribological properties of Ni-based nanocomposite coatings:

The nickel composite of silicon carbide showed the minimum wear rate than a composite of alumina and zirconium nanoparticles. In comparison to pure Ni the wear rate reduced almost 30% with the addition of silicon carbide nanoparticles. Regarding the influence of ionic strength, the wear rate of Ni coatings deposited from B_{mc} type solution reduced 50% as compared to B_{lc} type and 25 % than B_{hc} type coatings. In composite coatings, the B_{hc} and B_{lc} type composite coatings showed the best wear rate as compared to B_{mc} type composite coatings. Therefore, in order to achieve better wear resistance performance in pure nickel coating the B_{mc} is favourable candidate. For composite coatings, both B_{hc} and B_{lc} are favourable candidates to get better

wear resistance results. The reinforcement of nanoparticles, not only resulted in significant improvement in wear resistance, but also in the reduction of friction coefficient of Ni-based composite coatings. However, no significant effect of depositing solution's ionic concentration on changing the coefficient of friction value was observed.

Corrosion resistance properties of Ni-based nanocomposite coatings:

The nickel composite of alumina nanoparticles showed the maximum corrosion resistance than a composite of silicon carbide and zirconium nanoparticles. When compared to pure Ni the corrosion resistant potential of Ni alumina composite increased from about 0.22 to 0.37 V vs Ag/AgCl. When comparing the influence of ionic power of electrodepositing solution, the Bmc has shown maximum corrosion resistance potential in pure nickel as well as in nanocomposite coating.

Adhesion and wettability properties of Ni-based nanocomposite coatings:

In the scratch test the nickel composite of alumina showed the maximum adhesion force of 79N followed by pure nickel (50), Ni-SiC (40) and nickel zirconium with a minimum value of 28N. Regarding the influence of various ionic concentrations on adhesion, when comparing within pure nickel coatings, the Ni (Bmc) presented the best adhesion force of 50N followed by Ni (Blc) with a value of 44N and Ni (Bhc) with a minimum value of 20N. When comparing nanocomposite coatings, all types of coatings exhibit the relatively higher adhesion than pure nickel with values; 60N/(Bhc), 76N/(Bmc) and 80N/(Blc).

The nickel composite of alumina nanoparticles showed minimum surface energy. Consequently, the water contact angle of nickel alumina is considerably higher than the rest of the coatings. The dispersive and polar component of all coatings was ranging from 29–36 mN/m and from 2–16 mN/m respectively. Regardless of depositing solution ionic strength all the coatings are mainly consisted of dispersive part of surface energy indicating covalent bonding between surface and liquids. The dispersive and polar component of coatings produced from electrodeposition technique ranging from 29–39 mN/m and from 2–18 mN/m respectively. There were not

considerable influences introduced by solution ionic strength on wettability behaviour both in pure nickel and nanocomposite coatings.

6.2. Recommendations for future work

The goal of current industrial project has been to investigate and understand the potential of the electrodeposited Ni-based composite coatings incorporating nanoparticles to improve the tribological performance of water-lubricated tribological systems. Therefore, a number of experimental investigations conducted to evaluate the industrial performance of the newly developed nanocomposite coating. These performance tests included, wear resistance, corrosion resistance, adhesion strength and wettability behaviour studies. Being an applied research numerous appealing questions raised during this research which needs to be investigated in future work.

A simulation based model should be designed to predict the optimal coating for water lubricated tribological systems. The experimental data in current research project are helpful for designing such model. For example, as discussed in chapter 4, the nickel composite of SiC nanoparticles is the best candidate for wear resistance and the nickel composite of alumina nanoparticles should be a better choice where more corrosion resistance performance of coatings required. In chapter 5: regarding the influence of various ionic concentrations in electroplating solutions, the B_{mc} type solution provided the best corrosion resistance behaviour for both Ni and Ni based co-deposits with reinforced particles. However, in case of wear rate performance the B_{mc} is suitable for pure Ni coating and for co-deposits coating the B_{hc} and B_{lc} type electrolytes are favourable candidates. Similarly, experimental findings concerning effect of other electroplating parameters on adhesion, wettability and tribological performance of coating can be incorporated into to the simulation model in order to achieve the optimal coating for specific industrial applications.

The modified rule of mixture has been widely used for prediction of hardness, modulus or poisson's ratio value of nanocomposite coatings (Kuo, M. et al., 2005). The modified rule of mixture is preferred over previous rule of mixture model because it include additional factor known as strengthening

efficiency factor β . The strengthening efficiency factor β depends upon the aspect ratio and distribution of the fillers in the matrix which significantly reduced the deviation between the experimental and theoretical curves. The strengthening efficiency factor β within the context of tribological properties of nanocomposite can be an effective tool for prediction of wear or corrosion properties as well.

In present work all tribological tests were conducted under distilled water lubrication. However, in a real application the sand particles and various salinities of marine environment may alter the tribological performance of newly developed coatings. Therefore, the influences of real sea water and sand particles on the tribological behaviour of newly developed coatings should be investigated in future work.

6.3. Reference

- Aal, A. A., Bahgat, M., and Radwan, M., 2006. Nanostructured ni–al composite coatings. *Surface and Coatings Technology*, 201 (6), 2910-2918.
- Abbott, A., 2011. *The electrodeposition of composite materials using deep eutectic solvents*. Thesis.
- Abbott, A. P., Boothby, D., Capper, G., Davies, D. L., and Rasheed, R. K., 2004. Deep eutectic solvents formed between choline chloride and carboxylic acids: Versatile alternatives to ionic liquids. *Journal of the American Chemical Society*, 126 (29), 9142-9147.
- Abbott, A. P., Dalrymple, I., and Endres, F., 2008. Why use ionic liquids for electrodeposition? *Electrodeposition from Ionic Liquids*, 1.
- Abbott, A. P., El Ttaib, K., Frisch, G., Ryder, K. S., and Weston, D., 2012. The electrodeposition of silver composites using deep eutectic solvents. *Physical Chemistry Chemical Physics*, 14 (7), 2443-2449.
- Agarwal, M., Kumar, V., Malladi, S. R. K., Balasubramaniam, R., and Balani, K., 2010. Effect of current density on the pulsed co-electrodeposition of nanocrystalline nickel-copper alloys. *JOM*, 62 (6), 88-92.
- Argañaraz, M., Ribotta, S., Folquer, M., Gassa, L., Benitez, G., Vela, M., and Salvarezza, R., 2011. Ni–W coatings electrodeposited on carbon steel: Chemical composition, mechanical properties and corrosion resistance. *Electrochimica Acta*, 56 (17), 5898-5903.
- Armand, M., Endres, F., Macfarlane, D. R., Ohno, H., and Scrosati, B., 2009. Ionic-liquid materials for the electrochemical challenges of the future. *Nature materials*, 8 (8), 621-629.
- Aruna, S., Bindu, C., Ezhil Selvi, V., William Grips, V., and Rajam, K., 2006. Synthesis and properties of electrodeposited Ni/Ceria nanocomposite coatings. *Surface and Coatings Technology*, 200 (24), 6871-6880.
- Bajwa, R. S., Khan, Z., Bakolas, V., and Braun, W., 2015a. Effect of bath ionic strength on adhesion and tribological properties of pure nickel

and Ni-based nanocomposite coatings. *Journal of Adhesion Science and Technology*, 1-13.

- Bajwa, R. S., Khan, Z., Bakolas, V., and Braun, W., 2015b. Water-lubricated Ni-based composite (Ni– Al₂O₃, Ni–SiC and Ni–ZrO₂) thin film coatings for industrial applications. *Acta Metallurgica Sinica (English Letters)*, 1-9.
- Balasubramanian, A., Srikumar, D., Raja, G., Saravanan, G., and Mohan, S., 2009. Effect of pulse parameter on pulsed electrodeposition of copper on stainless steel. *Surface Engineering*, 25 (5), 389-392.
- Barcena, J., Maudes, J., Coletto, J., Baldonado, J. L., and Gomez De Salazar, J. M., 2008. Microstructural study of vapour grown carbon nanofibre/copper composites. *Composites Science and Technology*, 68 (6), 1384-1391.
- Beattie, S., and Dahn, J., 2003. Single bath, pulsed electrodeposition of copper-tin alloy negative electrodes for lithium-ion batteries. *Journal of The Electrochemical Society*, 150 (7), A894-A898.
- Bełtowska-Lehman, E., Goral, A., and Indyka, P., 2011. Electrodeposition and characterization of Ni/Al₂O₃ nanocomposite coatings. *Archives of Metallurgy and Materials*, 56 (4), 919-931.
- Beltowska-Lehman, E., Indyka, P., Bigos, A., Szczerba, M., and Kot, M., 2015. Ni–W/ZrO₂ nanocomposites obtained by ultrasonic DC electrodeposition. *Materials & design*, 80, 1-11.
- Benea, L., 2009. Electrodeposition and tribocorrosion behaviour of ZrO₂–Ni composite coatings. *Journal of applied electrochemistry*, 39 (10), 1671-1681.
- Benea, L., Başa, S.-B., Dănăilă, E., Caron, N., Raquet, O., Ponthiaux, P., and Celis, J.-P., 2015. Fretting and wear behaviors of Ni/nano-WC composite coatings in dry and wet conditions. *Materials & design*, 65, 550-558.

- Bonhote, P., Dias, A.-P., Papageorgiou, N., Kalyanasundaram, K., and Grätzel, M., 1996. Hydrophobic, highly conductive ambient-temperature molten salts. *Inorganic Chemistry*, 35 (5), 1168-1178.
- Borkar, T., and Harimkar, S., 2011. Microstructure and wear behaviour of pulse electrodeposited Ni-CNT composite coatings. *Surface Engineering*, 27 (7), 524-530.
- Borkar, T., and Harimkar, S. P., 2011. Effect of electrodeposition conditions and reinforcement content on microstructure and tribological properties of nickel composite coatings. *Surface and Coatings Technology*, 205 (17), 4124-4134.
- Burwell, J. T., 1957. Survey of possible wear mechanisms. *Wear*, 1 (2), 119-141.
- Chandrasekar, M., and Pushpavanam, M., 2008. Pulse and pulse reverse plating—conceptual, advantages and applications. *Electrochimica Acta*, 53 (8), 3313-3322.
- Changdong, G., Yihui, Y., Xuli, W., and Jiangping, T., 2012. Electrochemical preparation and characterization of Ni-PTFE composite coatings from a non-aqueous solution without additives.
- Chen, L., Wang, L., Zeng, Z., and Xu, T., 2006. Influence of pulse frequency on the microstructure and wear resistance of electrodeposited Ni-Al₂O₃ composite coatings. *Surface and Coatings Technology*, 201 (3), 599-605.
- Ciubotariu, A. C., Benea, L., Lakatos-Varsanyi, M., and Dragan, V., 2008. Electrochemical impedance spectroscopy and corrosion behaviour of Al₂O₃-Ni nano composite coatings. *Electrochimica Acta*, 53 (13), 4557-4563.
- Cui, G., Bi, Q., Zhu, S., Fu, L., Yang, J., Qiao, Z., and Liu, W., 2013. Synergistic effect of alumina and graphite on bronze matrix composites: Tribological behaviors in sea water. *Wear*, 303 (1), 216-224.

- Czichos, H., and Habig, K.-H., 2010. Tribologie-handbuch. *Tribologie-Handbuch: Tribometrie, Tribomaterialien, Tribotechnik*, ISBN 978-3-8348-0017-6. Vieweg+ Teubner Verlag| GWV Fachverlage GmbH, Wiesbaden, 2010, 1.
- Denny, T., and Andreas, B., 2008. Characterization of electrodeposited Ni–TiO₂ nanocomposite coatings. *Surface & Coatings Technology*, 202.
- El Abedin, S. Z., Pölleth, M., Meiss, S., Janek, J., and Endres, F., 2007. Ionic liquids as green electrolytes for the electrodeposition of nanomaterials. *Green Chemistry*, 9 (6), 549-553.
- Fan, H., 2010. *Electroplating of compound Ni–SiC coatings and improvement of wear resistance*. Paper presented at the Key Engineering Materials.
- Feng, Q., Li, T., Teng, H., Zhang, X., Zhang, Y., Liu, C., and Jin, J., 2008. Investigation on the corrosion and oxidation resistance of Ni–Al₂O₃ nano-composite coatings prepared by sediment co-deposition. *Surface and Coatings Technology*, 202 (17), 4137-4144.
- Fomin, A., 2010. *Studies on the electrodeposition of aluminium from different air and water stable ionic liquids*. Thesis; University of TU Clausthal, Germany.
- Golchin, A., Simmons, G., Glavatskih, S., and Prakash, B., 2013. Tribological behaviour of polymeric materials in water-lubricated contacts. *Proceedings of the Institution of Mechanical Engineers, Part J: Journal of Engineering Tribology*, DOI: 10.1177/1350650113476441.
- Gomes, A., Pereira, I., Fernández, B., and Pereiro, R., 2011. Electrodeposition of metal matrix nanocomposites: Improvement of the chemical characterization techniques. *Advances in Nanocomposites-Synthesis, Characterization and Industrial Applications*, Boreddy Reddy (Ed.), InTech, 503.
- Grimmett, D. L., Schwartz, M., and Nobe, K., 1993. A comparison of DC and pulsed Fe-Ni alloy deposits. *Journal of The Electrochemical Society*, 140 (4), 973-978.

- Grischke, M., Hieke, A., Morgenweck, F., and Dimigen, H., 1998. Variation of the wettability of DLC-coatings by network modification using silicon and oxygen. *Diamond and Related Materials*, 7 (2), 454-458.
- Gu, C., and Tu, J., 2011. One-step fabrication of nanostructured ni film with lotus effect from deep eutectic solvent. *Langmuir*, 27 (16), 10132-10140.
- Gu, C., You, Y., Wang, X., and Tu, J., 2012. Electrodeposition, structural, and corrosion properties of Cu films from a stable deep eutectics system with additive of ethylene diamine. *Surface and Coatings Technology*, 209 (25) Pages 117–123.
- Gül, H., Kılıç, F., Aslan, S., Alp, A., and Akbulut, H., 2009. Characteristics of electro-co-deposited Ni–Al₂O₃ nano-particle reinforced metal matrix composite (MMC) coatings. *Wear*, 267 (5), 976-990.
- Gül, H., Kılıç, F., Uysal, M., Aslan, S., Alp, A., and Akbulut, H., 2012. Effect of particle concentration on the structure and tribological properties of submicron particle sic reinforced Ni metal matrix composite (MMC) coatings produced by electrodeposition. *Applied Surface Science*, 258 (10), 4260-4267.
- Gül, H., Uysal, M., Akbulut, H., and Alp, A., 2014. Effect of PC electrodeposition on the structure and tribological behavior of Ni–Al₂O₃ nanocomposite coatings. *Surface and Coatings Technology*, 258, 1202-1211.
- Gyftou, P., Pavlatou, E., and Spyrellis, N., 2008. Effect of pulse electrodeposition parameters on the properties of Ni/Nano-SiC composites. *Applied Surface Science*, 254 (18), 5910-5916.
- Haerens, K., Matthijs, E., Chmielarz, A., and Van Der Bruggen, B., 2009. The use of ionic liquids based on choline chloride for metal deposition: A green alternative? *Journal of environmental management*, 90 (11), 3245.

- Hamrock, B. J., and Dowson, D., 1981. Ball bearing lubrication: Elastohydrodynamics of elliptical contacts. Publisher, Wiley-Interscience (New York), 1981. 409 p.
- Hamrock, B. J., Schmid, S. R., and Jacobson, B. O., 2004. *Fundamentals of fluid film lubrication*. CRC press.
- Haq, I. U., Akhtar, K., Khan, T. I., and Ali Shah, A., 2013. Electrodeposition of Ni-Fe₂O₃ nanocomposite coating on steel. *Surface and Coatings Technology*, 235, 691-698.
- Horio, K., Kasai, T., and Kobayashi, A., 1991. A study on laser-enhanced plating. *CIRP Annals-Manufacturing Technology*, 40 (1), 195-198.
- Hou, K.-H., Chang, Y.-F., Chang, S.-M., and Chang, C.-H., 2010. The heat treatment effect on the structure and mechanical properties of electrodeposited nano grain size Ni-W alloy coatings. *Thin Solid Films*, 518 (24), 7535-7540.
- Hou, K.-H., and Chen, Y.-C., 2011. Preparation and wear resistance of pulse electrodeposited Ni-W/Al₂O₃ composite coatings. *Applied Surface Science*, 257 (15), 6340-6346.
- Hou, K.-H., Hwu, W.-H., Ke, S.-T., and Ger, M.-D., 2006. Ni-P-SiC composite produced by pulse and direct current plating. *Materials chemistry and physics*, 100 (1), 54-59.
- Hou, K.-H., Jeng, M.-C., and Ger, M.-D., 2007. A study on the wear resistance characteristics of pulse electroforming Ni-P alloy coatings as plated. *Wear*, 262 (7), 833-844.
- Hou, K., Ger, M., Wang, L., and Ke, S., 2002. The wear behaviour of electro-codeposited Ni-SiC composites. *Wear*, 253 (9), 994-1003.
- Hou, K. H., Jeng, M. C., Shen, Y. K., and Ger, M. D., 2008. The wear behavior of pulse current electroforming Ni-P-SiC composite coatings. *Key Engineering Materials*, 364, 358-363.
- Hovestad, A., and Janssen, L., 1995. Electrochemical codeposition of inert particles in a metallic matrix. *Journal of applied electrochemistry*, 25 (6), 519-527.

- Huang, S., Hu, Y., and Pan, W., 2011. Relationship between the structure and hydrophobic performance of Ni–TiO₂ nanocomposite coatings by electrodeposition. *Surface and Coatings Technology*, 205 (13), 3872-3876.
- Jegan, A., and Venkatesan, R., 2013. Characterization and optimization of pulse electrodeposition of Ni/Nano-Al₂O₃ composite coatings. *International Journal of Minerals, Metallurgy, and Materials*, 20 (5), 479-485.
- Jiang, J., Arnell, R., and Dixit, G., 2000. The influence of ball size on tribological behaviour of MoS₂ coating tested on a ball-on-disk wear rig. *Wear*, 243 (1), 1-5.
- Johnson, K., 1974. Contact mechanics. 1985. *Cam-bridge University Press, Cambridge*.
- Jung, A., Natter, H., Hempelmann, R., and Lach, E., 2009. Nanocrystalline alumina dispersed in nanocrystalline nickel: Enhanced mechanical properties. *Journal of materials science*, 44 (11), 2725-2735.
- Kanani, N., 2004. *Electroplating: Basic principles, processes and practice*. Elsevier Science.
- Kartal, M., Uysal, M., Gul, H., Alp, A., and Akbulut, H., 2015. Effect of surfactant concentration in the electrolyte on the tribological properties of nickel-tungsten carbide composite coatings produced by pulse electro co-deposition. *Applied Surface Science*.
- Kelly, J., Bradley, P., and Landolt, D., 2000. Additive effects during pulsed deposition of Cu-Co nanostructures. *Journal of The Electrochemical Society*, 147 (8), 2975-2980.
- Kelly, J., Cantoni, M., and Landolt, D., 2001. Three-dimensional structuring of electrodeposited Cu-Co multilayer alloys. *Journal of The Electrochemical Society*, 148 (9), C620-C626.
- Kelly, R. G., Scully, J. R., Shoesmith, D., and Buchheit, R. G., 2002. *Electrochemical techniques in corrosion science and engineering*. CRC Press.

- Khan, T. I., 2011. Tribological behavior of electrodeposited Ni–SnO₂ nanocomposite coatings on steel. *Surface and Coatings Technology*, 205 (8), 2871-2875.
- Khazrayie, M., and Aghdam, A., 2010. Si₃N₄/Ni nanocomposite formed by electroplating: Effect of average size of nanoparticulates. *Transactions of Nonferrous Metals Society of China*, 20 (6), 1017-1023.
- Kim, D.-W., and Kim, K.-W., 2012. Effects of sliding velocity and normal load on friction and wear characteristics of multi-layered diamond-like carbon (DLC) coating prepared by reactive sputtering. *Wear*.
- Kumar, K. A., Mohan, P., Kalaignan, G. P., and Muralidharan, V., 2012. Electrodeposition and characterization of Ni-ZrO₂ nanocomposites by direct and pulse current methods. *Journal of nanoscience and nanotechnology*, 12 (11), 8364-8371.
- Kuo, M., Tsai, C., Huang, J., and Chen, M., 2005. Peek composites reinforced by nano-sized SiO₂ and Al₂O₃ particulates. *Materials chemistry and physics*, 90 (1), 185-195.
- Lampke, T., Leopold, A., Dietrich, D., Alisch, G., and Wielage, B., 2006. Correlation between structure and corrosion behaviour of nickel dispersion coatings containing ceramic particles of different sizes. *Surface and Coatings Technology*, 201 (6), 3510-3517.
- Landolt, D., and Marlot, A., 2003. Microstructure and composition of pulse-plated metals and alloys. *Surface and Coatings Technology*, 169, 8-13.
- Langdon, T. G., 2009. Research on bulk nanostructured materials in ufa: Twenty years of scientific achievements. *Materials Science and Engineering: A*, 503 (1), 6-9.
- Lee, C., 2012. Wear and corrosion behavior of electrodeposited nickel-carbon nanotube composite coatings on Ti-6Al-4V alloy in hanks' solution. *Tribology International*.

- Leyland, A., and Matthews, A., 2000. On the significance of the H/E ratio in wear control: A nanocomposite coating approach to optimised tribological behaviour. *Wear*, 246 (1), 1-11.
- Lille, H., and Koo, J., 2005. Determination of the modulus of elasticity, poisson's ratio and the coefficient of thermal expansion of electrochemically metallized nickel coatings. *Materials Science*, 11 (4), 356-359.
- Liu, Y.-S., and Pan, G.-B., 2011. Ionic liquids for the future electrochemical applications. *Ionic liquids: Applications and perspectives*, 627-642.
- Liu, Z., Abedin, S., and Endres, F., 2012. Electrodeposition of zinc films from ionic liquids and ionic liquid/water mixtures. *Electrochimica Acta*.
- Liu, Z., Zheng, M., Hilty, R. D., and West, A. C., 2010. Effect of morphology and hydrogen evolution on porosity of electroplated cobalt hard gold. *Journal of The Electrochemical Society*, 157 (7), D411-D416.
- Liu, Z., Zheng, M., Hilty, R. D., and West, A. C., 2011. The effect of pulse reversal on morphology of cobalt hard gold. *Electrochimica Acta*, 56 (5), 2546-2551.
- Lou, H. H., and Huang, Y., 2005. *Encyclopedia of chemical processing*. Thesis. Taylor & Francis.
- Low, C., Wills, R., and Walsh, F., 2006. Electrodeposition of composite coatings containing nanoparticles in a metal deposit. *Surface and Coatings Technology*, 201 (1), 371-383.
- Lugscheider, E., and Bobzin, K., 2001. The influence on surface free energy of PVD-coatings. *Surface and Coatings Technology*, 142, 755-760.
- Marlot, A., Kern, P., and Landolt, D., 2002. Pulse plating of Ni–Mo alloys from Ni-rich electrolytes. *Electrochimica Acta*, 48 (1), 29-36.
- Mishra, R., Basu, B., and Balasubramaniam, R., 2004. Effect of grain size on the tribological behavior of nanocrystalline nickel. *Materials Science and Engineering: A*, 373 (1), 370-373.

- Mo, J., Zhu, M., Lei, B., Leng, Y., and Huang, N., 2007. Comparison of tribological behaviours of AlCrN and TiAlN coatings—deposited by physical vapor deposition. *Wear*, 263 (7), 1423-1429.
- Morgenstern, T., and Schultze, J., 1997. Laser deposition of metals and polymers in Si-microstructures. *Electrochimica Acta*, 42 (20), 3057-3064.
- Musiani, M., 2000. Electrodeposition of composites: An expanding subject in electrochemical materials science. *Electrochimica Acta*, 45 (20), 3397-3402.
- Nakahara, S., Okinaka, Y., Okinaka, Y., Sard, S. N. R., Leidheiser, H., and Ogburn, F., 1976. Properties of electrodeposits—their measurement and significance, electrochemical society (1975) ch. 3 j. *Electrochem. Soc*, 123, 1284.
- Nakanishi, T., Ozaki, M., Nam, H.-S., Yokoshima, T., and Osaka, T., 2001. Pulsed electrodeposition of nanocrystalline conife soft magnetic thin films. *Journal of The Electrochemical Society*, 148 (9), C627-C631.
- Navas, C., García, I., Ye, X., Damborenea, J. D., and Celis, J.-P., 2006. Role of contact frequency on the wear rate of steel in discontinuous sliding contact conditions. *Wear*, 260 (9), 1096-1103.
- Notter, I., and Gabe, D., 1992. Porosity of electrodeposited coatings: Its cause, nature, effect and management. *Corrosion Reviews*, 10 (3-4), 217-280.
- Ogihara, H., Safuan, M., and Saji, T., 2012. Effect of electrodeposition conditions on hardness of Ni-B/diamond composite films. *Surface and Coatings Technology*, 212 pages 180–184.
- Oloruntoba, D., Eghwubare, O., and Oluwole, O., 2010. Effect of some process variables on nickel electroplating of low carbon steel. *Leonardo Electronic Journal of Practices and Technologies*, A18, pages 079-094.
- Owens, D. K., and Wendt, R., 1969. Estimation of the surface free energy of polymers. *Journal of applied polymer science*, 13 (8), 1741-1747.

- Pondicherry, K. S., Grün, F., Gódor, I., Bertram, R., and Offenbecher, M., 2013. Applicability of ring-on-disc and pin-on-plate test methods for Cu–steel and Al–steel systems for large area conformal contacts. *Lubrication Science*, 25 (3), 231-247.
- Puippe, J. C., and Ibl, N., 1980. Influence of charge and discharge of electric double layer in pulse plating. *Journal of applied electrochemistry*, 10 (6), 775-784.
- Ramanauskas, R., Gudavičiūtė, L., Ščit, O., Bučinskienė, D., and Juškėnas, R., 2008. Pulse plating effect on composition and corrosion properties of zinc alloy coatings. *Transactions of the Institute of Metal Finishing*, 86 (2), 103-108.
- Ramesh, C., Adarsha, H., Pramod, S., and Khan, Z., 2013. Tribological characteristics of innovative Al6061–carbon fiber rod metal matrix composites. *Materials & design*, 50, 597-605.
- Saha, R., Haq, I., Khan, T., and Glenesk, L., 2010. Development of wear resistant nano dispersed composite coating by electrodeposition. *Key Engineering Materials*, 442, 187-194.
- Shi, L., Sun, C., Zhou, F., and Liu, W., 2005. Electrodeposited nickel–cobalt composite coating containing nano-sized Si₃N₄. *Materials Science and Engineering: A*, 397 (1), 190-194.
- Spies, H., 2014. Corrosion behaviour of nitrided, nitrocarburised and carburised steels. *Thermochemical Surface Engineering of Steels: Improving Materials Performance*, 267.
- Su, F.-H., and Huang, P., 2012. Microstructure and tribological property of nanocrystalline Co–W alloy coating produced by dual-pulse electrodeposition. *Materials chemistry and physics*, 134 (1), pages 350–359.
- Su, F., Liu, C., and Huang, P., 2013a. Friction and wear of nanocrystalline Co and Co-W alloy coatings produced by pulse reverse electrodeposition. *Wear*.

- Su, F., Liu, C., Zuo, Q., Huang, P., and Miao, M., 2013b. A comparative study of electrodeposition techniques on the microstructure and property of nanocrystalline cobalt deposit. *Materials chemistry and physics*.
- Surender, M., Balasubramaniam, R., and Basu, B., 2004a. Electrochemical behavior of electrodeposited Ni–WC composite coatings. *Surface and Coatings Technology*, 187 (1), 93-97.
- Surender, M., Basu, B., and Balasubramaniam, R., 2004b. Wear characterization of electrodeposited Ni–WC composite coatings. *Tribology International*, 37 (9), 743-749.
- Tao, S., and Li, D., 2006. Tribological, mechanical and electrochemical properties of nanocrystalline copper deposits produced by pulse electrodeposition. *Nanotechnology*, 17 (1), 65.
- Thiemig, D., and Bund, A., 2009. Influence of ethanol on the electrocodeposition of Ni/Al₂O₃ nanocomposite films. *Applied Surface Science*, 255 (7), 4164-4170.
- Thiemig, D., Lange, R., and Bund, A., 2007. Influence of pulse plating parameters on the electrocodeposition of matrix metal nanocomposites. *Electrochimica Acta*, 52 (25), 7362-7371.
- Thuvander, M., Abraham, M., Cerezo, A., and Smith, G., 2001. Thermal stability of electrodeposited nanocrystalline nickel and iron–nickel alloys. *Materials science and technology*, 17 (8), 961-970.
- Vaezi, M., Sadrnezhad, S., and Nikzad, L., 2008. Electrodeposition of Ni–SiC nano-composite coatings and evaluation of wear and corrosion resistance and electroplating characteristics. *Colloids and Surfaces A: Physicochemical and Engineering Aspects*, 315 (1), 176-182.
- Wang, L., He, Y., Zhou, J., and Duszczyk, J., 2010. Effect of temperature on the frictional behaviour of an aluminium alloy sliding against steel during ball-on-disc tests. *Tribology International*, 43 (1), 299-306.
- Wang, Q., Zhou, F., Ding, X., Zhou, Z., Wang, C., Zhang, W., Li, L. K.-Y., and Lee, S.-T., 2013. Microstructure and water-lubricated friction and wear

properties of CrN (c) coatings with different carbon contents. *Applied Surface Science*, 268, 579-587.

Wang, S.-C., and Wei, W.-C. J., 2003. Characterization of electroplated Ni/SiC and Ni/Al₂O₃ composite coatings bearing nanoparticles. *Journal of materials research*, 18 (07), 1566-1574.

Wang, Y., Ju, Y., Wei, S., Gao, W., Lu, W., and Yan, B., 2014. Au-Ni-TiO₂ nano-composite coatings prepared by sol-enhanced method. *Journal of The Electrochemical Society*, 161 (14), D775-D781.

Wielage, B., Lampke, T., Zacher, M., and Dietrich, D., 2008. *Electroplated nickel composites with micron-to nano-sized particles*. Paper presented at the Key Engineering Materials.

Xia, Y., Sasaki, S., Murakami, T., Nakano, M., Shi, L., and Wang, H., 2007. Ionic liquid lubrication of electrodeposited nickel-Si₃N₄ composite coatings. *Wear*, 262 (7), 765-771.

Xue, Y.-J., Jia, X.-Z., Zhou, Y.-W., Ma, W., and Li, J.-S., 2006. Tribological performance of Ni-CeO₂ composite coatings by electrodeposition. *Surface and Coatings Technology*, 200 (20), 5677-5681.

Xue, Y.-J., Liu, H.-B., Lan, M.-M., Li, J.-S., and Li, H., 2010. Effect of different electrodeposition methods on oxidation resistance of Ni-CeO₂ nanocomposite coating. *Surface and Coatings Technology*, 204 (21), 3539-3545.

You, Y., Gu, C., Wang, X., and Tu, J., 2012. Electrodeposition of Ni-Co alloys from a deep eutectic solvent. *Surface and Coatings Technology*.

Yuan, X.-D., and Yang, X.-J., 2010. A study on friction and wear properties of PTFE coatings under vacuum conditions. *Wear*, 269 (3), 291-297.

Zein El Abedin, S., Borissenko, N., and Endres, F., 2004. Electrodeposition of nanoscale silicon in a room temperature ionic liquid. *Electrochemistry communications*, 6 (5), 510-514.

Zein El Abedin, S., Ryder, K., Höfft, O., and Farag, H., 2012. Ionic liquids: Potential electrolytes for electrochemical applications. *International Journal of Electrochemistry*, 2012.

Zein El Abedin, S., Welz-Biermann, U., and Endres, F., 2005. A study on the electrodeposition of tantalum on NiTi alloy in an ionic liquid and corrosion behaviour of the coated alloy. *Electrochemistry communications*, 7 (9), 941-946.

Zhou, Q., He, C. L., and Cai, Q. K., 2009. Effect of Al₂O₃ powders on properties of electrodeposited Ni matrix. *Advanced Materials Research*, 79, 631-634.

Appendix A

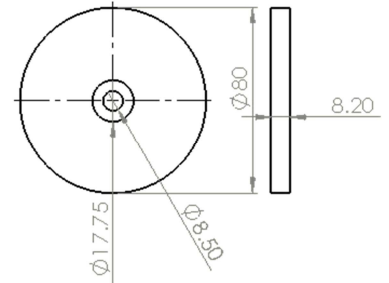
Surface area and pulse plating calculations

Surface area of cathode for electrodeposition

$$\begin{aligned} \text{Surface area (dm}^2\text{)} &= \text{Area of top} + \text{area of side} \\ &= \pi r^2 + 2\pi r h \\ &= 0.70 \text{ dm}^2 \end{aligned}$$

Surface area of anode sheet

$$\text{Surface area (dm}^2\text{)} = 2hw + 2lh + 2wh$$



Steel cathode disc



Pulse plating parameter calculations

$$\text{Duty cycle} = \frac{T_{ON}}{T_{ON} + T_{OFF}} = \frac{4_{mS}}{4_{mS} + 16_{mS}} = 20\%$$

$$\text{Frequency} = \frac{1}{T_{ON} + T_{OFF}} = \frac{1}{4_{mS} + 16_{mS}} = 50\text{Hz}$$

$$\text{Current density} = \frac{\text{Peak current A}}{\text{Surface area /dm}^2} = \frac{2.10}{0.70} = 3 \text{ A/dm}^2$$

$$\text{Average current} = \text{Peak current} \times \text{Duty cycle} = 2.10 \times 0.20 = 0.42\text{A}$$

C. Pulse Mathematics

This section describes how to calculate various setting for Pulse and Pulse Reverse plating.

C.1. Pulse Plating Calculations

The following sections give the details for calculating the plating parameters when using pulsed power supplies.

C.1.1. Overview - DC versus Pulse

This Section discusses how to determine Duty Cycle, Average Current, Peak Current, Average Voltage, Peak Voltage, and Plating Cycle Preset.

Platers are accustomed to calculating plating time (ampere-time) using D.C. amperage which, for practical purposes, is a steady, unchanging current. See **Figure 9.1a**. When a pulse power supply is used, the current is no longer steady and unchanging. It now is ON for some time and OFF for some time. This is depicted in **Figure 9.1b**.

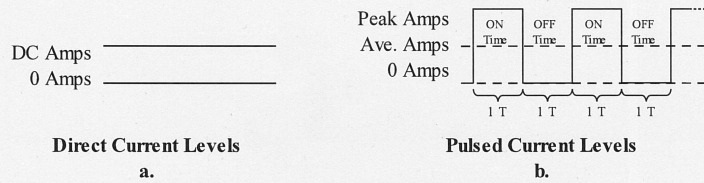


Figure 9.1: DC versus Pulse Currents

This ON and OFF current introduces the parameter DUTY CYCLE into the calculations. This is the ratio that the power supply is ON in relation to the total ON and OFF (cycle) time.

As shown in **Figure 9.1**, the level of current during the ON time of the Pulsed Current is twice the amplitude of the D.C. Current. However, the current is only there half of the time since both the ON and OFF times are 1 Time unit long. Therefore, twice the amplitude times half of the time will equal one ($1/2 \times 2 = 1$) or if the upper half of the pulse ON Time in Figure 7-1b were placed in the lower half of the OFF time the energy in the output would equal one times the D.C. level shown in **Figure 9.1a**.

The amplitude of the pulse (ON time) is called PEAK current. The level of energy which is equal to the D.C. level when time (or DUTY CYCLE) is considered is called AVERAGE current. The relationship of these 3 parameters is:

$$\text{Average_Current} = \text{Peak_Current} \times \text{Duty_Cycle}$$

Basically, all pulse plating calculations are performed to obtain the D.C. equivalent (AVERAGE) current to allow the plater to control the plating thickness. Pulse mathematics

are straight-forward when calculating unipolar (single direction ON and OFF) parameters. Unipolar may be either cathodic or anodic. As the pulse waveform becomes more complicated, so do the calculations. This will be apparent when PERIODIC REVERSE is introduced. Also remember that the same relationship (Avg. = Pk. x Duty Cycle) given above for current is true when calculating voltage.

C.1.2. Duty Cycle for Pulse

As previously stated, DUTY CYCLE is the ratio of the ON time to the total ON and OFF period (cycle) time. Referring to **Figure 9.2**, the total ON and OFF period time is 10 milliseconds (ms). The ON time is 1ms. and the OFF time is 9ms. This is a 10% DUTY CYCLE because the ON time is 1/10 of the period (ON + OFF).

$$Duty_Cycle (DC) = \frac{ON_Time}{ON_Time + OFF_Time}$$

$$DC \% = \frac{1ms}{1ms + 9ms} \times 100 = \frac{1ms}{10ms} \times 100 = 0.1 \times 100 = 10\%$$

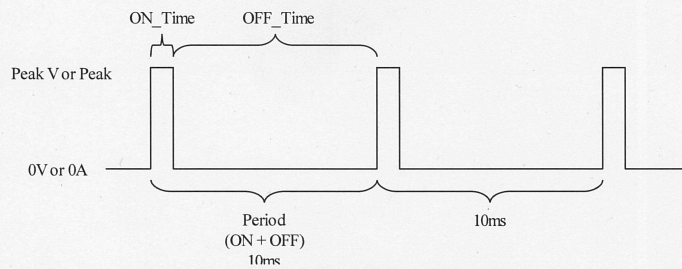


Figure 9.2: Duty Cycle

If the ON time increases and the OFF time decreases by the same amount, the ON + OFF period time would remain the same while the DUTY CYCLE would increase. For example, if the ON time was 2ms and the OFF time 8ms the ON + OFF period would be the same, 10ms, but the DUTY CYCLE would become 20%.

The fact that the PERIOD did not change means that the FREQUENCY of the pulsed waveform is not changing either since:

$$Frequency = \frac{1}{Period}$$

Therefore, DUTY CYCLE can be changed while maintaining a certain FREQUENCY by changing ON and OFF time equal but opposite amounts.

Appendix A

Dynatronix, Inc.

MicroStar DP DPR DPD Group1 Manual

Conversely, FREQUENCY can be changed while DUTY CYCLE remains unchanged by changing both ON and OFF times by proportionate amounts in the same direction. For example, if, in the previous example where ON time was increased to 2 mS, the OFF time was increased two-fold also instead of decreased by 1 mS, the DUTY CYCLE would be:

$$DC (\%) = \frac{2ms}{2ms + 18ms} \times 100 = \frac{2ms}{20ms} \times 100 = 0.2 \times 100 = 20\%$$

The FREQUENCY, however, would be:

$$Frequency = \frac{1}{2ms + 18ms} = \frac{1}{20ms} = 50Hz$$

Whereas, in the first example, it was:

$$Frequency = \frac{1}{1ms + 9ms} = \frac{1}{10ms} = 100Hz$$

C.1.3. Peak Regulation

Dynatronix power supplies are PEAK regulated whether they are constant current or constant voltage. This means that the operator control sets the PEAK current or voltage and the power supply holds that peak value constant (during ON_Time) despite any change in load resistance or DUTY CYCLE.

A change in DUTY CYCLE, with the PEAK being held constant, will change the AVERAGE output in accordance with:

$$Average_Current = Peak_Current \times Duty_Cycle$$

C.1.4. Average Readbacks

All Dynatronix Power Supplies, whether manual, programmable or both, measure, display and/or report output in AVERAGE. This is appropriate as AVERAGE is the equivalent of D.C. with which the majority of plating personnel are familiar. AVERAGE, which is the product of PEAK and DUTY CYCLE, is, therefore, used in calculating current density and AMPERE-TIME among other things.

Appendix B

Principle of instrumented indentation testing.

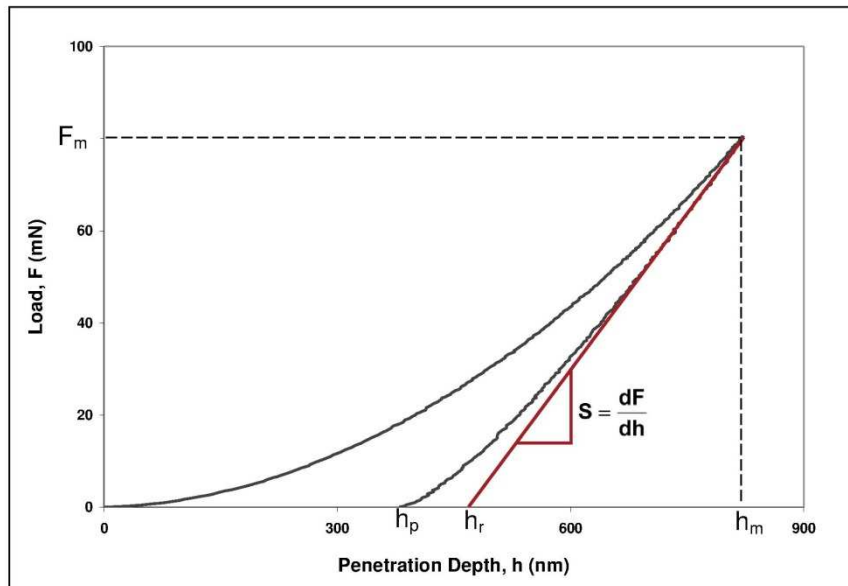
> Principle of Instrumented Indentation Testing (IIT)

The Nano Indentation Tester uses an already established method where an indenter tip with a known geometry is driven into a specific site of the material to be tested, by applying an increasing normal load. When reaching a pre-set maximum value, the normal load is reduced until partial or complete relaxation occurs. This procedure is performed repetitively; at each stage of the experiment the position of the indenter relative to the sample surface is precisely monitored with a differential capacitive sensor.

For each loading/unloading cycle, the applied load value is plotted with respect to the corresponding position of the indenter. The resulting load/displacement curves provide data specific to the mechanical nature of the material under examination. Established models are used to calculate quantitative Hardness and Elastic Modulus values for such data.

> Analysis of Indentation Curve

A typical load/displacement curve is shown below:



In order to determine Hardness and Elastic Modulus of the investigated material, we use the Power Law Method developed by Oliver & Pharr. This method describes the upper portion of the unloading curve by a power law relationship:

$$F = F_{\max} \left(\frac{h - h_p}{h_{\max} - h_p} \right)^m$$

Where F is the test force.

Appendix B

F_{\max} is the maximum applied force.
 h is the indentation depth under applied test force
 h_p is the permanent indentation depth after the removal of the test force.
 h_{\max} is the maximum indentation depth at F_{\max} .
 m is a power law constant exponent.

The power law exponent m is determined by a least squares fitting procedure and is a function of the indenter geometry.

The contact stiffness S is given by the derivative at peak load:

$$S = \left(\frac{dF}{dh} \right)_{\max} = m \cdot F_{\max} (h_{\max} - h_p)^{-1}$$

And the tangent depth, h_r , is thus given by:

$$h_r = h_{\max} - \frac{F_{\max}}{S}$$

Where h_r is the point of intersection of the tangent c to curve b at F_{\max} with the indentation depth-axis

The contact depth (depth of the contact of the indenter with the test piece at F_{\max}), h_c , is then:

$$h_c = h_{\max} - \epsilon(h_{\max} - h_r)$$

where ϵ depends on the power law exponent m .

> Calculation of the resulting values

▪ Indentation Testing Hardness H_{IT} :

The Indentation Testing Hardness H_{IT} is determined from the maximum load, F_{\max} , divided by the projected contact area A_p at the contact depth h_c :

$$H_{IT} = \frac{F_{\max}}{A_p(h_c)}$$

Where h_c is the depth of the contact of the indenter with the test piece at F_{\max}

$A_p(h_c)$ is the projected area of contact of the indenter at distance h_c from the tip.

where A_p is a function of the contact depth h_c and is determined by a calibration of the indenter tip.

Appendix B

▪ Vickers Hardness HV:

The Vickers Hardness HV is defined by:

$$HV = \frac{F_{\max}}{9.81 \cdot A_c(h_c)}$$

Where A_c is the developed contact area and can be calculated from the projected contact area A_p and the indenter geometry as:

$$A_c = \frac{A_p}{\sin \alpha}$$

Where α is the angle between the axis of the diamond pyramid and its faces. $\alpha = 68^\circ$ for a Vickers indenter and $\alpha = 65.27^\circ$ for a modified Berkovich indenter.

Finally, for a Vickers indenter: $HV = 0.0945 \cdot H_{IT}$

And for a modified Berkovich indenter: $HV = 0.0926 \cdot H_{IT}$

▪ Indentation Modulus E_r :

The reduced modulus of the indentation contact, E_r , is given by:

$$E_r = \frac{\sqrt{\pi} \cdot S}{2 \cdot \beta \cdot \sqrt{A_p(h_c)}}$$

Where β is a geometric factor depending on the diamond shape (circular: $\beta = 1$, triangular: $\beta = 1.034$, square: $\beta = 1.012$)

The Young's modulus of the sample, E_{IT} , can then be obtained from:

$$\frac{1}{E_r} = \frac{1 - \nu_s^2}{E_{IT}} + \frac{1 - \nu_i^2}{E_i}$$

Where

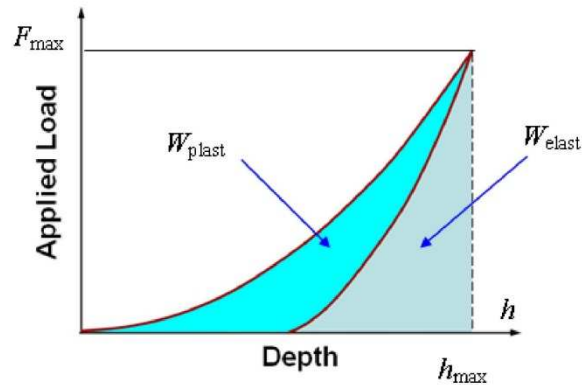
- ν_i is the Poisson's ratio of the indenter.
- ν_s is the Poisson's ratio of the sample.
- E_i is the modulus of the indenter.

▪ Elastic part of the indentation work η_{IT} :

CSM Instruments SA | A compagny of Anton Paar
Rue de la Gare 4 CH-2034 Peseux (Switzerland) T +41 32 557 56 00 F +41 32 557 56 10
info.csm@anton-paar.com www.csm-instruments.com - www.anton-paar.com

Appendix B

The mechanical work W_{total} induced by the indentation is only partly consumed as plastic deformation work W_{plast} . During the removal of the test force the remaining part is set free as work of the elastic reverse deformation W_{elast} .



The elastic part of the indentation work is then calculated as the ratio of the elastic deformation work W_{elast} divided by the total work:

$$\eta_{\text{IT}} = \frac{W_{\text{elast}}}{W_{\text{total}}} \text{ where } W_{\text{total}} = W_{\text{plast}} + W_{\text{elast}}$$

Where

W_{plast} is the plastic deformation work of indentation.
 W_{elast} is the elastic reverse deformation work of indentation.
 W_{total} is the total mechanical work of indentation

The plastic part of the indentation work follows as $\frac{W_{\text{plast}}}{W_{\text{total}}} = 100\% - \eta_{\text{IT}}$

▪ Indentation Creep C_{IT} :

If the change of the indentation depth is measured with a test force kept constant during a pause time, a relative change of the indentation depth can be calculated. This is a value for the creep of the material.

$$C_{\text{IT}} = \frac{h_2 - h_1}{h_1}$$

Where

h_1 is the indentation depth at the start of the pause
 h_2 is the indentation depth at the end of the pause

Appendix C

Calibration Certificate TE92 Microprocessor Controlled Rotary Tribometer

TE92CAL/COMPEND2000

CALIBRATION & MAINTENANCE PROCEDURE FOR TE92

Customer: Bournemouth University
Serial Number: TE92/8699
Date: 28th January 2014
Engineer: D. Willmont
Customer Contact: Rizwan BAJWA

Phoenix Tribology Ltd
29A Freemantle House
Kingsclere Park
Kingsclere
RG20 4SW
England

Phone: 44 (0) 1635 298279
Fax: 44 (0) 8707 877017
E-mail: info@phoenix-tribology.com

MAINTENANCE

- 1) Switch on multi-meter and thermocouple simulator.
- 2) Disconnect TE92 control cabinet from machine. Inspect all plugs & sockets for damage. Reconnect control cabinet and leads. OK
- 3) Switch on control cabinet and computer. OK
- 4) Check operation of all push buttons and indicator lamps. Replace bulbs as necessary. **Mains lamp not working (68V bulb)**
- 5) Re-oil pillars with a light coating of light machine oil. OK
- 6) Run machine at 1000 rpm and listen for unusual sounds. Investigate where necessary.
- 7) Inspect high cross slide assembly for wear or stiffness. Check float. OK
- 8) Check all adaptors for damage and alignment. OK

Installed COMPEND v2.00

Old version installed on new pc (V2.00) Reinstalled V2.32.

CALIBRATION

ALLOW INSTRUMENTATION TO STABILISE FOR 30 MINUTES BEFORE CALIBRATION.

CALIBRATION OF TEMPERATURE MEASUREMENT INPUTS:

- 1) Ensure heater is switched off and disconnected.
- 2) Connect the thermocouple simulator to the thermocouple input T1 on the side of the machine. Set the simulator for K type simulation output.
- 3) Record the computer displayed readings of “Specimen Temp” at the set values in the table.

Simulator setting °C	Specimen Temp °C
0 (±1)	1
10 (±1)	10
20 (±1)	21
50 (±1)	51
100 (±2)	101
150 (±2)	150
200 (±2)	200

- 4) If outside of limits adjust calibration and repeat above.
- 5) Units Low = 0 Bits Low =
- 6) Units High = 600 Bits High =

7) CALIBRATION OF TORQUE MEASUREMENT INPUT

Torque

- 1) Remove the cell from the torque bracket and bolt it to the machine base plate. Note – the torque arm distance is 100mm.
- 2) Adjust the zero pot so that the torque reading = 0N with the weight hanger
- 3) Apply the following weights: -.

Applied Weight kg	Friction N	Indicated Friction N
0kg	0 ± 0.1	0.00
2kg	1.96 ± 0.1	1.99
5kg	4.91 ± 0.1	4.94
7kg	6.87 ± 0.1	6.93
10kg	9.81 ± 0.1	9.87
12kg	11.77 ± 0.1	11.85
20kg	19.62 ± 0.1	19.70

- 4) If outside of limits adjust calibration and repeat above.
- 8) Units Low = 0 Bits Low =
- 9) Units High = 9.81 Bits High =

CALIBRATION OF SPEED MEASUREMENT INPUT**High Speed**

- 1) Set up the machine in high-speed configuration. Remove the shaft guard. Check that the motor pulleys and speed transducer brackets are securely fitted. Attach a piece of reflective tape to the side of the specimen shaft.
- 2) Check that the optical sensor and disc are running true and are not damaged.
- 3) Using manual control and the optical tachometer, check the tachometer display (Speed) and the computer screen at the following speeds. When using the machine without the shaft guard fitted, take great care not to get clothing or hair caught in the rotating shaft.

Setpoint	Frequency meter	COMPEND
1000 rpm	1000 rpm	1000 rpm
2500 rpm	2500 rpm	2500 rpm
4000 rpm	4000 rpm	4000 rpm
5500 rpm	5500 rpm	5500 rpm
7000 rpm	7000 rpm	7000 rpm

Low Speed

- 4) Set up the machine in high-speed configuration. Remove the shaft guard. Check that the motor pulleys and speed transducer brackets are securely fitted. Attach a piece of reflective tape to the side of the specimen shaft.
- 5) Check that the optical sensor and disc are running true and are not damaged.
- 6) Using manual control and the optical tachometer, check the tachometer display (Speed) and the computer screen at the following speeds. When using the machine without the shaft guard fitted, take great care not to get clothing or hair caught in the rotating shaft.

Setpoint	Frequency meter	COMPEND
100 rpm	100	100
500 rpm	500	500
1000 rpm	1000	1000
2000 rpm	2000	2000
3000 rpm	3000	3000

CALIBRATION OF LOAD**High Load**

- 1) Remove any specimen assembly from the machine including the specimen carrier.
- 2) Place the calibrated force button and spacer in place of the specimen assembly.

Setpoint	Actual Load
0.10 kN ± 0.01	0.100
0.20 kN ± 0.01	0.198
0.50 kN ± 0.01	0.498
0.75 kN ± 0.02	0.744
1.00 kN ± 0.02	0.995
1.50 kN ± 0.02	1.498
2.00 kN ± 0.02	2.000

- 3) If outside of limits, adjust recalibration and repeat above.
- 4) Units Low = Bits Low =
- 5) Units High = Bits High =

Low Load

- 1) Remove any specimen assembly from the machine including the specimen carrier.
- 2) Place the calibrated force button and spacer in place of the specimen assembly.

Setpoint	Actual Load	
20 N ± 1	20	21
50 N ± 1	50	51
100 N ± 1	100	101
200 N ± 2	198	201
400 N ± 2	386	400
600 N ± 2	573	600
800 N ± 3	767	800
1000 N ± 3	960	1000

- 3) If outside of limits adjust calibration and repeat above.
- 4) Units Low = 40 Bits Low = 484
- 5) Units High = 1075 Bits High = 3149

OTHER COMMENTS:

Configuration Files

TE92HS 10kN
 TE92HS 1kN
 TE92LS 10kN
 TE92LS 1kN

Calibrations Before

	Units low	units high	bits low	bits high
Speed SP Low	211	2230	300	3000
Speed SP High	0	10000	0	4095
Load SP high	0	10	0	4095
Load SP low	0	1000	0	4095
Temperature SP	0	200	0	4095
Anpout 4	0	4095	0	4095
SPEED HS	0	1421	0	500
Total Revs	0	1421	0	500
Anin 1	0	4095	0	4095
Anin 2	0	4095	0	4095
Anin 3	0	4095	0	4095
Anin 4	0	4095	0	4095
SPECIMEN TEMP	0	200	824	3485
Anin 6	0	4095	0	4095
TORQUE	0	9.81	11	1406
LOAD 10kN	0.366	5.083	209	1723
LOAD 1kN	0	1037	484	2954

Appendix C

TE92CAL/COMPEND2000

Calibrations After

	Units low	units high	bits low	bits high
Speed SP Low	211	2230	300	3000
Speed SP High	0	10000	0	4095
Load SP high	0	10	0	4095
Load SP low	0	1000	0	4095
Temperature SP	0	200	0	4095
Anpout 4	0	4095	0	4095
SPEED HS	0	2892	0	1000
Total Revs HS	0	2892	0	1000
Anin 1	0	4095	0	4095
Anin 2	0	4095	0	4095
Anin 3	0	4095	0	4095
Anin 4	0	4095	0	4095
SPECIMEN TEMP	0	200	824	3485
Anin 6	0	4095	0	4095
TORQUE	0	9.81	38	1406
LOAD 10kN	0.366	5.083	209	1723
LOAD 1kN	0	1075	484	3149

Appendix C

TE92CAL/COMPEND2000

Notes:-

Need to keep check on motor cooling fan, signs of bearing failed bearings.

Calibration

Certificate

TE92 Microprocessor Controlled Rotary Tribometer

Serial No. TE92/8699

Phoenix Tribology Ltd

29A Freemantle House

Kingsclere Park

Kingsclere

RG20 4SW

England

Phone:44 (0) 1635 276064298279

Fax: 44 (0) 8707 877017

E-mail: info@phoenix-tribology.com

This is to certify that the above unit has been Calibrated in accordance with our standard procedures and conforms to the specification. Calibration covers:

Thermocouple inputs, linearity and scale.

Speed, actual value and display, linearity and scale.

Friction transducers & amplifier, linearity and scale.

Load-cell transducer & amplifier, linearity and scale.

CALIBRATION EQUIPEMNT

Multimeter, test leads & Probes

Thermocouple simulator

Optical tachometer and reflective tape

Loadcell

Serial Number

14400367

3075

2015652

078668

Signed



David Willmont

For and on behalf of

Phoenix Tribology Ltd.

Date 28th January 2014

Appendix D**Water-Lubricated Ni-Based Composite (Ni–Al₂O₃, Ni–SiC and Ni–ZrO₂) Thin Film Coatings for Industrial Applications**

Rizwan Sarwar Bajwa, Zulfiqar Khan, Vasilios Bakolas & Wolfgang Braun

Acta Metallurgica Sinica (English Letters), First online: 16 Dec 2015,
29 (1), 8-16, [DOI: 10.1007/s40195-015-0354-1](https://doi.org/10.1007/s40195-015-0354-1).



Water-Lubricated Ni-Based Composite (Ni–Al₂O₃, Ni–SiC and Ni–ZrO₂) Thin Film Coatings for Industrial Applications

Rizwan Sarwar Bajwa¹ · Zulfiqar Khan¹ · Vasilios Bakolas² · Wolfgang Braun²

Received: 22 July 2015 / Revised: 3 November 2015
© The Chinese Society for Metals and Springer-Verlag Berlin Heidelberg 2015

Abstract In this work, pure nickel and Ni-based nanocomposite coatings (Ni–Al₂O₃, Ni–SiC and Ni–ZrO₂) were produced on steel substrate by using pulse electrodeposition technique. The industrial performance tests were conducted to evaluate the wear resistance, corrosion resistance, adhesion strength and wettability behaviour of newly developed coatings. Rolling contact ball-on-disc tribometer was used to assess anti-wear behaviour of these coatings under water-lubricated contacts. The results showed that the wear- and corrosion resistance properties of nickel alumina and Ni–SiC composite coatings significantly improved than that of pure Ni and Ni–ZrO₂ coatings. The adhesion and wettability results of Ni–Al₂O₃ composite showed better performance when compared to the rest of the coatings. The effects of incorporating nanoparticles on the surface microstructure, interface adhesion and distribution of the particles were also investigated. The coatings were characterized by using scanning electron microscopy, X-ray diffraction analysis and 3D white light interferometry. The wear failure behaviour of these coatings was further examined by post-test surface observation under optical microscope.

KEY WORDS: Electrodeposition; Wear-resistant; Corrosion-resistant; Tribology; Nanocoatings; Water-lubrication

1 Introduction

Material's surfaces or components have limited life due to the mechanical interactions of components within the system and/or chemical or electrochemical influences of operating environment. During the last decade, extensive work has been completed in the field of electrodeposition coating technique, especially with a focus on wear and

corrosion-resistant coatings, self-lubricating systems and dispersion-strengthened coatings [1–6].

Recently, Gül et al. [7, 8] compared the effect of current density on the tribological performance of Ni–Al₂O₃ composite coatings deposited using DC and pulse current techniques. The surface morphology results showed that the composite coatings produced from PC deposition contain a higher-loaded percentage of incorporating particles and better particle distributions. The wear results demonstrated that in DC-plated coatings the increasing current density contributed to reduced wear rate. However, in case of PC-plated composite coating, insignificant effect was observed on the wear rate with increasing current density. Researchers have also reported the optimum values for incorporating particles [9] and sodium dodecylsulfate (SDS) [10] concentrations in the electrolyte of Ni–SiC and Ni–WC composite coatings, respectively. These values are 20 g/L for particle

Available online at <http://link.springer.com/journal/40195>

✉ Rizwan Sarwar Bajwa
rbajwa@bournemouth.ac.uk

¹ Faculty of Science and Technology, Sustainable Design Research Centre, Bournemouth University Talbot Campus, Poole, Dorset, UK

² Advanced Bearing Analysis, Schaeffler Technologies GmbH & Co. KG, 91074 Herzogenaurach, Germany

Published online: 16 December 2015

Springer

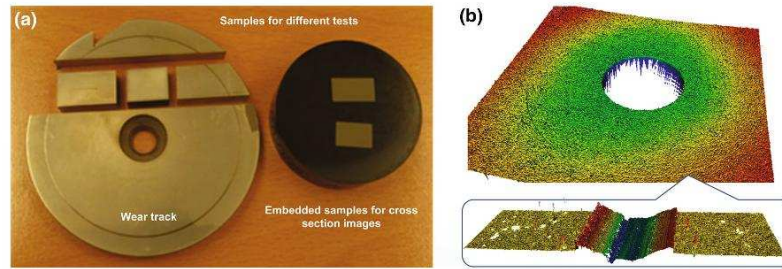
R. S. Bajwa *et al.*: Acta Metall. Sin. (Engl. Lett.)

Fig. 1 a Subsections images (by using precision cutting method) of electrodeposited coated disc used for different tests, b 3D profile of the sample wear track after wear-resistant test

concentration and 0.10 g/L for SDS in order to achieve distinctly improvement of the mechanical and wear-resistant properties. The effect of ultrasonic treatment on incorporation of zirconia particles into a nickel matrix was investigated by Beltowska-Lehman *et al.* [11]. It was found that the Ni-W/ZrO₂ composite coatings exhibit uniform particle distribution, enhanced content of the particles at lower ultrasonic treatment and consequently improved the mechanical properties achieved.

Considerable studies were conducted to examine the tribological performance of nanocomposite coatings embedded with nanoparticles into nickel as matrix [12–17]. Nanoparticles present unique and novel properties, typically when their size is below 100 nm. The effect of nanosized Al₂O₃ composite with nickel matrix on anti-corrosion properties of nickel coating was studied by Zhou *et al.* [18]. They demonstrate that the incorporation of Al₂O₃ nanoparticles improves the corrosion resistance by reducing the porosity of nickel coatings and also improves the abrasion resistance due to better dispersion of nano-Al₂O₃ as compared to micro-Al₂O₃. The microhardness and anti-wear resistance performance of electrodeposited nanocomposite coatings was studied by Borkar *et al.* [19]. They showed that the increasing weight content of the nanoparticles into the electrolyte bath (up to 40 g/L) significantly improves the microhardness and the wear resistance of the nickel coating due to the enhanced strengthening effect of the nanoparticles into nanocomposite coatings. They also investigate the effect of plating conditions and concluded that the pulse current and pulse reverse current enhanced the weight percentage of reinforcement of the nanoparticles into the coating better as compared to direct current deposition.

The influence of pulse frequency on the sliding wear property of the nanocomposite coatings was examined by Chen *et al.* [20]. They indicated that the volume fraction of alumina particles in coatings increased with the increase in pulse frequency and the wear behaviour of coating depends

on reinforcement content of the particles into coating rather than pulse frequency. They demonstrated that the anti-wear properties of electrodeposited coatings under various pulse frequencies behave significantly different under dry and oil-lubricated environments.

Previous studies [21–25] investigated the rolling contact fatigue behaviour of thermal plasma sprayed coated rolling elements under various tribological conditions. They indicated that the coating failure mechanisms under rolling contact based on two kinds of failure modes: the surface wear and coating delamination. Additionally, Khan *et al.* [26–29] studied the failure mechanisms of hybrid ceramic rolling contact bearing elements in rolling or rolling/sliding contact with conventional oil and saturated liquid refrigerant lubrication.

The tribological performance of electrodeposited nickel-based coatings was studied by various researchers as reported above. However, the tribological performance of electrodeposited nanocomposite coatings in rolling contact subject to water-lubricated regime has been left obscure. Earlier investigations have utilized pin-on-disc or ball-on-disc sliding tribotest conditions under dry or oil-lubricated environments.

In current work, a high-speed microprocessor rotary tribometer (HSMRT) was used to simulate industrial applications in terms of rolling contacts. The pulse current electrodeposition technique was utilized to electrodeposit pure nickel as a mean of benchmarking, and nickel composite coatings incorporating nanosized alumina, SiC and ZrO₂ particles. These coatings were investigated in terms of their tribological and mechanical properties, coatings–substrate interface adhesion strength, wettability behaviour and surface free energies. The pure nickel and nickel alumina composite coatings have been extended from our previously published work in which [30] the influences of the different ionic strength of electrolyte were studied.

The surface energy of the coatings plays an important role in the substrate–coating interface adhesion and

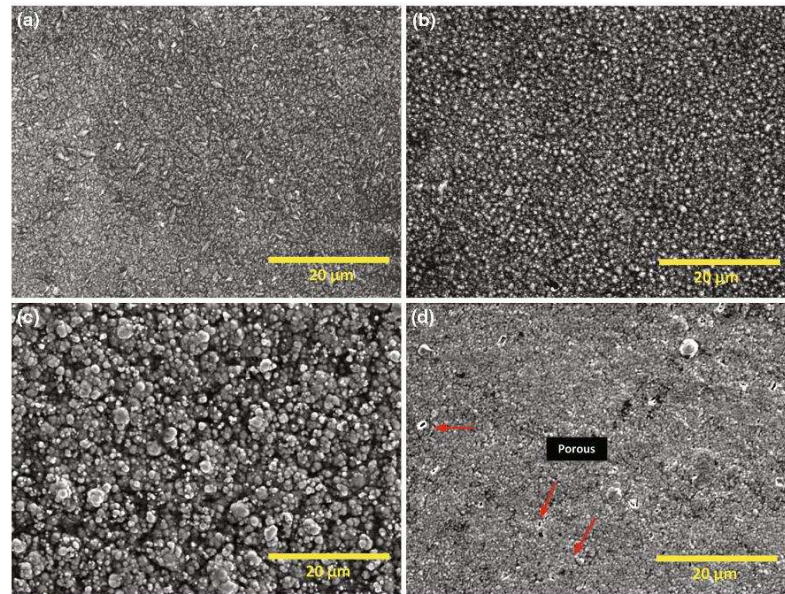
R. S. Bajwa *et al.*: Acta Metall. Sin. (Engl. Lett.)

Fig. 2 Surface morphologies of pulse electrodeposited nickel-based composite coatings: **a** pure nickel, **b** Ni-Al₂O₃, **c** Ni-SiC, **d** Ni-ZrO₂

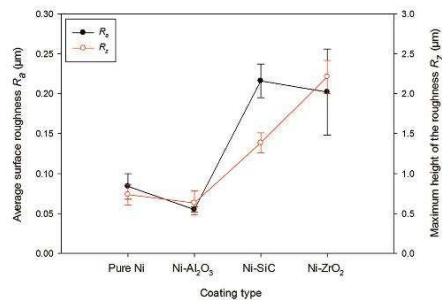


Fig. 3 Surface roughness parameters (R_a and R_z) of pure nickel and nickel composite coatings

adhesion resistance on counter body in tribological applications. Therefore, the effect of various embedded nanoparticles into electrodeposited nanocomposite coatings subject to surface energy and wettability behaviour was also investigated in this study [31].

2 Experimental

2.1 Electrodeposition and Characterization of the Coatings

All coatings, pure nickel, Ni-Al₂O₃, Ni-SiC and Ni-ZrO₂, were pulse electrodeposited with the expected thickness of $\sim 10 \mu\text{m}$ over steel substrate. The electrolyte composition consists of NiSO₄·6H₂O (265 g/L), NiCl₂·6H₂O (48 g/L) and H₃BO₃ (31 g/L). For composite coatings, the nanoparticles ($\sim 50 \text{ nm}$) with an amount of 20 g/L were ultrasonically dispersed in the electrolyte. The electrodeposition process parameters were kept constant as current density (3 A/dm^2) and pulse on-off time (20–80 ms) with a duty cycle of 20%. A high-quality nickel sheet was used as an anode, and a steel circular disc of 80 mm diameter and 8.20 mm thick was used as a cathode.

Scanning electron microscopy (JSM-6010, JEOL) was used to analyse the microstructure of the deposits. The weight percentages of embedded particles were calculated by the energy-dispersive X-ray spectroscopy (EDS). X-ray diffraction (XRD) analysis was performed by using a D8 Advance (Bruker) with 2θ range of 20° – 100° and

R. S. Bajwa *et al.*: Acta Metall. Sin. (Engl. Lett.)

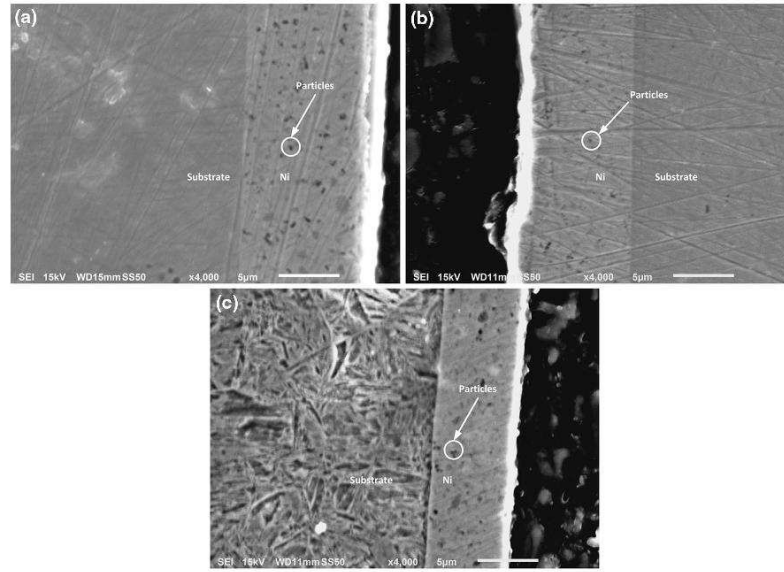


Fig. 4 Cross-sectional SEM micrographs of incorporated nanoparticle distributions in the nickel-based composite coatings: **a** Ni–Al₂O₃, **b** Ni–SiC, **c** Ni–ZrO₂

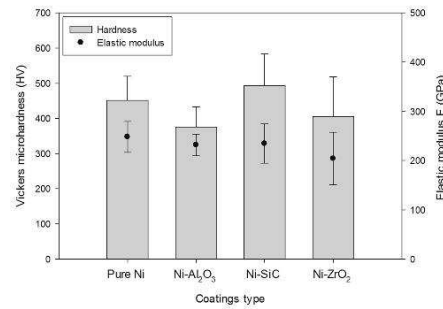


Fig. 5 Hardness and elastic modulus values of pure nickel and nickel composite coatings

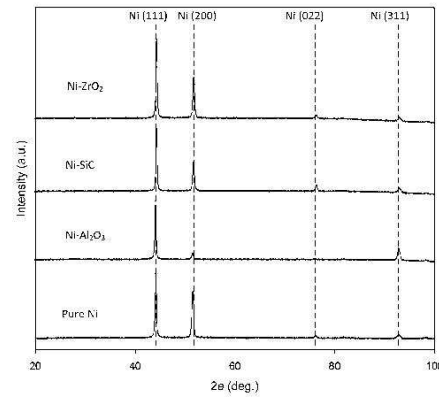


Fig. 6 X-ray diffraction patterns from electrodeposited pure nickel and nickel-based composite (Ni–Al₂O₃, Ni–SiC and Ni–ZrO₂) coatings

with a step increment of 0.02°. For coating-substrate interfacial adhesion analysis, the specimens were embedded by using ATM OPAL 460 equipment as

shown in Fig. 1. The hardness and elastic modulus of the coatings were measured by using CSM microindentation tester (MHT) at a loading force of 300 mN.

2.2 Wear and Corrosion Resistance Testing

The wear resistance tests conducted by using a unidirectional ball-on-disc tribometer in distilled water at a rolling speed of 1 m/s and normal load of 45 N. The corresponding Hertzian contact pressure [32] can be estimated to be 1.75 GPa. The tribometer consists of an upper plated specimen and lower three balls (100Cr6) spaced at 120°. 3D profile of one sample's wear track is shown in Fig. 1. The wear volume was calculated as $V = AL$, where A is the cross-sectional area of worn scar in mm^2 and L is the length of the worn scar in millimetres. A specific wear rate is determined as $v = V/(Fl)$, where F is the load in N and l is the rolling distance in metres [33]. All wear tests were conducted at least two times to ensure repeatability and minimize uncertainty.

The electrochemical measurements were taken by using a system of three electrodes. The deposit part was used as a working electrode, and a platinum wire was used as counter electrode. The reference electrode was an Ag/AgCl. The electrochemical results were obtained at opening circuit potential (OCP) with scanning rate of 0.001 V/s.

2.3 Adhesion Performance and Surface Energies Testing

The scratch tests were conducted DIN EN 1071-3 standard method by using a CSM REVETEST machine. The scratch was made with a length of 10 mm on each type of the coating with a sliding speed of 10 mm/min and increasing load from 0 to 100 N/min. The critical load value (L_c) is defined as the load value at which the first mode of failure was observed. The surface free energy was conducted using Owens and Wendt (OWRK) method considering

water and diiodomethane as reference liquids of known surface energies [34].

3 Results and Discussion

3.1 Surface Morphology and Mechanical Properties of the Coatings

Pure nickel and nickel composite coatings were electrodeposited under same pulse parameters exhibit shiny grey appearance, surface uniformity and good adherence to the mild steel substrate. The micrographs of pulse electrodeposited pure nickel and nickel composite of nanosized particles of alumina, silicon carbide and zirconium are shown in Fig. 2. All the pulsed deposited coatings exhibit compact fine grain size. However, the grain size of co-deposited Ni-SiC exhibits the highest grain size when compared to the rest of the coatings which causes higher surface roughness parameters ($R_a \sim 0.21 \mu\text{m}$; $R_z \sim 1.38 \mu\text{m}$). The variation in average surface roughness (R_a) and the maximum height of the roughness (R_z) values for deposited coatings are shown in Fig. 3. The presence of agglomerated particles and pores on the Ni-ZrO₂ coatings resulted in higher surface roughness values ($R_a \sim 0.20 \mu\text{m}$; $R_z \sim 2.2 \mu\text{m}$). The surface roughness values were minimum ($R_a \sim 0.05 \mu\text{m}$; $R_z \sim 0.63 \mu\text{m}$) for Ni-alumina followed by pure nickel ($R_a \sim 0.08 \mu\text{m}$; $R_z \sim 0.73 \mu\text{m}$) due to finer surface morphology. The cross-sectional SEM micrographs of incorporating nanoparticle distributions of composite coatings are shown in Fig. 4.

The weight percentage of reinforcement content was calculated through energy-dispersive spectroscopy to be 2.5–3 for the nickel composite coatings. The microhardness and elastic modulus properties of the nickel and nickel composite coatings, electrodeposited under same pulse conditions, but with different types of incorporated particles are shown in Fig. 5. There was no significant difference observed in the hardness values between all types of the coatings which contradicts the previous finding. Previously, it has been reported that the hardness of the composite coatings was significantly improved due to the strengthening effects of incorporated hard particles. However, the reinforcement content of hard particles in that study was (8–12) wt% [19]. Generally, the increase in the weight percentage of incorporated hard particles into nickel matrix results in enhanced mechanical properties. However, in practice the hardness to elastic modulus ratio (H/E) is an important parameter in predicting the better mechanical properties of materials [11]. Thus, lower hardness of Ni-Al₂O₃ (375HV) and Ni-ZrO₂ (405HV)

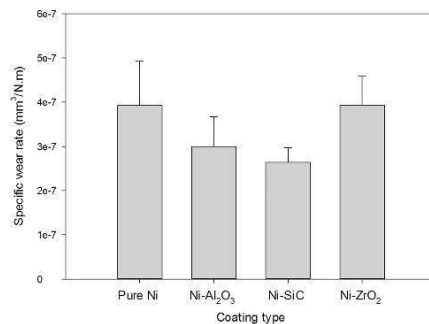


Fig. 7 Comparison of the wear rates of pure nickel and nickel composite coatings in water-lubricated rolling contacts

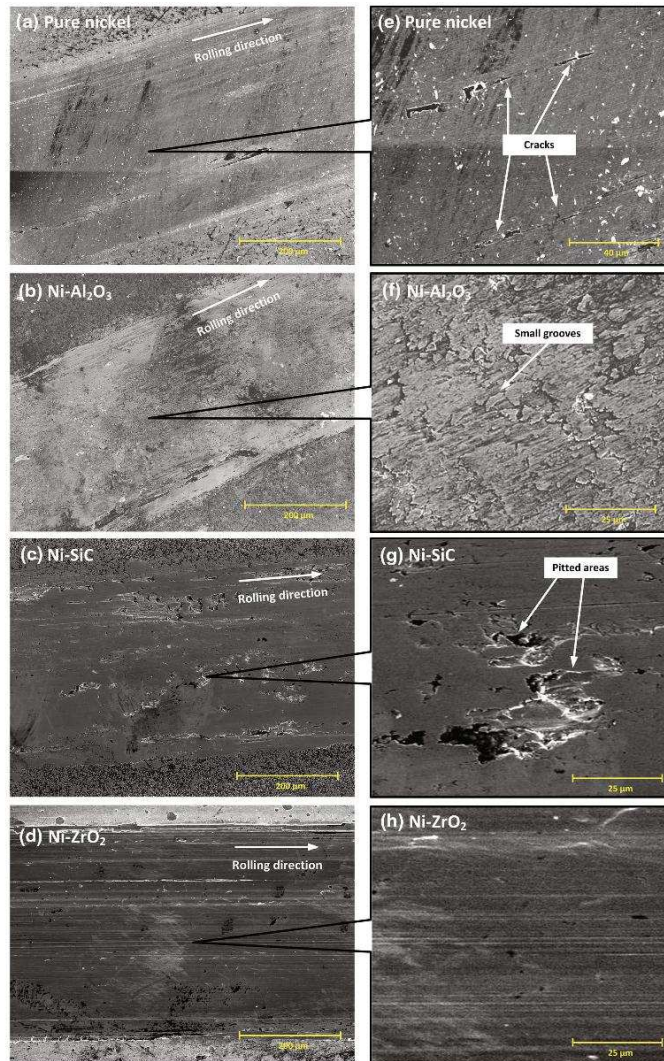
R. S. Bajwa *et al.*: Acta Metall. Sin. (Engl. Lett.)

Fig. 8 SEM micrographs of worn surfaces of pure nickel and nickel composite coatings in water-lubricated rolling contacts; overall **a-c**, magnified **d-f** views

composites than pure nickel coating can be attributed to lower plasticity index ratio (H/E) and porous surface morphology, respectively. As shown in Fig. 5, the Ni-SiC

coating exhibits the higher hardness to elastic modulus (H/E) ratio, which is an indication of good wear resistance property. This is because that H/E ratio is a better

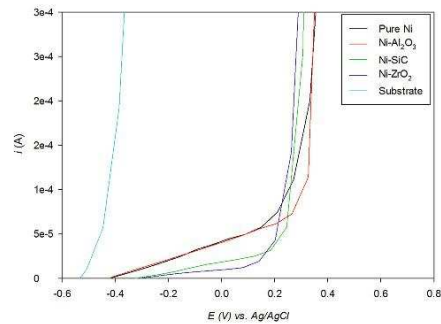
R. S. Bajwa *et al.*: Acta Metall. Sin. (Engl. Lett.)

Fig. 9 Potentiodynamic polarization curves for bare substrate, pure nickel and nickel composite of different nanoparticles in 3.5% NaCl solution

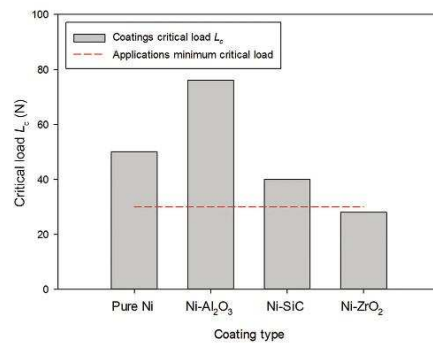


Fig. 10 Critical loads for different types of nickel and nickel composite coatings according to DIN EN 1071-3

parameter for predicting wear resistance property than hardness alone [35].

The X-ray diffraction (XRD) patterns for pure nickel and nickel-based composite (Ni-Al₂O₃, Ni-SiC and Ni-ZrO₂) coatings are shown in Fig. 6. For all the coatings, the XRD patterns show typical high peaks for (111) and (200) crystal planes of nickel and also evidenced by other researchers [7, 9, 11]. There are visible changes in orientation between the four samples; in particular, the changes affect the (311) reflection, which grows more intense for the Ni-alumina where the (002) grows less intense. For the Ni-SiC, there is a visible more intense orientation indicated by the (022) reflection. Note that due to very low reinforcement content percentage of nanoparticles, the corresponding peaks could not be resolved [19]. The

crystalline grain sizes were calculated by using XRD patterns and observed less than 50 nm for all coatings: pure Ni = 39 nm, Ni-alumina = 33 nm, Ni-SiC = 34 nm and Ni-ZrO₂ = 30 nm. The average grain size slightly reduced with the addition of the nanoparticles into a nickel matrix. Many studies have shown that the reinforcement of the nanosized particles into Ni matrix reduces the average grain size of Ni matrix [8, 10, 36].

3.2 Wear and Corrosion Properties of the Coatings

The wear rates of pure nickel and nickel composite coatings in water-lubricated rolling contacts are shown in Fig. 7. The Ni-SiC showed the minimum wear rate followed by Ni-Al₂O₃ in water-lubricated contacts. There was no significant difference in wear rates of Ni-ZrO₂ and pure nickel electrodeposited coatings. For all coatings, the two-body abrasive wear and plastic deformation were observed due to the higher hardness of counter steel balls than coatings as shown in Fig. 1. However, relatively severe plastic deformation in a form of continuous wide grooves in the case of pure nickel and nickel-ZrO₂ was an indication of poor wear resistance property. Post-test surface examinations of worn wear tracks were further investigated through SEM and are shown in Fig. 8a-d and magnified view in Fig. 8e-h. Similar severe plastic deformation appearances of the pure nickel and Ni-ZrO₂ led to the smoothing of the surface as shown in Fig. 8e, h, while, in the analysis of worn Ni-Al₂O₃ and Ni-SiC, the surfaces microplothing and delamination wear mechanism were observed, respectively, as shown in Fig. 8f, g. It may relate to SiC and Al₂O₃ particles pulling out of the matrix and contribute to three-body abrasion wear [33]. However, lower wear rate in Ni-SiC and Ni-Al₂O₃ composites indicates that SiC and Al₂O₃ hard particles are restricting severe plastic deformation in worn surfaces.

The potentiodynamic curves for the steel substrate and electrodeposited coatings are shown in Fig. 9. As can be seen, the corrosion resistance potential for deposited coating is significantly higher than the smooth substrate surface. In comparison, the Ni-Al₂O₃ exhibits the higher corrosion resistance potential followed by pure nickel. This can be attributed to finer grain structure with the addition of Al₂O₃ particles and validates the previous findings [37, 38]. It is interesting to observe that the corrosion potential of Ni-SiC and Ni-ZrO₂ is lower than pure nickel and exhibits similar behaviour. The lower corrosion potential behaviour in nickel composite coatings incorporating SiC and ZrO₂ can be because of higher surface roughness (R_a) and maximum height of the roughness (R_z) parameter values. The roughness valleys in these coatings can provide weak points for penetration of aggressive corrosive solution

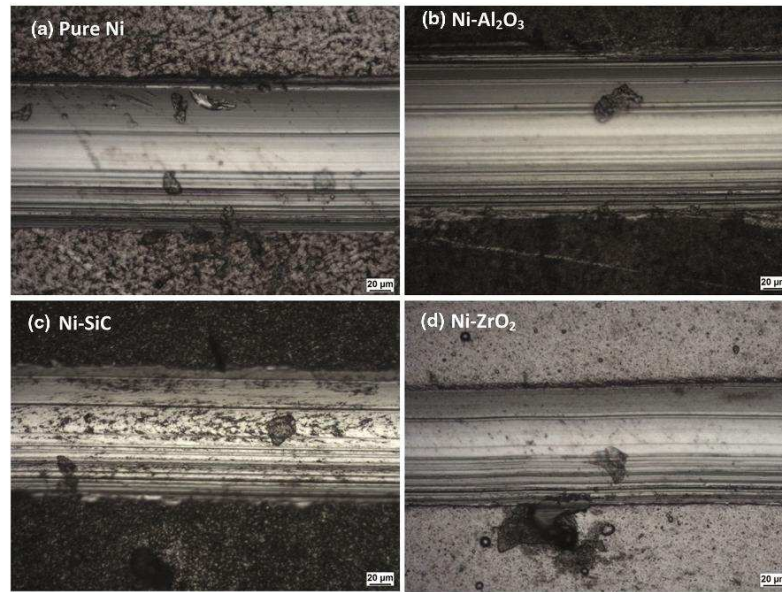


Fig. 11 Optical microscopic examinations for failure mechanism according to DIN EN 1071-3 for nickel and nickel composite coatings

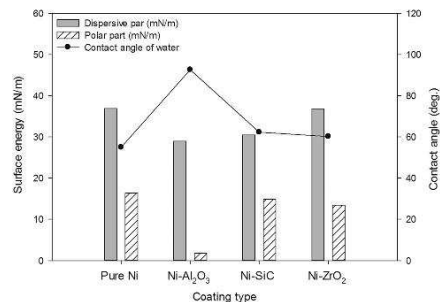


Fig. 12 The comparison of the surface energy and changing wettability behaviour of the pure nickel and nickel composite coatings

towards substrate and consequently cause lower pitting potential.

3.3 Adhesion Strength and Wettability Behaviour of the Coatings

The adhesion performance of all coatings was investigated to evaluate their suitability in industrial application. The

adhesion critical load values (L_c) measured in scratch tests for pure nickel and nickel composite coatings are compared in Fig. 10. All coatings except Ni-ZrO₂ showed adhesion strength above the critical load of 30 N which is generally required as a minimum critical load value for industrial applications. Nickel composite of alumina nanoparticles showed the maximum L_c value of 79 N and lowest L_c value of 28 N and was observed in Ni-ZrO₂ composite coatings. Note that these coatings were deposited on mild steel substrate without any intermediate coating which can further improve adhesion strength. Coatings failure mechanism in scratch testing was observed through microscopy and is shown in Fig. 11.

Figure 12 shows the polar and dispersive component of the surface free energy and water contact angle measurement results of all coatings. In all coatings, the higher dispersive component share reveals that the coatings mainly possess covalent bonds. Their disperse shares vary from 29 to 36 mN/m, and polar shares vary from 2 to 16 mN/m. It is noticeable that no significant differences were observed in wettability behaviour between pure nickel and nickel composite coating. However, the polar component of Ni-Al₂O₃ composite coating was remarkably reduced by addition of nanosized alumina particles.

R. S. Bajwa *et al.*: Acta Metall. Sin. (Engl. Lett.)

The reduced polar component in nickel alumina composite coatings results into the higher contact angle of water as compared to the rest of the coatings. The surfaces become less hydrophilic with reducing polar shares due to reduction in dipole interactions [39]. Furthermore, it is noticeable that lower surface energy of Ni–Al₂O₃ coating exhibits the highest adhesion to the substrate which is contrasting to previous investigations [31]. Their studies concluded that the high adhesion can be achieved with increasing high surface energies. However, they used PVD method for coating development which may be the reason for the present contradiction.

4 Conclusions

1. The wear-resistant results show that the Ni–SiC and Ni–Al₂O₃ provide a better wear resistance performance than pure nickel and Ni–ZrO₂ coatings.
2. Nickel composite of nanosized alumina exhibits the maximum corrosion resistance potential followed by pure nickel, Ni–SiC and Ni–ZrO₂.
3. In scratch test, the Ni–alumina composite showed a better adhesion strength on a substrate as compared to rest of the coatings.
4. The low surface energy and in return the higher water contact angle of nickel–alumina composite coating predict a better corrosion resistance performance in water-lubricated contacts.
5. The cross-sectional images of the coatings show that all the coatings are uniform and well adhere to the substrate without cracks at the coating–substrate interface.

Acknowledgments The authors would like to acknowledge Schaeffler Technologies GmbH & Co. KG (Germany) and Bournemouth University (UK) for financial and in-kind support. The authors also thank Dr Loma from the Experimental Techniques Centre, Brunel University, for her assistance with XRD analysis.

References

- [1] P. Gyftou, E. Pavlatou, N. Spyrellis, *Appl. Surf. Sci.* **254**, 5910 (2008)
- [2] F. Su, C. Liu, P. Huang, *Wear* **300**, 114 (2013)
- [3] C. Lee, *Tribol. Int.* **55**, 7 (2012)
- [4] M. Musiani, *Electrochim. Acta* **45**, 3397 (2000)
- [5] A.K. Pradhan, S. Das, *Tribol. Trans.* **57**, 46 (2014)
- [6] H. Lee, C. Lin, D. Wu, C. Lee, *Tribol. Trans.* **54**, 497 (2011)
- [7] H. Gül, M. Uysal, H. Akbulut, A. Alp, *Surf. Coat. Technol.* **258**, 1202 (2014)
- [8] H. Gül, F. Kılıç, S. Aslan, A. Alp, H. Akbulut, *Wear* **267**, 976 (2009)
- [9] H. Gül, F. Kılıç, M. Uysal, S. Aslan, A. Alp, H. Akbulut, *Appl. Surf. Sci.* **258**, 4260 (2012)
- [10] M. Kartal, M. Uysal, H. Gül, A. Alp, H. Akbulut, *Appl. Surf. Sci.* **354**, 328 (2015)
- [11] E. Beltowska-Lehman, P. Indyka, A. Bigos, M. Szczerba, M. Kot, *Mater. Des.* **80**, 1 (2015)
- [12] C. Lee, *Tribol. Trans.* **55**, 640 (2012)
- [13] X. Guo, K. Song, S. Liang, X. Wang, Y. Zhang, *Tribol. Trans.* **57**, 283 (2014)
- [14] K. Dass, S. Chauhan, B. Gaur, *Tribol. Trans.* **57**, 157 (2014)
- [15] L. Xu, S. Wei, Q. Liu, G. Zhang, J. Li, *Tribol. Trans.* **56**, 833 (2013)
- [16] I. Imanieh, E. Yousefi, A. Dolati, M. Mohammadi, *Acta Metall. Sin. (Engl. Lett.)* **26**, 558 (2013)
- [17] M. Sheng, C. Lv, L. Hong, M. Shao, K. Wan, F. Lv, *Acta Metall. Sin. (Engl. Lett.)* **26**, 735 (2013)
- [18] Q. Zhou, C.L. He, Q.K. Cai, *Adv. Mater. Res.* **79**, 631 (2009)
- [19] T. Borkar, S.P. Harimkar, *Surf. Coat. Technol.* **205**, 4124 (2011)
- [20] L. Chen, L. Wang, Z. Zeng, T. Xu, *Surf. Coat. Technol.* **201**, 599 (2006)
- [21] R. Ahmed, M. Hadfield, *Surf. Coat. Technol.* **82**, 176 (1996)
- [22] R. Ahmed, *Wear* **253**, 473 (2002)
- [23] R. Ahmed, M. Hadfield, *Wear* **220**, 80 (1998)
- [24] S. Stewart, R. Ahmed, *Wear* **253**, 1132 (2002)
- [25] Z.A. Khan, M. Hadfield, S. Tobe, Y. Wang, *Ceram. Int.* **32**, 751 (2006)
- [26] Z.A. Khan, M. Hadfield, Y. Wang, *Mater. Des.* **26**, 680 (2005)
- [27] Z.A. Khan, M. Hadfield, S. Tobe, Y. Wang, *Mater. Sci. Eng., A* **404**, 221 (2005)
- [28] Z.A. Khan, M. Hadfield, *Mater. Des.* **28**, 2688 (2007)
- [29] C. Ramesh, M. Shreeshail, G. Harsha, K. Zulfiqar, *Mater. Sci. Forum* **773**, 547 (2014)
- [30] R.S. Bajwa, Z. Khan, V. Bakolas, W. Braun, J. Adhes. Sci. Technol., 1–13 (2015). doi:10.1080/01694243.2015.1117276
- [31] E. Lugscheider, K. Bobzin, *Surf. Coat. Technol.* **142**, 755 (2001)
- [32] K. Johnson, *Contact Mechanics* (Cambridge University Press, Cambridge, 1974)
- [33] G. Cui, Q. Bi, S. Zhu, L. Fu, J. Yang, Z. Qiao, W. Liu, *Wear* **303**, 216 (2013)
- [34] D.K. Owens, R. Wendt, *J. Appl. Polym. Sci.* **13**, 1741 (1969)
- [35] A. Leyland, A. Matthews, *Wear* **246**, 1 (2000)
- [36] L. Benea, S.-B. Başa, E. Dănilă, N. Caron, O. Raquet, P. Ponthiaux, J.-P. Celis, *Mater. Des.* **65**, 550 (2015)
- [37] Q. Feng, T. Li, H. Teng, X. Zhang, Y. Zhang, C. Liu, J. Jin, *Surf. Coat. Technol.* **202**, 4137 (2008)
- [38] C. Ramesh, H. Adarsha, S. Pramod, Z. Khan, *Mater. Des.* **50**, 597 (2013)
- [39] M. Grischke, A. Hieke, F. Morgenweck, H. Dimigen, *Diam. Relat. Mater.* **7**, 454 (1998)

Effect of Bath Ionic Strength on Adhesion and Tribological Properties of Pure Nickel and Ni-Based Nanocomposite Coatings

Rizwan Sarwar Bajwa, Zulfiqar Khan, Vasilios Bakolas & Wolfgang Braun

Journal of Adhesion Science and Technology, First online 30 Nov 2015,
30 (6), 653-665, [DOI:10.1080/01694243.2015.1117276](https://doi.org/10.1080/01694243.2015.1117276).

Effect of bath ionic strength on adhesion and tribological properties of pure nickel and Ni-based nanocomposite coatings

Rizwan Sarwar Bajwa^a, Zulfiqar Khan^a, Vasilios Bakolas^b and Wolfgang Braun^b

^aFaculty of Science & Technology, Sustainable Design Research Centre, Bournemouth University, Poole, UK;

^bAdvanced Bearing Analysis, Schaeffler Technologies GmbH & Co. KG, Herzogenaurach, Germany

ABSTRACT

The effect of electrolytic chemical concentration on wear-resistance, corrosion-resistance, adhesion and wettability properties of pure nickel and nickel–alumina composite coatings has been investigated in this paper. Coatings were electroplated over steel substrates under constant pulse conditions using pulse electrodeposition technique. Corrosion-resistance results show that the anti-corrosion properties are increasing with medium concentration (MC) both for pure nickel and nickel–alumina composite coating. For anti-wear properties, the MC showed increasing trend in case of pure nickel coatings but decreased in nickel–alumina composite coatings. In composite coating, the higher and low concentrations of electrolyte showed the higher wear resistance properties. Furthermore, the influence of electrolyte concentration on changing surface morphologies, mechanical, wettability and adhesion properties have been investigated and reported here. Surface morphologies of the synthesized coatings were studied with scanning electron microscopy (SEM) and energy-dispersive spectroscopy. Coatings surface mapping and wear analyses were examined by using 3D white light interferometry.

ARTICLE HISTORY

Received 18 August 2015
 Revised 21 October 2015
 Accepted 3 November 2015

KEYWORDS

Wear-resistance; corrosion resistance; adhesion; water-lubrication

1. Introduction

Electrodeposited composite coatings incorporating hard nanoparticle oxides as Al₂O₃, [1,2] ZrO₂, [3,4] TiO₂, [5] Fe₂O₃, [6] CeO₂ [7] and carbides as SiC [8,9] or WC [10] demonstrated excellent tribological and mechanical properties with wide-ranging industrial applications in engineering.

The electrodeposition techniques provide a freedom of controlling a variety of coating parameters with enhanced mechanical and tribological properties. This freedom allows significant contribution for the design of nanocomposite coatings in terms of surface engineering. Due to wide range of experimental parameters in pulse electrodeposition technique, many experimental results presented in the literature are contradictory or difficult to compare. [11–13] There are two main types of electrodeposition conditions (1) pulse

CONTACT Rizwan Sarwar Bajwa  rbajwa@bournemouth.ac.uk

© 2015 Taylor & Francis

2  R. S. BAJWA ET AL.

parameters which include current density, pulse-on time/pulse-off time, duty cycle and frequency and (2) bath conditions; these include bath composition, additives, pH, temperature and composite micro-/nano-sized particles. Extensive studies have been conducted with improved mechanical and tribological properties of electrodeposited coatings by properly controlling these parameters.[14–19] However, the effect of ionic strength of electrolyte solution on wear-resistance and corrosion-resistance properties left obscure and needs to be explored due to their utmost important in wide range of industrial applications as a wear and corrosion resistance protective coatings.

This work is the continuation of research within our group.[20–24] The purpose of this investigation is to demonstrate an optimized bath concentration for electrodeposited coatings in terms of improved tribological and mechanical properties for water-lubricated tribological systems/components. Previously, Lehman and co-workers have conducted experimental investigations to understand the influence of electrolyte composition on the electrodeposited coatings.[25] They presented that lower ionic concentration contribute to better deposition with respect to microstructure and better dispersion of particles in matrix of pure nickel and Ni–Al₂O₃ composite coatings. The effect of bath volume for electrodeposition was explored by Oloruntoba et al. [26]. Their findings were that the high volume of bath solution progressively increased the deposition rate of nickel coating through electrodeposition process. They investigated the microstructure and mechanical properties analysis of the coatings without tribological performance measures.

During the current work, electrolytes were prepared with three varying strengths (high, medium and low concentrations) in total six baths (every two baths with same strength) for electrodeposition of Ni–Al₂O₃ composite and pure nickel coatings.

The tribological properties of these coatings investigated using High Speed Microprocessor Rotary Tribometer (HSMRT) to simulate industrial applications in terms of rolling contacts. Pure nickel coatings were manufactured as a reference coating and investigated under the same chemical and tribo test conditions.

2. Experimental methods

2.1. Preparation and characterization of coatings

All coatings, the pure nickel and the composites incorporating nano-Al₂O₃, were deposited under constant pulse parameters as; current density 3 A/dm², pulse on/off time 20/80 ms, respectively, and with a duty cycle of 20% with expected thickness of ~10 μm.

The Watt's-type bath is prepared with different ionic strength of bath solution as high concentration (HC), medium concentration (MC) and low concentration (LC) for both pure nickel and composite coatings. 20 g/L of nano-alumina (~50 nm) supplied by Io-Li-Tec (Germany) was added to bath for developing composite coatings. The solutions had been magnetically stirred overnight to yield better suspension prior to the start of the deposition process. In addition, these nanoparticles were ultrasonically dispersed in the electrolyte during the deposition process. The composition of chemical within the bath included nickel sulphate, nickel chloride, boric acid and nanoparticles which are provided in Table 1.

Nickel sheet (99.99% purity) was used as anode and a steel substrate (80 mm diameter and 8.20 mm thick) was used as a cathode. The chemical composition of steel substrate is given in Table 2. The substrate disc with a surface area (0.70 dm²) to be deposited was

Table 1. Chemical and nanoparticles composition for varying bath concentration.

Bath number	Chemical composition (g/L)			
	Nickel sulphate	Nickel chloride	Boric acid	Nano-Al ₂ O ₃
		High concentration (HC)		
1	331	60	38	–
2	331	60	38	20
		Medium concentration (MC)		
3	265	48	31	–
4	265	48	31	20
		Low concentration (LC)		
5	200	48	31	–
6	200	48	31	20

Table 2. Chemical composition of the steel substrate.

C (wt.%)	Si (wt.%)	Mn (wt.%)	S (wt.%)	P (wt.%)
0.14	0.27	0.91	0.25	0.02

mechanically polished to achieve naked substrate constant roughness (Ra) of 0.05 μm for all samples. The surface area which was not required to be electroplated was sealed with polyvinyl chloride. Prior to each coating deposition, the substrate surface conditioning was performed using deionized water and acetone under ultrasonic treatment. The pH of the bath was adjusted between 4.0 and 4.5 by sodium hydroxide or diluted sulphuric acid and recorded using Tecpel pH meter. The surface roughness measurements were performed by using three-dimensional scanning interferometry (ZYGO). The roughness parameters Ra and Rz, defined as the arithmetic mean of roughness profile and sum of maximum values of profile peak height and depth, respectively, over the entire sampling length.

Scanning Electron Microscopy (JSM-6010, JEOL) was used to analyse the surface morphology of the coatings. For cross-sectional view of coating–substrate interface adhesion the samples were imbedded by ATM OPAL 460 equipment keeping coatings cross-sectional areas on top. Mechanical properties including hardness and elastic modulus of coatings were calculated by using CSM Micro Indentation Tester (MHT) at a loading force of 300 mN. At least 12 indentations were made on each sample and average value is report with error bars.

2.2. Tribological and anti-corrosion properties testing

The wear resistance tests conducted using a ball-on-plate machine assembled to a HSMRT and described in [27]. The unidirectional ball-on-disc tribometer consists of upper coated disc and lower three steel balls (100Cr6) equally spaced at 120°. Previously, such ball-on-plate rig have been used to study rolling contact fatigue response when ball is in rolling contact with a flat surface. [28,29] The hardness and elastic modulus of ball was 740 + 140 HV10 and 210 GPa, respectively. All tests performed in distilled water at a rolling speed of 1 m/s and normal load of 45 N under boundary/mixed lubrication regimes condition. The corresponding Hertzian contact pressure [30] can be estimated to 1.75 GPa, assuming contact between steel ball (210 GPa, Poisson's ratio 0.30) and coated flat disc (230 GPa, Poisson's ratio 0.28 [31]).

The cross-sectional area of worn surface was measured by using a three-dimensional surface profiler (ZYGO) to calculate the amount of wear of the coating. The wear volume is defined as $V = AL$, where A is the cross-sectional area of wear track (mm^2) and L is the length of the wear track (mm). A specific wear rate was determined as: Specific wear rate (mm^3/Nm) = wear volume (mm^3)/[load (N) \times rolling distance (m)]. [32] To ensure repeatability and to minimize uncertainty, each test was performed at least two times under the same testing conditions.

The potentiodynamic anodic polarization measurements were carried out using three-electrode system with a platinum wire as counter electrode and Ag+/AgCl electrode as reference electrode. The coated samples were used as working electrode. The coated specimens were immersed in 3.5 wt.% NaCl electrolyte at a temperature of 20 °C till the open circuit potential (OCP) was stable before starting the test at scanning rate 0.001 V/s. The corrosion resistance properties of the coatings were studied from potentiodynamic anodic polarization curves.

2.3. Adhesion and wettability testing

The scratch testing method was used to study the adhesion of coating according to DIN EN 1071-3 standard method (Determination of adhesion and other mechanical failure modes by a scratch test). The scratch tests were conducted using a CSM REVETEST machine with Rockwell C diamond with a tip radius of 200 μm . The scratch length of 10 mm was made with sliding speed of 10 mm/min. The load was increased from 0 N to 100 N/min. The smallest load at which first failure mode was observed defined critical load value.

The wettability behaviour of coatings was studied using Owens and Wendt (OWRK) method. [33] To ensure the statistical validity of the results, two to three droplets were made for contact angle measurements using water and diiodomethane as reference liquids of known surface energies. The determination of the surface energies of the solid coatings based on contact angle measurements methodology is explained in detail elsewhere. [34]

3. Results and discussion

3.1. Surface morphology and mechanical properties

Figure 1 compares the engineered surfaces through SEM micrographs of which were produced by using various bath concentrations (HC, MC and LC). As can be seen from Figure 1, in case of HC and MC the surface morphologies of nickel and nickel composite coatings were not affected with deposition from different concentration of ionic strength of electrolyte. Whilst, for coatings deposited from LC concentration resulted into bigger grain structure and agglomeration clusters in pure nickel and Ni–alumina composite coatings, respectively. This change in morphology subject to lower concentration of bath was also evident from surface roughness parameters (R_a and R_z), shown in Figure 2. Due to the presence of agglomerated particles, Ni– Al_2O_3 (LC) composite exhibits the maximum surface roughness ($R_a \sim 0.64 \mu\text{m}$; $R_z \sim 4.36 \mu\text{m}$), followed by pure nickel (LC) coatings with $R_a \sim 0.08 \mu\text{m}$ and $R_z \sim 0.98 \mu\text{m}$ because of bigger grain structure. Agglomerated particles on the surface resulted in larger standard deviation value of roughness parameters of Ni– Al_2O_3 (LC) composite coating. It was interesting to note that similar behaviour was observed in microhardness results of these coatings with variation in ionic strength of electrolyte. Likewise, there were not

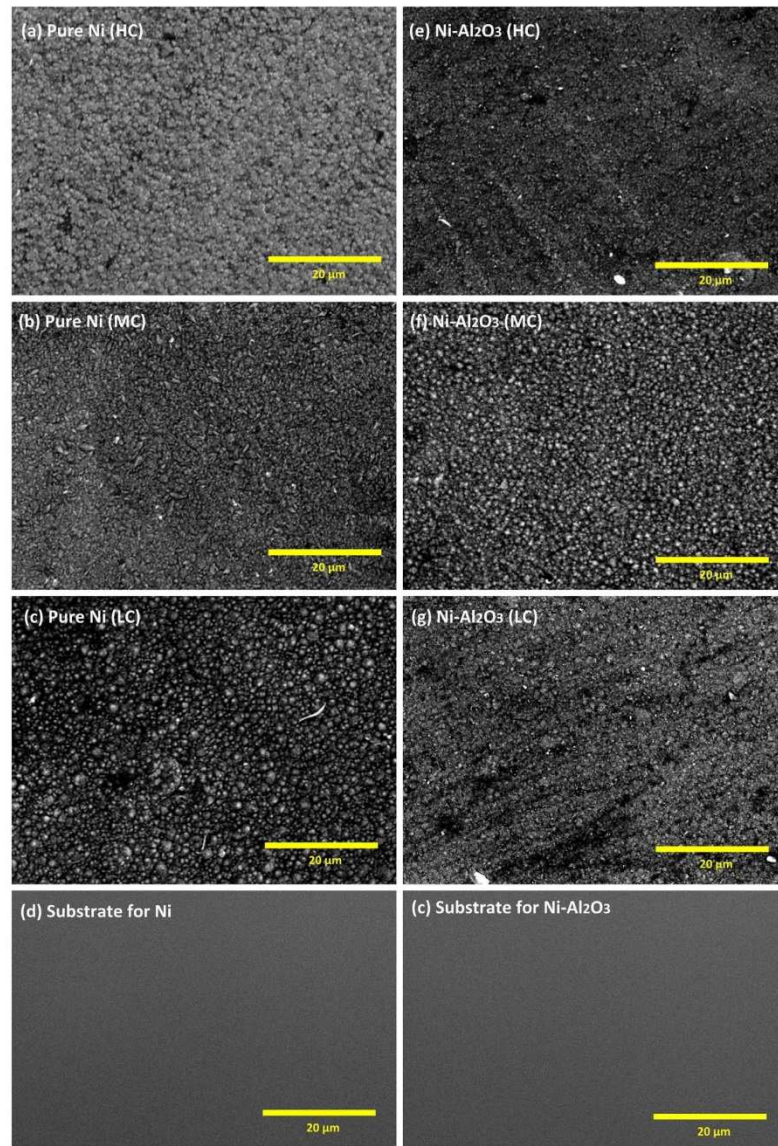


Figure 1. Surface micrographs of pure nickel (a–c) and Ni–Al₂O₃ composite (e–g) coatings deposited through various bath concentrations (10 kV, WD 11 and $\times 2000$).

significant differences in measured hardness (350–450 HV), deposited from HC and MC strength for both pure and composite coatings except the LC type coatings (Figure 3).

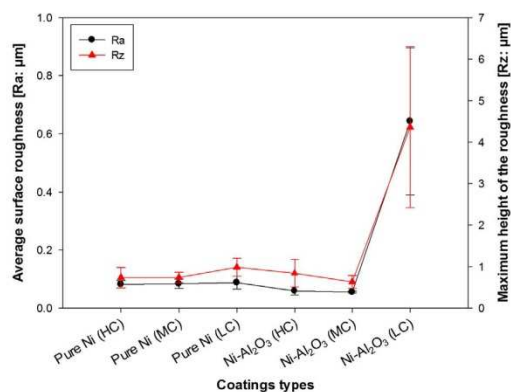


Figure 2. The variation in surface roughness parameters (Ra and Rz) of electrodeposited coatings with different electrolyte ionic strength.

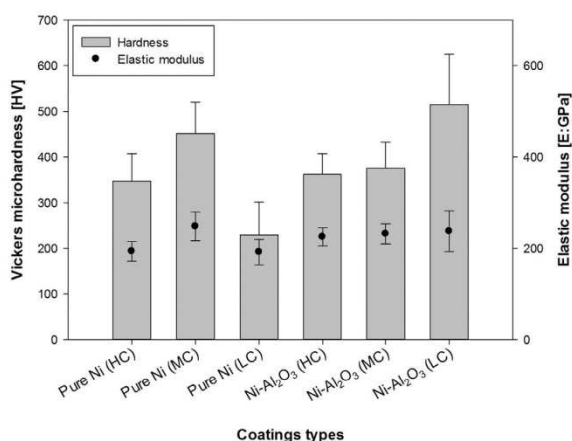


Figure 3. Hardness and elastic modulus values of all coatings deposited from different bath concentration.

The reason for the highest hardness for pure Ni (MC) when compared to pure Ni (HC) and pure Ni (LC) can be attributed to relatively much finer, more compact and smaller grain size morphology as shown in Figure 1(a)–(c). The microhardness of Ni–Al₂O₃ (LC) was significantly improved in LC bath with average value of 515 HV as compared to pure nickel deposited from LC bath with average value of 230 HV. The maximum value of hardness in Ni–alumina composite deposited LC type bath predicts better anti-wear performance of these coatings. However, the higher surface roughness parameters of these type of coatings can be attributed to surface friction which can be reduced through surface polishing prior to real applications. Note that the samples were mechanically polished to achieve relative

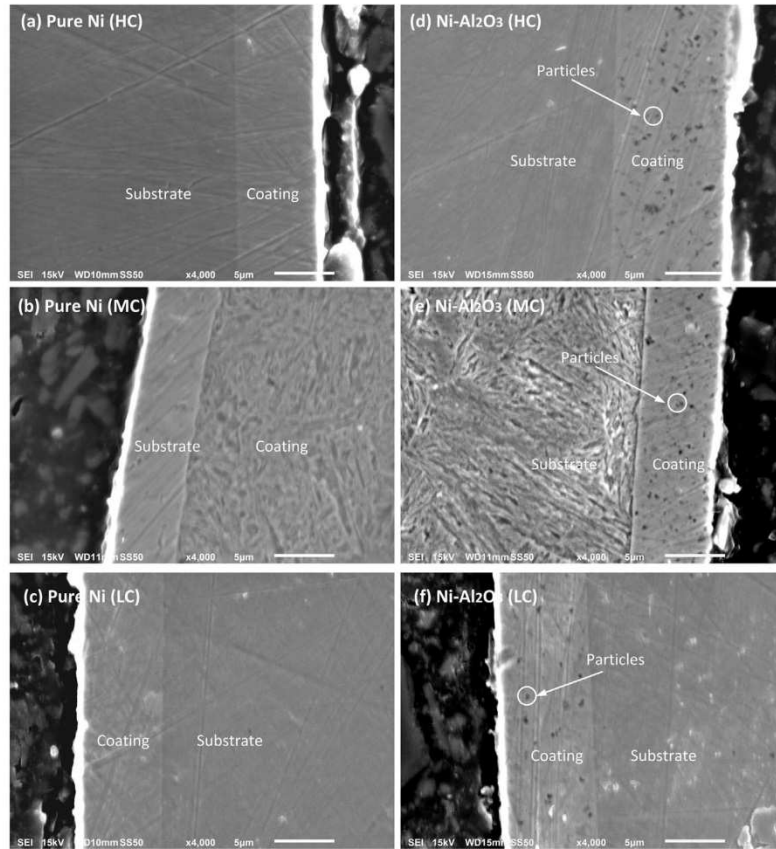


Figure 4. Cross-sectional SEM images of pure nickel and nickel-based composite coatings electrodeposited with different electrolyte ionic strength.

smoother surface prior to mechanical testing. This is because the roughness peak coming in contact to indenter can result in a greater depth of indent at relatively lower load due to increased localized stress at the point of contact.

In comparison, the typical pyramidal and spherical globular shape microstructure morphologies observed in pure nickel and nickel-based composite coatings, respectively. Similar morphologies in nickel and nickel-based composite have been reported previously by different researchers.[35–38] Moreover, addition of alumina nanoparticles in nickel matrix resulted into the compact morphology as compared to pure nickel coatings. This attributed to well-known cathodic polarization phenomenon due to the adsorption of particles at substrate surface. All pure nickel and nickel-based coatings were smooth, crack free and adhered well to the substrate without an interfacial delamination as shown in Figure 4(a)–(f). To see the effect of electrolyte concentration on nano-alumina particles

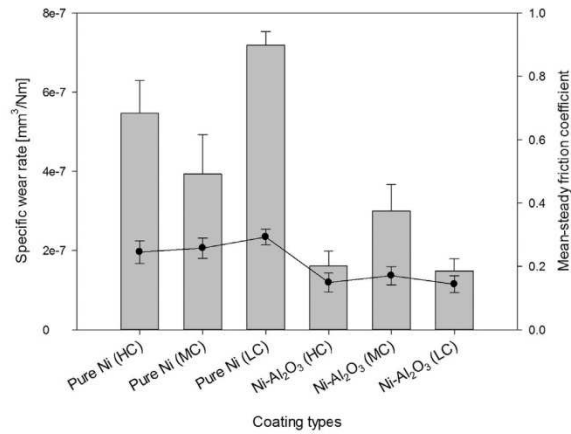


Figure 5. The comparison of wear rates and mean-steady friction coefficient of pure nickel and nickel composite coatings electrodeposited with different electrolyte ionic strength.

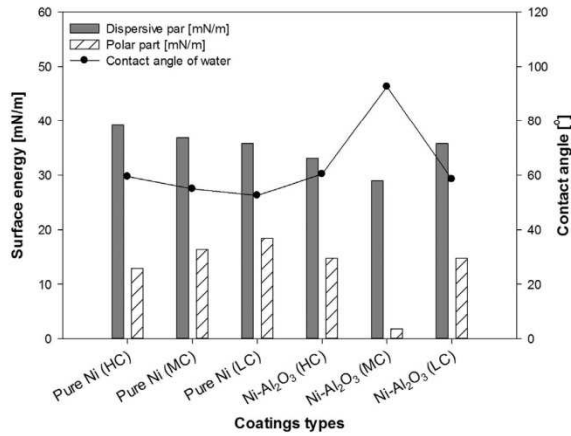


Figure 6. The comparison of the surface energy and changing wettability behaviour of electrodeposited coatings with different electrolyte ionic strength.

distribution in composite coatings magnified view of cross-sectional images is presented in Figure 4(d)–(f). All composite coatings exhibit the homogenous nano-alumina particles distribution. However, less agglomerated nano-Al₂O₃ particles were observed in LC type coatings than those produced by HC and MC type electrolyte. In addition to homogenous particle distribution, the less agglomeration behaviour can be the reason for the higher hardness value of Ni–Al₂O₃ (LC) coating.

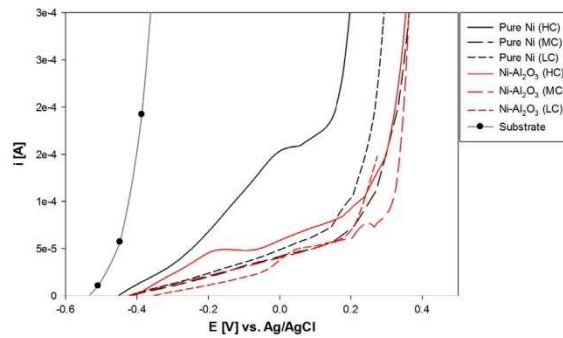


Figure 7. Potentiodynamic polarization curves for electroplated coatings deposited with different electrolytic strength, in 3.5% NaCl solution.

3.2. Tribological and wettability properties

Generally, the wear-resistance properties of electroplated coatings improved with addition of hard nanoparticles into matrix materials as can be seen from Figure 5. This is attributed to the strengthening effects of loaded hard particles into nickel matrix and in agreement with previous findings.[3,39,40] The influence of reagent concentration on pure nickel coatings demonstrated that the MC type coating has less wear about 30% than HC and about half of LC type coatings. A reason for this can be the higher hardness of MC as compared to HC and LC type's coatings. Also, the higher plasticity index H/E ratio of pure Ni (MC) than those pure Ni (HC) and pure Ni (LC) can result in better wear resistance properties.[41] A comparison between composite coatings showed that HC and LC type composites exhibit the similar wear-resistance behaviour and almost half of the composite coating deposited from MC electrolyte. When compared with pure nickel coatings, the wear resistance of composite coating is improved, almost doubled, except MC type which enhanced about 25% of the MC type pure nickel coating. Also, mean-steady friction coefficient values are lower for composite coatings than that of pure nickel coatings, as can be seen in Figure 5. The strengthening effect of incorporated nano-alumina particle is the reason for the lower friction coefficient of composite coatings. It is known that the friction coefficient in composite coatings was reduced with increasing the reinforcement content of nanoparticles in the coatings.[3,42] The higher wear rate in MC type composite coating may be due to the lower surface wettability behaviour, resulting in dry contact wear scenario. The effect of changing bath concentration on coatings surface wettability behaviour plotted in Figure 6. In all coatings, the higher dispersive part than polar part of surface free energy reveals that coatings exhibit mainly covalent bonds. However, MC type nickel alumina composite showed the minimum value of polar component, consequently the maximum contact angle of water was observed. This can be the one reason for higher wear rate than other composite coatings due to decreased wettability. These results indicate that in order to achieve better anti-wear properties, MC composition is suitable in pure nickel coatings. On the other hand, HC and LC electrolytes can produce better wear resistance properties in nickel-based composite coatings reinforced with nano-alumina particles.

10 R. S. BAJWA ET AL.

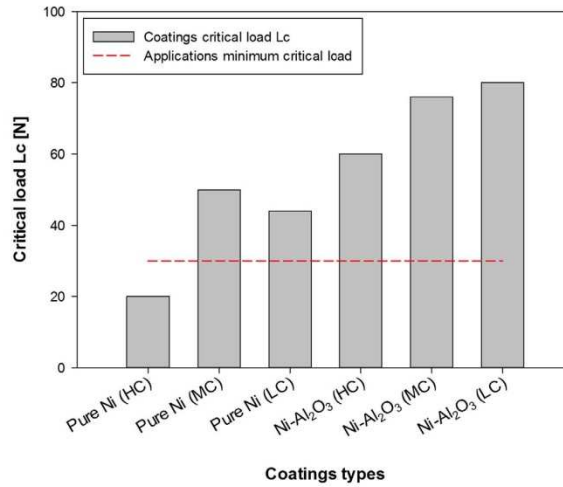


Figure 8. Critical load values for electroplated coatings deposited with different electrolytic strength according to DIN EN 1071-3.

3.3. Electrochemical corrosion-resistance properties

To evaluate the optimized bath concentration for pure nickel and nickel composite coatings, the electrochemical corrosion measurements deployed and resulting potentiodynamic polarization curves are plotted in Figure 7. As can be seen from Figure 7, under the same conditions the composite coatings showed better anti-corrosion property than pure nickel coatings and validates the previous finding in the literature.[43] It is interesting to observe that the coatings deposited from MC type electrolyte exhibits the maximum corrosion resistance potential both in pure nickel and nickel-based nano-alumina composites. Note that in pure nickel coatings deposited from MC bath also performed better in term of wear resistance. Therefore, MC is suitable solution to get better wear and corrosion resistance properties for pure nickel coatings. For Ni-Al₂O₃ composite coatings the MC better candidate to corrosion resistance but not suitable for wear resistance in comparison to HC and LC solutions. However, the corrosion performance of LC type composite coatings can be improved by surface polishing to reduce surface roughness which can be the main reason for poor corrosion resistance behaviour. This is well known that the roughness valleys in the surface can provide weak point for the penetration of aggressive corrosive solution towards substrate and can result in poor corrosion resistance performance.

3.4. Adhesion strength properties

The coating-substrate interface adhesion strength is one of the important factors of the coating in industrial applications. Therefore, adhesion strength was evaluated through scratch test for these coatings and compared with minimum critical load value required in industrial applications. The effects of different bath conditions on adhesion critical load values (L_c) for

electrodeposited coatings are compared and presented in Figure 8. As can be seen, all the coatings showed good adhesion strength except in the case of pure nickel deposited from HC electrolyte. In pure nickel coatings the maximum critical load value of 44 N observed in MC type bath and followed by LC and HC with values 50 and 44 N, respectively. For nickel composite coatings, the critical load values range between 60 and 80 N which is significantly higher than pure nickel coatings. Note that these coatings were deposited on mild steel substrate without any intermediate coating which can further improve adhesion strength.

4. Conclusions

Tribological and adhesion properties of electrodeposited pure nickel and nickel composite coatings with incorporated nano-alumina particle coatings have been studied. The effects of different ionic strength of electrolyte on these properties investigated to evaluate optimized concentration of bath. The following conclusions can be drawn from experimental results.

- In general, the influence of bath concentration on surface morphology and mechanical properties of all coatings was much significant. However, MC and LC type baths showed better hardness values in pure nickel and nickel–alumina composites, respectively.
- Wear-resistance properties increase with HC and LC type bath in nickel–alumina composite coatings. Whereas, wear-resistance properties decreased in HC and LC type and increased in MC type bath.
- The electrochemical corrosion results show that the MC type bath is suitable candidate to achieve increased corrosion resistance properties both in pure nickel and nickel composite coatings.
- The scratch tests show that independent from bath type, the adhesion significantly increases with incorporation of nanoparticles into nickel matrix. The minimum adhesion strength observed in LC type pure nickel coatings.

Disclosure statement

No potential conflict of interest was reported by the authors.

Funding

This work was supported with financial and kind support from Schaeffler Technologies GmbH & Co. KG (Germany) and Bournemouth University (UK) as part of a collaborative research programme.

References

- [1] Lee C. Wear and corrosion behavior of electrodeposited nickel–carbon nanotube composite coatings on Ti–6Al–4V alloy in Hanks' solution. *Tribol. Int.* 2012;55:7–14.
- [2] Lee C. Corrosive wear and mechanical properties of Ni/Al₂O₃ micro- and nanoparticulates-reinforced coatings on Ti–6Al–4V alloy. *Tribol. Trans.* 2012;55:640–651.
- [3] Borkar T, Harimkar SP. Effect of electrodeposition conditions and reinforcement content on microstructure and tribological properties of nickel composite coatings. *Surf. Coat. Technol.* 2011;205:4124–4134.

- [4] Dass K, Chauhan S, Gaur B. Study on mechanical and dry sliding wear characteristics of meta-cresol novalac epoxy composites filled with silicon carbide, aluminum oxide, and zinc oxide particulates. *Tribol. Trans.* 2014;57:157–172.
- [5] Lajevardi S, Shahrabi T. Effects of pulse electrodeposition parameters on the properties of Ni–TiO₂ nanocomposite coatings. *Appl. Surf. Sci.* 2010;256:6775–6781.
- [6] Haq IU, Akhtar K, Khan TI, et al. Electrodeposition of Ni–Fe₂O₃ nanocomposite coating on steel. *Surf. Coat. Technol.* 2013;235:691–698.
- [7] Xue Y-J, Liu H-B, Lan M-M, et al. Effect of different electrodeposition methods on oxidation resistance of Ni–CeO₂ nanocomposite coating. *Surf. Coat. Technol.* 2010;204:3539–3545.
- [8] Rudnik E, Burzyńska L, Dolasiński Ł, et al. Electrodeposition of nickel/SiC composites in the presence of cetyltrimethylammonium bromide. *Appl. Surf. Sci.* 2010;256:7414–7420.
- [9] Pradhan AK, Das S. Dry sliding wear and friction behavior of Cu–SiC nanocomposite coating prepared by pulse reverse electrodeposition. *Tribol. Trans.* 2014;57:46–56.
- [10] Surender M, Basu B, Balasubramaniam R. Wear characterization of electrodeposited Ni–WC composite coatings. *Tribol. Int.* 2004;37:743–749.
- [11] Hovestad A, Janssen L. Electrochemical codeposition of inert particles in a metallic matrix. *J. Appl. Electrochem.* 1995;25:519–527.
- [12] Gomes A, Pereira I, Fernández B, et al. Electrodeposition of metal matrix nanocomposites: improvement of the chemical characterization techniques. In: Reddy B, editor. *Advances in nanocomposites-synthesis, characterization and industrial applications*. Rijeka: InTech; 2011. p. 503–526.
- [13] Golchin A, Simmons G, Glavatskih S, et al. Tribological behaviour of polymeric materials in water-lubricated contacts. *Proc. Inst. Mech. Eng., Part J: J. Eng. Tribol.* 2013;227:811–825.
- [14] Low C, Wills R, Walsh F. Electrodeposition of composite coatings containing nanoparticles in a metal deposit. *Surf. Coat. Technol.* 2006;201:371–383.
- [15] Chandrasekar M, Pushpavanam M. Pulse and pulse reverse plating – conceptual, advantages and applications. *Electrochim. Acta.* 2008;53:3313–3322.
- [16] Scharf T, Prasad S. Solid lubricants: a review. *J. Mater. Sci.* 2013;48:511–531.
- [17] Balasubramanian A, Srikumar D, Raja G, et al. Effect of pulse parameter on pulsed electrodeposition of copper on stainless steel. *Surf. Eng.* 2009;25:389–392.
- [18] Rashidi A, Amadeh A. Effect of electroplating parameters on microstructure of nanocrystalline nickel coatings. *J. Mater. Sci. Technol.* 2010;26:82–86.
- [19] Xuetao Y, Yu W, Dongbai S, et al. Influence of pulse parameters on the microstructure and microhardness of nickel electrodeposits. *Surf. Coat. Technol.* 2008;202:1895–1903.
- [20] Nazir M, Khan ZA, Stokes K. Optimisation of interface roughness and coating thickness to maximise coating–substrate adhesion – a failure prediction and reliability assessment modelling. *J. Adhes. Sci. Technol.* 2015;29:1415–1445.
- [21] Khan ZA, Pashaei P, Bajwa R, et al. Fabrication and characterisation of electropdeposited and magnetrton-sputtered thin films. *Int. J. Comput. Methods Exp. Meas.* 2015;3:1–10.
- [22] Nazir M, Khan ZA, Stokes K. A holistic mathematical modelling and simulation for cathodic delamination mechanism – a novel and an efficient approach. *J. Adhes. Sci. Technol.* 2015;29:1–39.
- [23] Nazir M, Khan ZA, Stokes K. A unified mathematical modelling and simulation for cathodic blistering mechanism incorporating diffusion and fracture mechanics concepts. *J. Adhes. Sci. Technol.* 2015;29:1200–1228.
- [24] Nazir M, Khan Z, Stokes K. Modelling of metal-coating delamination incorporating variable environmental parameters. *J. Adhes. Sci. Technol.* 2015;29:392–423.
- [25] Bełtowska-Lehman E, Goral A, Indyka P. Electrodeposition and characterization of Ni/Al₂O₃ nanocomposite coatings. *Arch. Metall. Mater.* 2011;56:919–931.
- [26] Oloruntoba D, Eghwubare O, Oluwole O. Effect of some process variables on nickel electroplating of low carbon steel. *Leonardo Electron. J. Pract. Technol.* 2010;18:79–94.
- [27] Khan ZA, Hadfield M, Wang Y. Pressurised chamber design for conducting rolling contact experiments with liquid refrigerant lubrication. *Mater. Des.* 2005;26:680–689.

- [28] Kikuchi K, Yoshioka T, Kitahara T, et al. Rolling contact fatigue life of ceramics for rolling bearing materials. *Jpn. Soc. Lubr. Eng., J. Int. Ed.* 1984;5:137–142. (ISSN 0389-5483).
- [29] Fujiwara T, Yoshioka T, Kitahara T, et al. Study on load rating property of silicon nitride for rolling bearing material. *Jpn. Soc. Lubr. Eng., J. Int. Ed.* 1989;33:81–86.
- [30] Johnson K. *Contact mechanics*. 1985. Cambridge: Cambridge University Press; 1974.
- [31] Lille H, Koo J. Determination of the modulus of elasticity, Poisson's ratio and the coefficient of thermal expansion of electrochemically metallized nickel coatings. *Mater. Sci.* 2005;11:356–359.
- [32] Cui G, Bi Q, Zhu S, et al. Synergistic effect of alumina and graphite on bronze matrix composites: tribological behaviors in sea water. *Wear.* 2013;303:216–224.
- [33] Owens DK, Wendt R. Estimation of the surface free energy of polymers. *J. Appl. Polym. Sci.* 1969;13:1741–1747.
- [34] Lugscheider E, Bobzin K. The influence on surface free energy of PVD-coatings. *Surf. Coat. Technol.* 2001;142–144:755–760.
- [35] Jegan A, Venkatesan R. Characterization and optimization of pulse electrodeposition of Ni/nano- Al_2O_3 composite coatings. *Int. J. Miner. Metall. Mater.* 2013;20:479–485.
- [36] Jung A, Natter H, Hempelmann R, et al. Nanocrystalline alumina dispersed in nanocrystalline nickel: enhanced mechanical properties. *J. Mater. Sci.* 2009;44:2725–2735.
- [37] Thiemig D, Lange R, Bund A. Influence of pulse plating parameters on the electrocodeposition of matrix metal nanocomposites. *Electrochim. Acta.* 2007;52:7362–7371.
- [38] Thiemig D, Bund A. Influence of ethanol on the electrocodeposition of Ni/ Al_2O_3 nanocomposite films. *Appl. Surf. Sci.* 2009;255:4164–4170.
- [39] Wang S-C. Characterization of electroplated Ni/SiC and Ni/ Al_2O_3 composite coatings bearing nanoparticles. *J. Mater. Res.* 2003;18:1566–1574.
- [40] Wielage B, Lampke T, Zacher M, et al. Electroplated nickel composites with micron-to nano-sized particles. Zurich: *Trans Tech*; 2008. p. 283–309.
- [41] Wang Q, Zhou F, Ding X, et al. Microstructure and water-lubricated friction and wear properties of CrN(C) coatings with different carbon contents. *Appl. Surf. Sci.* 2013;268:579–587.
- [42] Fan H. Electroplating of compound Ni–SiC coatings and improvement of wear resistance. Zurich: *Trans Tech*; 2010. p. 399–402.
- [43] Feng Q, Li T, Teng H, et al. Investigation on the corrosion and oxidation resistance of Ni– Al_2O_3 nano-composite coatings prepared by sediment co-deposition. *Surf. Coat. Technol.* 2008;202:4137–4144.

Wear and Friction Properties of Electrodeposited Ni-based
Coatings Subject to Nano-enhanced Lubricant and Composite
Coating

Rizwan Bajwa, Zulfiqar Khan, H Nazir, Vivek Chacko and Adil Saeed

Acta Metallurgica Sinica (English Letters),
DOI 10.1007/s40195-016-0470-6,
Accepted: 7th July 2016.



Wear and Friction Properties of Electrodeposited Ni-Based Coatings Subject to Nano-enhanced Lubricant and Composite Coating

Rizwan Bajwa¹ · Zulfiqar Khan¹ · H. Nazir¹ · Vivek Chacko¹ · Adil Saeed¹

Received: 10 April 2016/Revised: 13 June 2016
© The Chinese Society for Metals and Springer-Verlag Berlin Heidelberg 2016

Abstract This paper presents research findings on the tribological performance of electrodeposited coatings subject to nano-lubricants with the addition of nano-Al₂O₃ and graphene and Ni/nano-Al₂O₃ composite coatings. Electrodeposited coatings were produced by using a pulse electrodeposition method. Tribological experiments were conducted by using a linear reciprocating ball on flat sliding tribometer. Experimental results confirmed that the wear and friction resistance properties were significantly enhanced by doping of nano-effects in the lubricating oil and composite coating. The addition of Al₂O₃ nanoparticles in the lubricating oil showed the best tribological properties, followed by Ni-Al₂O₃ composite coatings and nano-oil with graphene. The surface morphology and microstructure of electrodeposited coatings were examined by scanning electron microscopy, energy-dispersive spectroscopy and X-ray diffraction. The wear mechanisms of these coatings subjected to tribological testing were investigated by post-test surface analyses. This research provides a novel approach to design durable nano-coatings for tribological applications in various industries such as automotive, aerospace, locomotive and renewable energy technologies.

KEY WORDS: Tribology; Nanoparticles; Graphene; Nano-additives; Nano-coatings

1 Introduction

This paper enables researchers to fully understand the advantages of two distinct approaches of nano-additives within lubricants and nano-coatings, to solve complex tribological issues in terms of design for durability and reliability. Optimisation of surfaces in contact and in relative motion is needed to enhance their tribological performance. This research is focus on enhancing the tribological performance of contact surfaces through nano-composite coatings and nano-additives in lubrication. Almost one-

third of the energy losses in mechanically interacting systems or components are attributed to friction or wear behaviour. For a long time, oil lubricants or greases have been used to reduce these frictional forces and wear asperities between two interacting surfaces. In recent years, nanoparticles have been widely studied in various applications due to their unique wear, friction and corrosion resistant properties. Nanoparticles are used both as an additive in the lubricant oil and as a metal matrix nano-composite (MMC) materials. The term nano-additive is commonly used for nanoparticles when they are used as an additive to conventional lubricants. Many studies have reported an effective role of nano-additives in lubricants in terms of the improvement of anti-friction and anti-wear properties of materials [1–3]. These nano-additives are made up of nano-sized metals [4], metal-oxides [5] and diamond nanoparticles [6]. The optimum fraction of nano-additives in lubricants is an important factor. Several studies have been conducted to investigate the optimised

Available online at <http://link.springer.com/journal/40195>.

✉ Rizwan Bajwa
rbajwa@bournemouth.ac.uk

¹ NanoCorr, Energy and Modelling Research Group,
Bournemouth University, Poole, UK

Published online: 05 August 2016

Springer

percentage of nanoparticles in lubricants to achieve the best tribological properties [7–9]. Their results concluded that the optimised concentration of nano-sized particles in lubricants is always <1%. This is because of the higher concentration can lead to surface damage due to extensive wear and high frictional heat.

On the other hand, the use of nanoparticles in composite coatings is also widely investigated in the last decades. Likewise, the composite coatings incorporating a variety of nanoparticles made up of nano-sized alumina oxide [10–12], zirconium oxide [13–15], titanium oxide [16], iron (III) oxide Fe_2O_3 [17], cerium oxide CeO_2 [18] and carbides such as silicon carbide [19, 20] and tungsten carbide WC [21] have enhanced anti-wear, anti-friction, anti-corrosion and mechanical properties. In addition, in composite coatings/materials the concentration of reinforcement content of nanoparticles is an important factor to obtain optimum tribological properties. Recently, Gül *et al.* [22] investigated the influences of particle concentration on the tribological properties of nickel composite incorporating silicon carbide particles. It was found that 20 g L^{-1} concentration of immersed particles in the electrolyte demonstrated excellent anti-wear properties of co-deposited coatings. Beltowska-Lehman *et al.* [23] examined the influence of ultrasonic treatment during the deposition process of nickel–zirconia nano-composite coating on their microstructural and functional properties. It was established that the lower ultrasonic treatment demonstrated excellent nanoparticles distribution in the matrix, and consequently, enhanced mechanical properties were achieved.

In recent years, a few studies have been reported on the use of graphene as an additive in the lubricating oil [24–26]. It was found that the anti-wear and anti-friction properties were improved significantly with the addition of graphene in the lubricant. Researchers investigated the effects of varying content ratios of graphene in lubricants on their tribological behaviour [26]. It was found that the average friction coefficient was reduced by 24% with the addition of 0.5 vol% of graphene. Lin *et al.* [25] studied the tribological properties of chemically modified graphene platelets in stearic and oleic acids. They concluded that the optimal value of 0.07 wt% of modified graphene platelets can significantly enhance the anti-wear and anti-friction properties than that of raw oil.

The influence of micro- and nano-sized alumina particles on the corrosion resistance of Ni-based coatings was investigated by Zhou *et al.* [27]. It was found that the reinforcement of nano-alumina presented better corrosion resistance than that of microalumina particles in nickel composite. This is because of better particle distributions and relatively refined compact microstructure of nano-alumina composite coatings. Previously, the effect of chemical solution concentration on the tribological

performance of pure nickel and nickel–alumina composite coatings was investigated [12]. It was found that the ionic strength of electrolyte has significant influence on the tribological and mechanical properties of electrodeposited coatings. The effect of electrodeposition methods and incorporating various nanoparticles such as Al_2O_3 , SiC and ZrO_2 were studied by Borkar and Harimkar [13]. It was concluded that pulse current can present better tribological properties of electrodeposited composite coatings. Furthermore, the nickel composite of alumina nanoparticle exhibits better mechanical and anti-wear properties than Ni–SiC and Ni– ZrO_2 composites.

Tribological performance of various nano-lubricants and nano-composite coatings has been investigated extensively as reported above. Nevertheless, it has been left ambiguous that whether nano-lubricant or nano-composite coatings approach provides a more favourable solution to ever growing tribological operational challenges. Therefore, tribological properties of nano-dispersed lubricants and nano-composite are experimentally evaluated and comparative results are presented here. X-ray diffraction (XRD) results are extended from the previous reported work [15] in which the tribological performance of various nano-composite was investigated. This research is a continuation of existing work in terms of enhancing tribological and anti-corrosive properties in harsh environment [28–41].

2 Experimental

2.1 Preparation and Characterisation of Coated Samples

Pure Ni and Ni–alumina nano-composite coatings ($\sim 10 \mu\text{m}$ in thickness) were produced by electrodeposition method. Pulse current condition was controlled by using a MicroStar Pulse Interface connected to Dynatronix pulse power supply. The pulse current conditions were kept persistent as current density 3 A/dm^2 , pulse on/off time (20–80 ms) and a duty cycle of 20%. An optimised Watt's bath chemical composition was used for deposition process based on previous findings [12]. For the development of nano-enhanced composite coating, alumina nanoparticles (40–50 nm; supplied by Lo-Li-Tech) were added into an electroplating bath under continuous magnetic stirring process. Moreover, to ensure better suspension of particles, the chemical solution was ultrasonically stirred during the deposition process. A nickel sheet with high purity was used as anode and a steel rectangular plate of dimensions $30 \text{ mm} \times 10 \text{ mm} \times 3 \text{ mm}$ to be coated on both sides as a cathode. Standard surface conditioning was deployed before coating development process. Flat plate specimen,

R. Bajwa *et al.*: Acta Metall. Sin. (Engl. Lett.)

to be coated with a surface area of 0.09 dm^2 , was mechanically polished to an average roughness of $0.05 \mu\text{m}$ and ultrasonically conditioned with acetone.

Surface morphology of electrodeposited samples was studied by using a scanning electron microscope (SEM, JSM-6010, JEOL). The elements content analysis was conducted by using an energy-dispersive X-ray spectroscope (EDS). X-ray diffraction (XRD) analysis (D8 Advance, Bruker) was conducted in 2θ range of 20° – 100° and with a step increment of 0.02° .

2.2 Preparation of Nano-lubricants

Nano-enhanced lubricants were fabricated by using a commercial oil SAE10W40 with the addition of $0.1 \text{ wt}\%$ Al_2O_3 nanoparticles and graphene, respectively. Nanoparticles and graphene were added into oil under continuous sonication process to achieve better suspension and then cooled down to room temperature. Figure 1 displays a visual appearance of pure oil and nano-oils with uniformly dispersed nanoparticles and graphene platelets. A clear yellow colour was apparent of pure oil as shown in Fig. 1a. However, nano-oils displayed darker yellow and black colour due to dispersed nanoparticle and graphene platelets, respectively, as shown in Fig. 1b, c.

2.3 Tribological Performance Testing

Tribological behaviour tests were conducted in accordance with ASTM G133 wear test principle by using a linearly reciprocating sliding wear/friction tribometer. A schematic diagram of reciprocating sliding contact set-up is shown in Fig. 2. Briefly describing the tribometer consisted of lower fixed electroplated plate ($30 \text{ mm} \times 10 \text{ mm} \times 3 \text{ mm}$) and

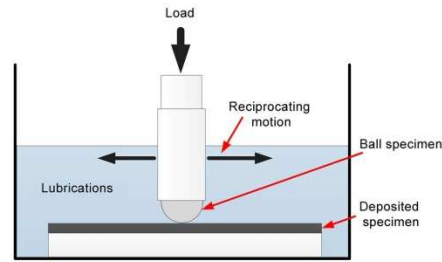


Fig. 2 Schematic diagram of reciprocating sliding contact testing

upper 100Cr6 steel ball (H: 740HV10, E: 210GPa and ν : 0.3) of a 9.525 mm diameter. All tests were performed under a constant load of 15 N , reciprocating frequency of 10 Hz and stroke length of 5 mm . These testing conditions were selected to maintain a boundary lubrication regime. Tribological performance data had been collected on coated specimen before these coatings were completely failed. Four different types of tribological tests were conducted as listed in Table 1. Each tribological test was repeated three times to ensure the repeatability and to achieve the minimum data scattering.

Post-test surface analyses of worn tracks during wear experiments were performed to investigate the wear mechanism and elemental contents by SEM and EDS, respectively. Three-dimensional white light interferometer (ZYGO) was used to measure the wear volume of the worn surfaces of the coated specimens. Wear volume was calculated as $V = AL$, where A is the cross-sectional area of the worn scar in mm^2 , and L is the length of the worn scar in mm . The specific wear rate (mm^3/Nm) was determined

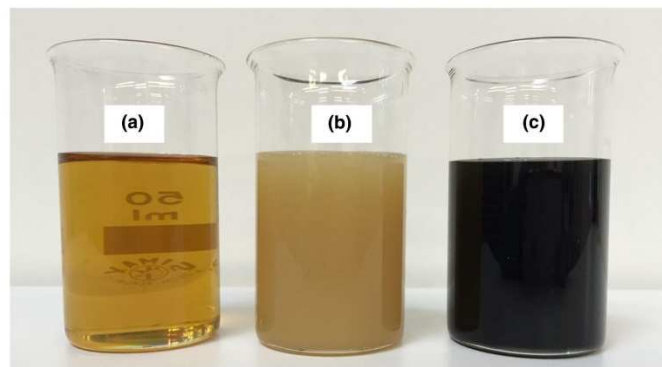
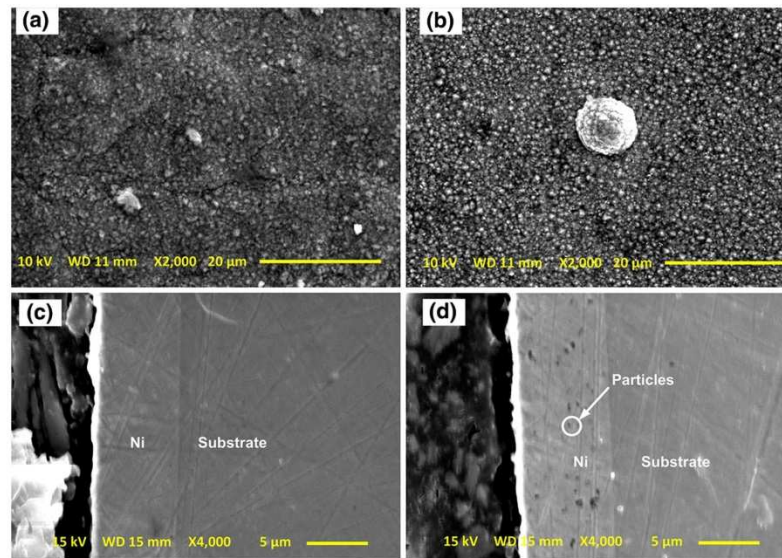


Fig. 1 Visual appearance of lubricants after combined ultrasonic and mechanical agitation: a pure oil, b oil + nano- Al_2O_3 , c oil + graphene

Table 1 List of tribopairs and corresponding lubricating oil conditions

Test type	Tribopairs	Lubricants
1	Steel ball/pure Ni coatings	Pure oil
2	Steel ball/Ni-Al ₂ O ₃ coatings	Pure oil
3	Steel ball/pure Ni coatings	Nano-oil with nano-alumina
4	Steel ball/pure Ni coatings	Nano-oil with graphene

**Fig. 3** SEM surface morphologies and cross-sectional deposited thickness of pure nickel **a, c** and Ni/nano-Al₂O₃ electrodeposited coatings **b, d**, respectively

as a function of the wear volume V (mm³) divided by the applied load (N) multiplied by sliding distance S (m) [15]. The tangential friction force at the contact interface was recorded continuously by using a piezoelectric transducer. The coefficient of friction was then calculated from measured friction force dividing by normal applied load.

3 Results and Discussion

3.1 SEM and XRD Surface Morphology of Electrodeposited Samples

Surface morphologies of electrodeposited pure nickel and nickel composite of nano-sized alumina coatings are shown

in Fig. 3a, b, respectively. The effect of reinforced Al₂O₃ nanoparticle on microstructure morphology of electrodeposited coating is evident from changes in grain structure of Ni coatings. Typical pyramidal and globular-shaped microstructure of composite coating is shown in Fig. 3b. In comparison with pure Ni, the crystallite grains of composite coating exhibit more compact morphology with clear grain edges. These surface morphologies of electrodeposited Ni and Ni-alumina composites are consistent with the previous observations [42, 43]. The reduced grain sizes and compact morphology of composite coatings incorporating nanoparticles have been attributed to the cathodic polarisation as a result of nanoparticles adsorption at cathode specimen surface. The addition of nano-sized alumina in the nickel matrix leads to the formation of

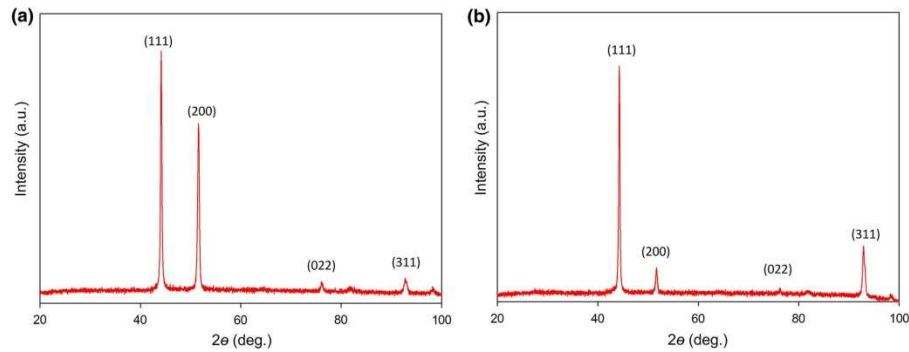


Fig. 4 XRD patterns of pure nickel **a** and Ni/nano-Al₂O₃ electrodeposited coatings **b**

agglomerated spherical particles on the surface of composite coatings as shown in Fig. 3b. This agglomerated morphology was also reported by Borkar and Harimkar [13] for Ni–Al₂O₃ composite coatings which contributed to the higher surface roughness of resulted coatings. The distribution of incorporated nanoparticles in the co-deposited coatings and cross-sectional thickness of deposited coatings were observed by SEM and are shown in Fig. 3c, d. It is evident that coatings are crack-free and well adhered to the substrate and nanoparticles are homogeneously distributed in the nickel matrix.

Figure 4a, b presents XRD results of pure Ni and Ni–alumina composite coatings. XRD patterns were categorised by the typical high intensity peaks of (111) and

(200) as reported previously by other researchers [44, 45] for Ni-based coatings. Reduction in crystallite size of the nickel–alumina composite is evident from low intensity peaks than pure Ni coatings intensity peaks. The corresponding peaks of nano-sized alumina particles were not possible to retrieve due to nano-sized and very low loaded content of particles in the nickel matrix.

3.2 Anti-wear Characteristics

In Fig. 5, the wear resistance results of electrodeposited coatings are compared when using nanoparticles as reinforced contents in nickel matrix and as an additive in the lubricating

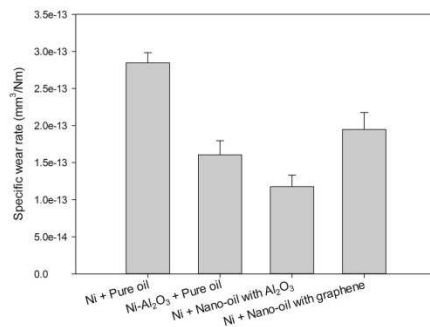


Fig. 5 Variation in specific wear rate post-tribotesting conditions of Ni coatings under pure oil, Ni–Al₂O₃ under pure oil, Ni coatings under nano-oil with nano-Al₂O₃ and Ni coatings under nano-oil with graphene

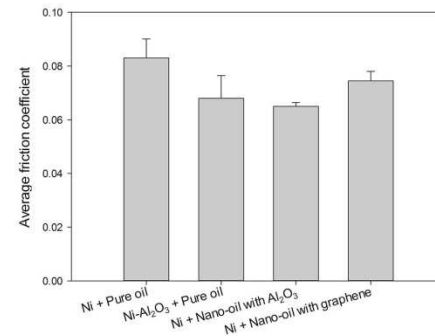


Fig. 6 Variation in average friction coefficient post-tribotesting conditions of Ni coatings under pure oil, Ni–Al₂O₃ under pure oil, Ni coatings under nano-oil with nano-Al₂O₃ and Ni coatings under nano-oil with graphene

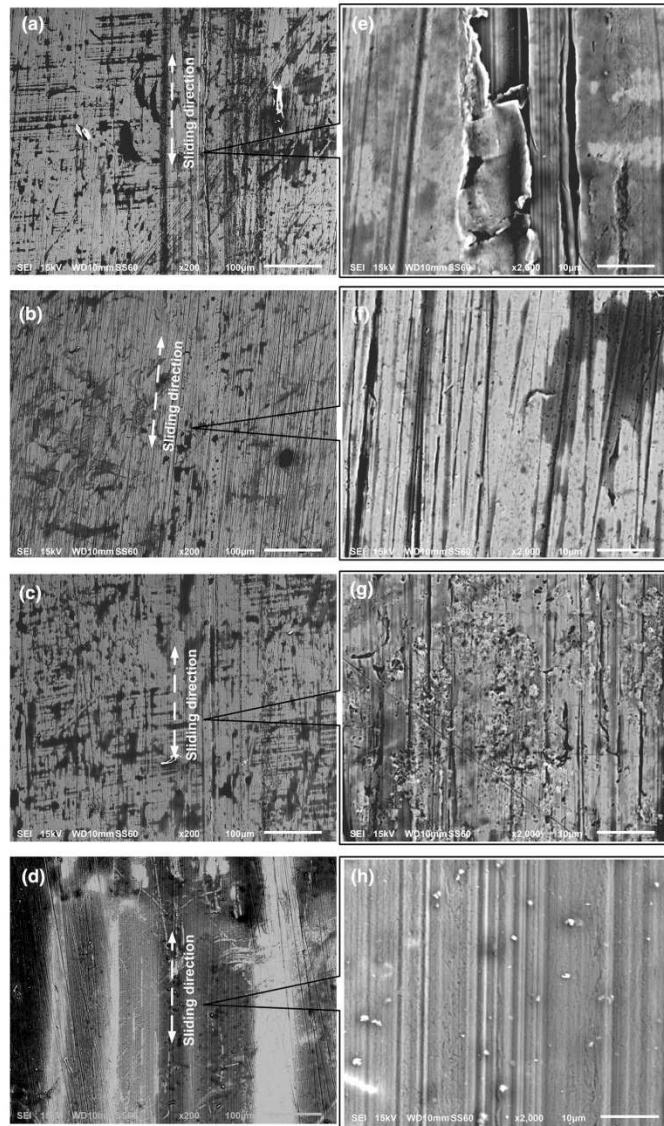
R. Bajwa *et al.*: Acta Metall. Sin. (Engl. Lett.)

Fig. 7 SEM images with overall and magnified view of worn surface post-tribotesting conditions: **a, e** Ni coatings under pure oil, **b, f** Ni-Al₂O₃ under pure oil, **c, g** Ni coatings under nano-oil with nano-Al₂O₃, **d, h** Ni coatings under nano-oil with graphene

R. Bajwa *et al.*: Acta Metall. Sin. (Engl. Lett.)

oil. By comparing with pure nickel coating under pure oil lubrication, nano-enhanced conditions (with the addition of nanoparticle in the matrix or oil) significantly enhanced anti-wear properties. Wear rate is reduced by 58.59% with 0.1 wt% addition of nano-alumina nanoparticle in pure lubricating oil. On the other hand, the wear rate is reduced by 43.86% with reinforcement of Al_2O_3 nanoparticles in nickel matrix followed by nano-oil with the addition of graphene with reduction of about 30%. Therefore, it is evident from Fig. 5 that the use of Al_2O_3 nanoparticle as an additive in the lubricating oil exhibits better wear resistance. This reduction in wear behaviour of electrodeposited coating with doping of nano-sized particles in both cases can be credited to three main reasons. First, the nanoparticles in lubricating oil or into the nickel matrix reduced the direct contact between two surfaces during sliding contact, and consequently the wear rate decreased [13]. Second, the self-repairing properties of nanoparticles contributed to the reduction in the abrasion

mechanism [46]. The formation of a protective triofilm with the presence of nanoparticles decreases the wear as confirmed by several researchers [47–49].

Similar wear rate results were observed in previous work [15] in which wear characteristic of pure nickel and Ni– Al_2O_3 composite were studied subject to water-lubricated conditions. However, microploughing and micro-cutting wear mechanisms were observed on the coatings wear tracks. In addition to nano-effects, the reduced surface damage behaviour in this study may relate to higher viscosity lubricating oil.

3.3 Friction Coefficient Characteristics

Experimental results of average coefficient of friction during sliding ball on disc test are shown in Fig. 6. As shown in Fig. 6, the friction coefficient is lower in nano-enhanced composite coatings and nano-oil (with nano- Al_2O_3 or

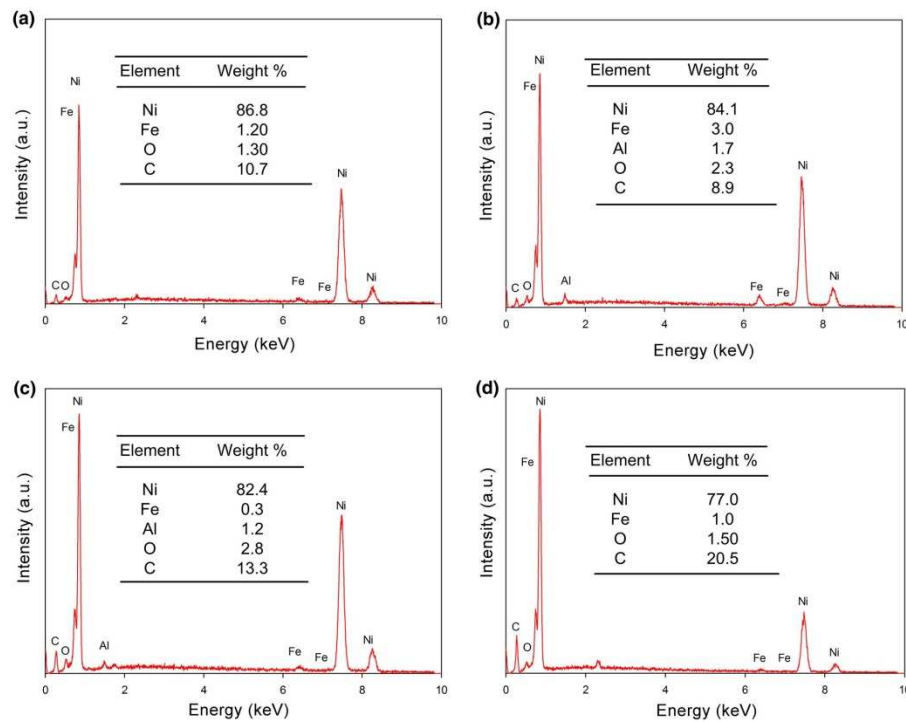


Fig. 8 EDS spectrum analysis of worn surface post-tribotesting conditions: **a** Ni coatings under pure oil, **b** Ni– Al_2O_3 under pure oil, **c** Ni coatings under nano-oil with nano- Al_2O_3 , **d** Ni coatings under nano-oil with graphene

graphene) than that of the pure nickel coating under pure oil friction testing. Friction coefficient is reduced by 21.69% in nano-oil incorporating nano-Al₂O₃ particles followed by Ni–Al₂O₃ composite coatings and nano-oil incorporating graphene with reduction of 18.07% and 9.64%, respectively. This is because of load-bearing effect of the addition of reinforced nano-alumina nanoparticles in the composite and as an additive in the lubricating oil. This premise is also confirmed by other researchers about various nano-sized nanoparticles [2, 50].

In summary, it can be concluded that by using 0.1 wt% Al₂O₃ nano-sized particles as a nano-additive in the lubricating oil can produce better anti-friction and anti-wear properties than if reinforced in the nickel matrix.

3.4 Worn Surface Characteristics

SEM and EDS were used to investigate worn surfaces. Figure 7 shows the overall and magnified view of worn tracks after the wear/friction tests with Ni coatings/pure oil, Ni–Al₂O₃/pure oil, Ni coatings/nano-oil with nano-Al₂O₃ and Ni coatings/nano-oil with graphene. Figure 7a, e presents the worn wear track of pure Ni coating after testing with pure lubricating oil. From magnified view in Fig. 7e, severe surface wear can be seen where grooves and coating delamination take place, whereas the tribological tests conducted with nano-composite and that of nano-enhanced lubricant oil incorporating nano-alumina particles and graphene showed relatively much smooth worn surface without coating delamination, as shown in Fig. 7b–d, f–h, respectively. Nano-lubricants with addition of nano-alumina particles exhibit relatively smoother worn surface. These observations also validate the wear rate results of the corresponding type of tribotest conditions. Similarly, the wear mechanism with various nano-sized particles, including Cu [47], ZnAl₂O₃ [2] and ZrO₂ [51], has been reported by other researchers. They reported that this is because of the bearing ball effect of the nanoparticles which reduces the contact between the interacting surfaces.

Post-test chemical element analyses of worn tracks were conducted by using EDS in order to validate the hypothesis that nanoparticles contributed to the reduction in wear scars. The EDS spectra of worn tracks subject to nano-composite coating and nano-oil showed the presence of Al, as shown in Fig. 8b, c, respectively. The formation graphene protective tribofilm is evident from relatively higher (C) content element of 20.51% as shown in Fig. 8d. This is also in agreement with previous investigations about using nanoparticles as Fe, Cu, and Co as nano-additives in the lubricants [47]. The EDS spectra of the worn track, testing with pure nickel and pure oil (without nanoparticles) are also shown in Fig. 8a for comparison purpose.

4 Conclusions

Experimental results showed that the use of Al₂O₃ nanoparticles and graphene in the lubricating oil and nano-alumina reinforcement in composite coating can considerably reduce the wear and friction. In comparison, the addition of Al₂O₃ nanoparticles in the lubricant can provide the best tribological performance than Ni–Al₂O₃ and using graphene as an additive in the lubricating oils. Also, the use of nanoparticle as an additive in lubricating oil is relatively cost-effective approach and a simple process, whereas the reinforcement of nanoparticles into the composite coating by electrodeposition technique is a complicated method involving a wide range of parameters to be controlled. Post-test surface analyses of worn tracks reveal that nano-enhanced lubricants and composite coatings display smoother surfaces and free of coating delamination, while pure nickel coatings which have been sliding against steel ball subjected to conventional oil presented severe surface deformation.

Moreover, during the EDS elemental surface analysis, the presence of Al₂O₃ hard nanoparticles and graphene within the worn track areas has confirmed the formation of, respectively, protective tribofilm.

References

- [1] S. Shahnazar, S. Bagheri, S.B.A. Hamid, *Int. J. Hydrogen Energy* **41**, 3153 (2016)
- [2] X. Song, S. Zheng, J. Zhang, W. Li, Q. Chen, B. Cao, *Mater. Res. Bull.* **47**, 4305 (2012)
- [3] Z.J. Zhang, D. Simionesie, C. Schaschke, *Lubricants* **2**, 44 (2014)
- [4] B.S. Zhang, B.S. Xu, Y. Xu, F. Gao, P.J. Shi, Y.X. Wu, *Tribol. Int.* **4**, 878 (2011)
- [5] A. Guerrero-Martínez, J. Pérez-Juste, L.M. Liz-Marzán, *Adv. Mater.* **22**, 1182 (2010)
- [6] H.Y. Chu, W.C. Hsu, J.F. Lin, *Wear* **268**, 960 (2010)
- [7] Y. Wu, W. Tsui, T. Liu, *Wear* **262**, 819 (2007)
- [8] L. Rapoport, M. Lvovsky, I. Lapsker, W. Leshchinsky, Y. Volovik, Y. Feldman, R. Tenne, *Wear* **249**, 149 (2001)
- [9] L. Rapoport, Y. Feldman, M. Homyonfer, H. Cohen, J. Sloan, J. Hutchison, R. Tenne, *Wear* **225**, 975 (1999)
- [10] C. Lee, *Tribol. Int.* **55**, 7 (2012)
- [11] C. Lee, *Tribol. Trans.* **55**, 640 (2012)
- [12] R.S. Bajwa, Z. Khan, V. Bakolas, W. Braun, *J. Adhes. Sci. Technol.* **30**, 653 (2016)
- [13] T. Borkar, S.P. Harimkar, *Surf. Coat. Technol.* **205**, 4124 (2011)
- [14] K. Dass, S. Chauhan, B. Gaur, *Tribol. Trans.* **57**, 157 (2014)
- [15] R.S. Bajwa, Z. Khan, V. Bakolas, W. Braun, *Acta Metall. Sin. (Engl. Lett.)* **1**, 8 (2016)
- [16] S. Lajevardi, T. Shahrabi, *Appl. Surf. Sci.* **256**, 6775 (2010)
- [17] I.U. Haq, K. Akhtar, T.I. Khan, A. Ali Shah, *Surf. Coat. Technol.* **235**, 691 (2013)
- [18] Y.J. Xue, H.B. Liu, M.M. Lan, J.S. Li, H. Li, *Surf. Coat. Technol.* **204**, 3539 (2010)
- [19] E. Rudnik, L. Burzyńska, Ł. Dolasiński, M. Misiak, *Appl. Surf. Sci.* **256**, 7414 (2010)

R. Bajwa *et al.*: Acta Metall. Sin. (Engl. Lett.)

- [20] A.K. Pradhan, S. Das, Tribol. Trans. **57**, 46 (2014)
- [21] M. Surender, B. Basu, R. Balasubramaniam, Tribol. Int. **37**, 743 (2004)
- [22] H. Gül, F. Kılıç, M. Uysal, S. Aslan, A. Alp, H. Akbulut, Appl. Surf. Sci. **258**, 4260 (2012)
- [23] E. Beltowska-Lehman, P. Indyka, A. Bigos, M. Szczerba, M. Kot, Mater. Des. **80**, 1 (2015)
- [24] D. Berman, A. Erdemir, A.V. Sumant, Mater. Today **17**, 31 (2014)
- [25] J. Lin, L. Wang, G. Chen, Tribol. Lett. **41**, 209 (2011)
- [26] C.G. Lee, Y.J. Hwang, Y.M. Choi, J.K. Lee, C. Choi, J.M. Oh, Int. J. Precis. Eng. Manuf. **10**, 85 (2009)
- [27] Q. Zhou, C.L. He, Q.K. Cai, Adv. Mater. Res. **79**, 631 (2009)
- [28] M.H. Nazir, Z.A. Khan, A. Saeed, K. Stokes, Eng. Fail. Anal. **63**, 43 (2016)
- [29] A. Saeed, Z.A. Khan, M.H. Nazir, Sustainability **7**, 16451 (2015)
- [30] M. Nazir, Z. Khan, A. Saeed, K. Stoke, Corrosion **72**, 500 (2016)
- [31] M. Nazir, Z.A. Khan, K. Stokes, J. Adhes. Sci. Technol. **29**, 1415 (2015)
- [32] M. Nazir, Z. Khan, K. Stokes, J. Adhes. Sci. Technol. **29**, 392 (2015)
- [33] C. Ramesh, H. Adarsha, S. Pramod, Z. Khan, Mater. Des. **50**, 597 (2013)
- [34] A. Saeed, Z.A. Khan, M. Hadfield, S. Davies, Tribol. Trans. **56**, 637 (2013)
- [35] A. Saeed, E.L. Montgomery, Z.A. Khan, Mater. Perform. Charact. **2**, 30 (2013)
- [36] A. Saeed, Z. Khan, M. Clark, M. Nel, R. Smith, Insight Non-Destr. Test. Cond. Monit. **53**, 382 (2011)
- [37] B. Karunamurthy, M. Hadfield, C. Vieillard, G. Morales-Espejel, Z. Khan, Ceram. Int. **36**, 1373 (2010)
- [38] Z.A. Khan, M. Hadfield, Mater. Des. **28**, 2688 (2007)
- [39] Z.A. Khan, M. Hadfield, S. Tobe, Y. Wang, Ceram. Int. **32**, 751 (2006)
- [40] Z.A. Khan, M. Hadfield, S. Tobe, Y. Wang, Mater. Sci. Eng., A **404**, 221 (2005)
- [41] Z.A. Khan, M. Hadfield, Y. Wang, Mater. Des. **26**, 680 (2005)
- [42] A. Jung, H. Natter, R. Hempelmann, E. Lach, J. Mater. Sci. **44**, 2725 (2009)
- [43] D. Thiemiig, A. Bund, Appl. Surf. Sci. **255**, 4164 (2009)
- [44] J. Calderón, J. Henaó, M. Gómez, Electron. Acta **124**, 190 (2014)
- [45] D. Thiemiig, A. Bund, Surf. Coat. Technol. **202**, 2976 (2008)
- [46] X. Kang, B. Wang, L. Zhu, H. Zhu, Wear **265**, 150 (2008)
- [47] J. Padgurskas, R. Rukuiza, I. Prosyčevs, R. Kreivaitis, Tribol. Int. **60**, 224 (2013)
- [48] Y. Choi, C. Lee, Y. Hwang, M. Park, J. Lee, C. Choi, M. Jung, Curr. Appl. Phys. **9**, e124 (2009)
- [49] A.H. Battez, R. González, J. Viesca, J. Fernández, J.D. Fernández, A. Machado, R. Chou, J. Riba, Wear **265**, 422 (2008)
- [50] A.H. Battez, J. Viesca, R. González, D. Blanco, E. Asedegbega, A. Osorio, Wear **268**, 325 (2010)
- [51] W. Li, S. Zheng, B. Cao, S. Ma, J. Nanopart. Res. **13**, 2129 (2011)

Tribological Properties of Ni/Al₂O₃, Ni/SiC, Ni/ZrO₂ and
Ni/Graphene Composite Coatings for Marine Applications

*Rizwan Sarwar Bajwa, Zulfiqar Khan, Vasilios Bakolas, Wolfgang Braun,
Christine Maggs, Saqib Rafique*

*Manuscript
[Click here to view linked References](#)

Tribological properties of Ni/Al₂O₃, Ni/SiC, Ni/ZrO₂ and Ni/Graphene composite coatings for marine applications

Rizwan Bajwa ^{1*}, Zulfiqar Khan ¹, Vasilios Bakolas ², Wolfgang Braun ², Christine Maggs ¹, Saqib Rafique ³

¹ NanoCorr, Energy & Modelling, Faculty of Science & Technology, Bournemouth University, Poole, United Kingdom

² Advanced bearing analysis, Schaeffler Technologies GmbH & Co. KG, 91074 Herzogenaurach, Germany

³ Low Dimensional Materials Research Centre, University of Malaya, 50603 Kuala Lumpur, Malaysia

*Email: rbajwa@bournemouth.ac.uk

Abstract

This paper presents tribological properties of Ni-based composite coatings incorporating nano-size Al₂O₃, SiC, ZrO₂ and graphene platelets (GPLs). Tribological tests were conducted in immersed seawater lubrication to simulate marine application conditions. Pulse electrodeposition process was used for co-deposition of composite coatings. Wear and friction resistance tests were conducted using a linear reciprocating ball on a flat sliding tribometer. The Ni/GPLs composite exhibited better tribological properties than composite coatings incorporating nanoparticles. Additionally, in worn surface analyses subjected to wear tests, the Ni/GPLs composite showed a relatively smoother surface without any severe surface failure or cracks. Post-test surface analyses were performed to investigate the failure mechanisms of coatings subjected to wear tests.

Keywords: Tribology; Nanoparticles; Graphene; Seawater.

1. Introduction

In recent years, extensive work has been reported on the potential of electrodeposited metal matrix composite (MMC) coatings for tribological systems. Reinforcement of the matrix with nanoparticles, especially if < 100nm results in novel tribological and mechanical properties. The wear and friction resistance behaviour of various nanocomposite coatings (Ni/Al₂O₃, Ni/SiC and Ni/ZrO₂) under dry sliding contact was studied by Borkar [1]. The addition of nanoparticles significantly enhanced the anti-

1 wear and anti-friction properties compared to pure Ni. Also, the microhardness of pure
2 nickel coatings significantly increased with increasing particle content in the composite.
3 The strengthening effect of hard nanoparticles in the composite provides a lubrication
4 effect by reducing direct contact between the interacting surfaces. The effect of
5 incorporated micro-size and nano-size alumina particles on the corrosion resistance
6 behaviour of nickel coatings was investigated by Zhou et al. The corrosion resistance
7 behaviour of nano-alumina/Ni was enhanced with the reduction of porosity of composite
8 coatings [2]. Similar improvements in wear, friction and corrosion resistance properties
9 have been reported for various other nanoparticles including, ZrO₂ [3], TiO₂ [4], Fe₂O₃
10 [5], CeO₂ [6] and SiC [7].

11 Unique thermal, electrical, chemical and mechanical properties of two-dimensional
12 graphene make it a potential candidate for numerous applications [8]. Significant
13 mechanical strength, inertness, highly atomically smooth surface and densely packed
14 characteristics of graphene predicts its impressive anti-wear and anti-frictional behaviour
15 [9-15]. Graphene was reported as one of the strongest material ever measured, which is an
16 important characteristic for wear protection [9]. The addition of graphene to Ni-graphene
17 composite has reduced grain size, resulting in increased hardness and corrosion
18 resistance, but tribological properties have not been investigated [11]. To the best of our
19 knowledge, first time in present work the tribological properties of Ni-graphene composite
20 has been investigated subject to seawater lubrication. The wear resistance and load-
21 carrying capacity of lubricating oil were improved with optimal concentration of graphite
22 nanosheets in paraffin oil [14]. Filletter et al. [15] investigated friction and dissipation in
23 graphene films grown epitaxially on SiC. They found that the friction on silicon carbide
24 was significantly reduced by a single and bilyer of graphene.

25 In recent years, extensive studies have been reported on tribological properties of
26 various nanocomposite coatings subjected to dry and oil lubrication, but fewer reports
27 cover the performance of electrodeposited coatings subject to water lubrication. Recently,
28 experimental investigations were conducted to study tribological properties of
29 nanocomposites under water lubrication to simulate water-lubricated bearing applications
30 [16]. Increasing operational demands on marine vessels, conventional power plants, tidal
31 and wave energy systems which have been deployed in harsh marine environments require
32 optimisation of advanced materials with enhanced wear and corrosion resistance
33 properties. For that reason, the tribological properties of electrodeposited coatings are

investigated here in seawater lubrication to simulate tribo-components working under sea environment.

2. Experimental procedures

2.1. Deposition process and characterization of composite coatings

The pulse electrodeposition method was used to produce Ni/Al₂O₃, Ni/SiC, Ni/ZrO₂ and Ni/graphene composite coatings, 10µm is thickness with a current density of 3 A/dm² for 2 hours electrodeposition process time. The chemical constituents of the electrolyte are given in Table 1. Prior to the deposition process the specimens were mechanically polished and ultrasonically cleaned with acetone. Nanoparticles and graphene were maintained in suspension by deploying continuous ultrasonic treatment and magnetic stirring during the deposition process. A mild steel specimen with dimensions 30mm×10mm×3mm was used as a cathode and deposition was on both sides.

Surface morphology of test samples was examined pre-test and post-test by using a scanning electron microscopy (SEM), energy-dispersive X-ray spectroscopy (EDS), and X-ray diffraction (XRD) analysis. X-ray diffraction (XRD) measurements were performed using an Ultima-IV (Rigaku, Japan) multipurpose X-ray diffraction system equipped with Cu K-α source ($\lambda=0.154060$ nm) to scan in 2θ range of 5 to 100 °.

Table 1 Chemical and nanoparticle constituents of bath solution

Electrolyte composition	
Nickel sulphate	265 g L ⁻¹
Nickel chloride	48 g L ⁻¹
Boric acid	31 g L ⁻¹
Nano-Al ₂ O ₃ (40-50 nm)	20 g L ⁻¹
Nano-SiC (50-60 nm)	20 g L ⁻¹
Nano-ZrO ₂ (40-50 nm)	20 g L ⁻¹
Graphene platelets (6-8 nm)	100 mg L ⁻¹

2.2. Wear and friction testing procedures

Tribological properties of electrodeposited nanocomposite coatings were studied using a linearly reciprocating sliding contact tribometer (Plint TE77). The tribometer consisted of lower fixed deposited specimen plate (30mm×10mm×3mm) and upper steel ball specimen (H: 740HV10, E: 210GPa and ν : 0.3) with 9.525mm diameter. All tests were performed with immersed seawater lubrication (Table 2). Tribo-conditions were chosen to ensure sliding contact subject to the boundary lubrication regime and to permit retrieval of data before coatings completely failed. Tribological tests for each type of coating were repeated at least three times. Note that, all the coatings were mechanically polished prior to tribological testing in order to overcome the influence of these bulging particles.

Table 2 Test conditions used for wear and friction experiments

Tribo test conditions	
Load	15 N
Sliding speed	0.05 m/sec
Frequency	10 Hz
Stroke length	5 mm
Steel ball diameter	9.525 mm
Lubrication	Sea water

Friction coefficient data were retrieved through COMPEND software which also controls the operating parameters of Plint-TE77 through a microprocessor coupled with a computer. The failure mechanism of coatings and elements content within worn tracks on coated specimen in wear tests were studied by using SEM and EDX analyses, respectively. The loss of material in wear testing was examined by using a three-dimensional white-light interferometer and measured wear volume was used to calculate specific wear rate [16].

3. Results and discussion

3.1. Surface morphology of electrodeposited coatings

Figure 1 shows the microstructure morphology of electroplated nanocomposite coatings reinforced with nano-sized alumina, silicon carbide, zirconium oxide and GPLs. All coatings exhibits the typical pyramid grain structure which is consistent with previous investigations by other researchers [1, 11, 17, 18]. The grain with clear edges and compact morphology is attributed to the cathodic polarization because of reinforced nanomaterials in the nickel matrix. However, the addition of the graphene in the nickel matrix results in the formation of agglomerated particles on the surface of Ni/graphene composite coatings (Fig. 2d). This can be related to the higher electrical conductivity of graphene platelets (GPLs) than nickel [19]. Therefore, during electrodeposition process the reduction rate of nickel ions on graphene platelets would be higher than that of nickel surface. This may results in the formation of agglomerated particles along with refined grain structure.

Fig. 1 SEM surface morphology: (a) Ni/Al₂O₃ (b) Ni/SiC (c) Ni/ZrO₂ and (d) Ni/graphene.

3.2. X-ray diffraction analysis

XRD patterns results (Figure 2) for the Ni-based composite coatings incorporating nano-size alumina (Al₂O₃), silicon carbide (SiC), zirconium (ZrO₂) and graphene platelets. The spectra exhibit intense reflections at 44.51°, 51.86° and relatively low intensity peaks at 76.40°, 92.97.80° and 98.48° respectively. The structural properties of the samples showed that films are crystalline, in accordance with the ICDD PDF-2 (Release 2011) DB card number 153681.

Fig. 2 The X-ray diffraction patterns from (a) Ni/Al₂O₃ (b) Ni/SiC (c) Ni/ZrO₂ and (d) Ni/graphene electrodeposited composite coatings.

Diffracted peaks show sharp and noise free spectra which confirms high crystallinity and well-arranged cubic symmetry of Ni crystal structure with cell dimension

Appendix D

as ; $\alpha = \beta = \gamma = 90^\circ$, $a = b = c$ (space group Fm-3m-225). The lattice parameters were calculated from the equation 1 and data is summarised in Table 3.

Lattice parameters calculations:

$$\frac{1}{d^2} = \frac{h^2 + k^2 + l^2}{a^2} \quad \text{Equation 1}$$

Where (hkl), a and d are miller indices, lattice constant and spacing between adjacent (hkl) lattice planes respectively.

Table 3 Lattice parameters and crystallite size as a function of different doping variants, namely alumina, silicon carbide, zirconium and graphene.

Sample	Lattice parameters			Crystallite size (nm)
	a (Å)	b (Å)	c (Å)	
Ni – Al ₂ O ₃	3.524454	3.524454	3.524454	16.08
Ni – SiC	3.52404	3.52404	3.52404	18.65
Ni – ZrO ₂	3.52587	3.52587	3.52587	19.68
Ni – Graphene	3.52312	3.52312	3.52312	11.21

There are no significant changes recorded in any of the spectra, however intensity of the characteristic peak (111) at 44.51° in ZrO₂ doped Ni sample is significantly higher as compared to rest of the composites. The intensity of the characteristic increased significantly with ZrO₂ doping as compared to other dopant which exhibit increasing level of crystallinity with ZrO₂ doping.

Table 3 also shows the crystallite size as a function of different doping agents. The crystallite size for each crystal plane had been calculated by using Scherrer equation as;

$$\tau = \frac{K\lambda}{\beta \cos\theta} \quad \text{Equation 2}$$

Where τ the mean size of the ordered (crystalline) domains, K is a dimensionless shape factor, λ is the X-ray wavelength, β is the line broadening at half the maximum and θ is Bragg's angle.

3.3. Wear resistance behaviour

Figure 3 presents the wear resistance outcomes of electrodeposited composite coatings subjected to sliding contact under seawater lubrication. As can be seen from Figure 3, the Ni/ZrO₂ composite exhibits the maximum wear rate. In comparison to Ni/ZrO₂ a reduction of 14 % and 43 % was observed in Ni/SiC and Ni/Al₂O₃ composite respectively. When compared with the nickel composite of graphene platelets (GPLs) a maximum reduction of 48 % was achieved in the wear rate. Likewise, wear characteristic were reported in previous findings in which tribological properties of these composites (except Ni/GPLs) were studied in water-lubricated rolling contact [16].

It is interesting to note that Ni/graphene composite showed the best wear resistant properties. Previously, only the corrosion behaviour of the Ni/graphene composite has been reported with better anti-corrosion behaviour than pure Ni coating [11]. It is evident from the current study that Ni/GPLs may also exhibit better anti-wear properties than composite coatings incorporating metal nanoparticles. The high anti-wear behaviour of Ni/GPLs composite may be due to the high strengthening effects in the presence of graphene. Secondly, this may be due to the significantly lower density of graphene than nanoparticles resulting into high volume fraction in the composite with decreasing wear rate.

Fig. 3 Specific wear rate of various types of electrodeposited composite coatings sliding against 100Cr6 steel ball under sea water lubrication.

3.4. Friction coefficient behaviour

Figure 4 shows variations in the average coefficient of friction of all coatings subjected to sliding contact under seawater lubrication. Overall, the variations in friction coefficient were not of much significance and ranges between ~0.16 to 0.23. In comparison, the Ni/SiC composite showed minimum friction value of 0.16, followed by Ni/GPLs (0.18), Ni/ZrO₂ (0.20) and Ni/Al₂O₃ (0.23). The reduced friction coefficient of

1 Ni/SiC may be related to the highest hardness of SiC nanoparticle (~1530 HV) than Al₂O₃
 2 (~1530 HV) and ZrO₂ (~1326 HV) as provided in the literature [1]. The harder
 3 nanoparticle induced better load bearing capacity and reduced a direct contact between the
 4 two surfaces during sliding contact more effectively [20, 21]. Similarly, the larger content
 5 of graphene in the Ni/GPLs composite may be resulting into formation of graphene tribo-
 6 film; consequently the friction coefficient was reduced. Furthermore, the counter steel ball
 7 surface sliding against Ni/GPLs composite exhibits the highest wear weight loss as shown
 8 in Figure 5d. This seems to be an indication of better hardness of Ni/GPLs composite than
 9 the counter steel ball. The highest friction coefficient of Ni/Al₂O₃ composite seems to be
 10 due to formation of wear debris, resulting in increasing friction force.
 11
 12
 13
 14
 15
 16
 17
 18
 19
 20

21 Fig. 4 Variation in average friction coefficient of different types of electrodeposited
 22 composite coatings sliding against 100Cr6 steel ball under sea water lubrication.
 23
 24
 25
 26

27 Fig. 5 Optical photographs of worn tracks of 100Cr6 steel ball sliding against: (a)
 28 Ni/Al₂O₃ (b) Ni/SiC (c) Ni/ZrO₂ and (d) Ni/Graphene under sea water lubrication.
 29
 30
 31
 32
 33

34 3.5. Appearances of worn surfaces

35 The worn surface morphologies of composite coatings after tribological testing
 36 subject to seawater lubrication are shown in Figure 6. It can be seen that mainly micro-
 37 cutting and micro-ploughing wear mechanisms are observed on the worn wear tracks.
 38 Micro-cutting and micro-ploughing are characteristics of plastic deformation. Likewise,
 39 wear mechanisms were observed in previous investigations [16] in which tribological
 40 behaviour of electrodeposited coating was studied under distilled water conditioned. The
 41 worn surfaces of Ni/SiC and Ni/ZrO₂ display almost similar surface morphologies (see
 42 Figure 6b and c). The parallel micro-grooves can be seen on both worn surfaces indicating
 43 severe plastic deformation [22]. In case of Ni/Al₂O₃ and Ni/graphene, the wear mechanism
 44 is micro-delamination and micro-ploughing respectively (see Figure 6a and d).
 45 Nevertheless, the worn surface of Ni/graphene composite under seawater lubrication is
 46 much smoother and free of micro-cutting. The removal of Ni/Al₂O₃ material due to micro-
 47 delamination wear mechanism may causes high average friction coefficient value as
 48 shown in Figure 4.
 49
 50
 51
 52
 53
 54
 55
 56
 57
 58
 59
 60
 61
 62
 63
 64
 65

Fig. 6 Worn surface morphology after tribo test under sea water lubrication: (a) Ni/Al₂O₃ (b) Ni/SiC (c) Ni/ZrO₂ and (d) Ni/Graphene.

An elemental analyses of worn surfaces were conducted by using EDS and corresponding spectrums are shown in Figure 7. The presence of nanoparticles and graphene spectrum peaks confirmed their influence on the tribological properties. The relative stronger peak of Fe element in Ni/graphene composite indicated that many wear debris from counter steel ball transferred on wear track [23]. As shown in Figure 6d, relatively high weight loss was observed on ball surface sliding against Ni/graphene composite.

Fig. 7 EDX spectra analysis of worn tracks after tribo test under sea water lubrication: (a) Ni/Al₂O₃ (b) Ni/SiC (c) Ni/ZrO₂ and (d) Ni/Graphene.

4. Conclusions

In this work, Ni-based composite coatings incorporating nano-size Al₂O₃, SiC, ZrO₂ and graphene were produced by using electrodeposition technique. Anti-wear and anti-friction properties of these composites were studied under seawater lubrication. The wear performance results showed the Ni/GPLs exhibits the best wear resistant property. The friction performance results showed that Ni/SiC and Ni/GPLs exhibit similar and better friction resistance than Ni/Al₂O₃ and Ni/ZrO₂. Post-test surface analyses of worn wear tracks on coatings revealed that Ni/GPLs composite is free of any severe surface damage in terms of micro-groove or surface delamination. The current study shows that graphene has significant potential to enhance the tribological properties of electrodeposited composite and feasible to deployment for engineering applications. The presence of incorporated nanoparticles and GPLs in the composite coating was validated by using energy-dispersive X-ray spectroscopy (EDS) element analyses after tribo-testing.

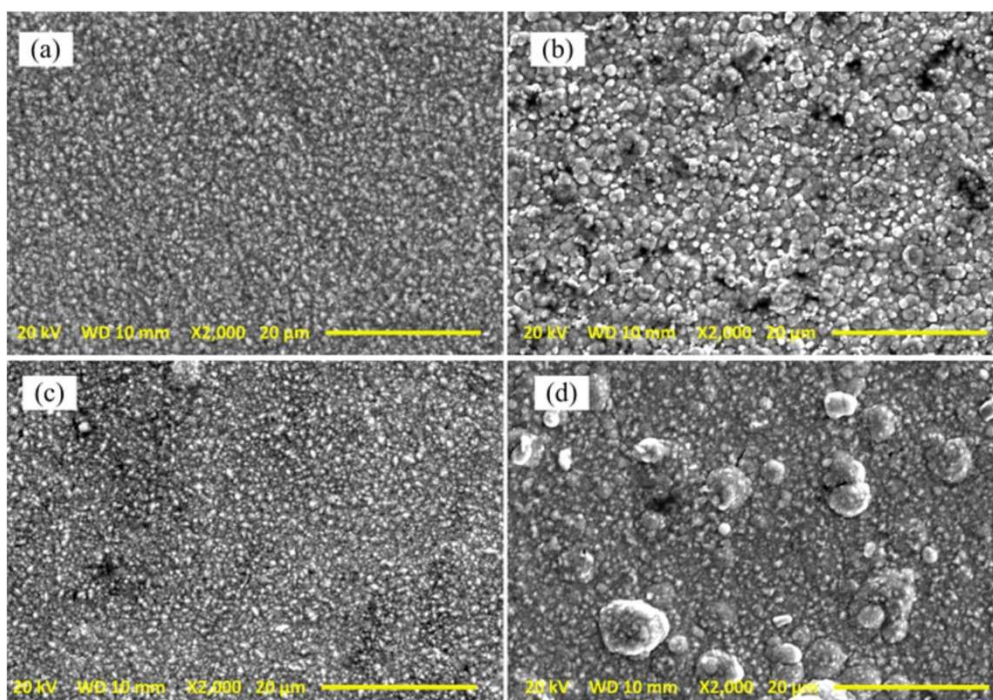
Reference

- 1
2
3
4
5
6
7
8
9
10
11
12
13
14
15
16
17
18
19
20
21
22
23
24
25
26
27
28
29
30
31
32
33
34
35
36
37
38
39
40
41
42
43
44
45
46
47
48
49
50
51
52
53
54
55
56
57
58
59
60
61
62
63
64
65
- [1] Borkar, T. and S.P. Harimkar, Effect of electrodeposition conditions and reinforcement content on microstructure and tribological properties of nickel composite coatings. *Surface and Coatings Technology*, 2011. 205(17): p. 4124-4134.
- [2] Zhou, Q., C.L. He, and Q.K. Cai, Effect of Al₂O₃ Powders on Properties of Electrodeposited Ni Matrix. *Advanced Materials Research*, 2009. 79: p. 631-634.
- [3] Dass, K., S. Chauhan, and B. Gaur, Study on Mechanical and Dry Sliding Wear Characteristics of Meta-Cresol Novalac Epoxy Composites Filled with Silicon Carbide, Aluminum Oxide, and Zinc Oxide Particulates. *Tribology Transactions*, 2014. 57(2): p. 157-172.
- [4] Lajevardi, S. and T. Shahrabi, Effects of pulse electrodeposition parameters on the properties of Ni-TiO₂ nanocomposite coatings. *Applied Surface Science*, 2010. 256(22): p. 6775-6781.
- [5] Haq, I.U., et al., Electrodeposition of Ni-Fe₂O₃ nanocomposite coating on steel. *Surface and Coatings Technology*, 2013. 235: p. 691-698.
- [6] Xue, Y.-J., et al., Effect of different electrodeposition methods on oxidation resistance of Ni-CeO₂ nanocomposite coating. *Surface and Coatings Technology*, 2010. 204(21): p. 3539-3545.
- [7] Pradhan, A.K. and S. Das, Dry Sliding Wear and Friction Behavior of Cu-SiC Nanocomposite Coating Prepared by Pulse Reverse Electrodeposition. *Tribology Transactions*, 2014. 57(1): p. 46-56.
- [8] Berman, D., A. Erdemir, and A.V. Sumant, Graphene: a new emerging lubricant. *Materials Today*, 2014. 17(1): p. 31-42.
- [9] Lee, C., et al., Frictional characteristics of atomically thin sheets. *Science*, 2010. 328(5974): p. 76-80.
- [10] Liu, J., H. Yan, and K. Jiang, Mechanical properties of graphene platelet-reinforced alumina ceramic composites. *Ceramics International*, 2013. 39(6): p. 6215-6221.

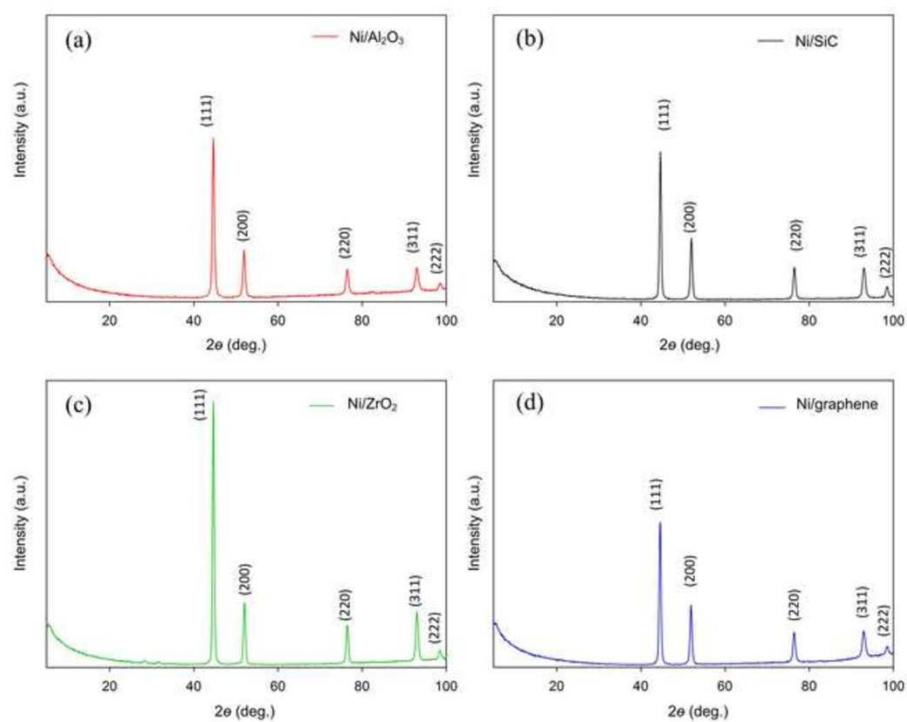
- 1
2
3
4
5
6
7
8
9
10
11
12
13
14
15
16
17
18
19
20
21
22
23
24
25
26
27
28
29
30
31
32
33
34
35
36
37
38
39
40
41
42
43
44
45
46
47
48
49
50
51
52
53
54
55
56
57
58
59
60
61
62
63
64
65
- [11] Kumar, C.P., T. Venkatesha, and R. Shabadi, Preparation and corrosion behavior of Ni and Ni-graphene composite coatings. *Materials Research Bulletin*, 2013. 48(4): p. 1477-1483.
- [12] Bandeira, P., et al., Influence of oxidized graphene nanoplatelets and [DMIM][NTf₂] ionic liquid on the tribological performance of an epoxy-PTFE coating. *Tribology International*, 2016. 97: p. 478-489.
- [13] Lin, J., L. Wang, and G. Chen, Modification of graphene platelets and their tribological properties as a lubricant additive. *Tribology letters*, 2011. 41(1): p. 209-215.
- [14] Huang, H., et al., An investigation on tribological properties of graphite nanosheets as oil additive. *Wear*, 2006. 261(2): p. 140-144.
- [15] Filleter, T., et al., Friction and dissipation in epitaxial graphene films. *Physical review letters*, 2009. 102(8): p. 086102.
- [16] Bajwa, R.S., et al., Water-Lubricated Ni-Based Composite (Ni-Al₂O₃, Ni-SiC and Ni-ZrO₂) Thin Film Coatings for Industrial Applications. *Acta Metallurgica Sinica (English Letters)*, 2015: p. 1-9.
- [17] Jung, A., et al., Nanocrystalline alumina dispersed in nanocrystalline nickel: enhanced mechanical properties. *Journal of materials science*, 2009. 44(11): p. 2725-2735.
- [18] Thiemig, D. and A. Bund, Influence of ethanol on the electrocodeposition of Ni/Al₂O₃ nanocomposite films. *Applied Surface Science*, 2009. 255(7): p. 4164-4170.
- [19] Liu, J., Fabrication of composite materials with addition of graphene platelets, in *School of Mechanical Engineering 2014*, University of Birmingham: 2014.
- [20] Battez, A.H., et al., Friction reduction properties of a CuO nanolubricant used as lubricant for a NiCrBSi coating. *Wear*, 2010. 268(1): p. 325-328.
- [21] Song, X., et al., Synthesis of monodispersed ZnAl₂O₄ nanoparticles and their tribology properties as lubricant additives. *Materials Research Bulletin*, 2012. 47(12): p. 4305-4310.
- [22] Binder, C., et al., Effect of nature of nitride phases on sliding wear of plasma nitrided sintered iron. *Wear*, 2015. 332: p. 995-1005.

- 1
2
3
4
5
6
7
8
9
10
11
12
13
14
15
16
17
18
19
20
21
22
23
24
25
26
27
28
29
30
31
32
33
34
35
36
37
38
39
40
41
42
43
44
45
46
47
48
49
50
51
52
53
54
55
56
57
58
59
60
61
62
63
64
65
- [23] Wang, Q., et al., Microstructure and water-lubricated friction and wear properties of CrN (C) coatings with different carbon contents. *Applied Surface Science*, 2013. 268: p. 579-587.

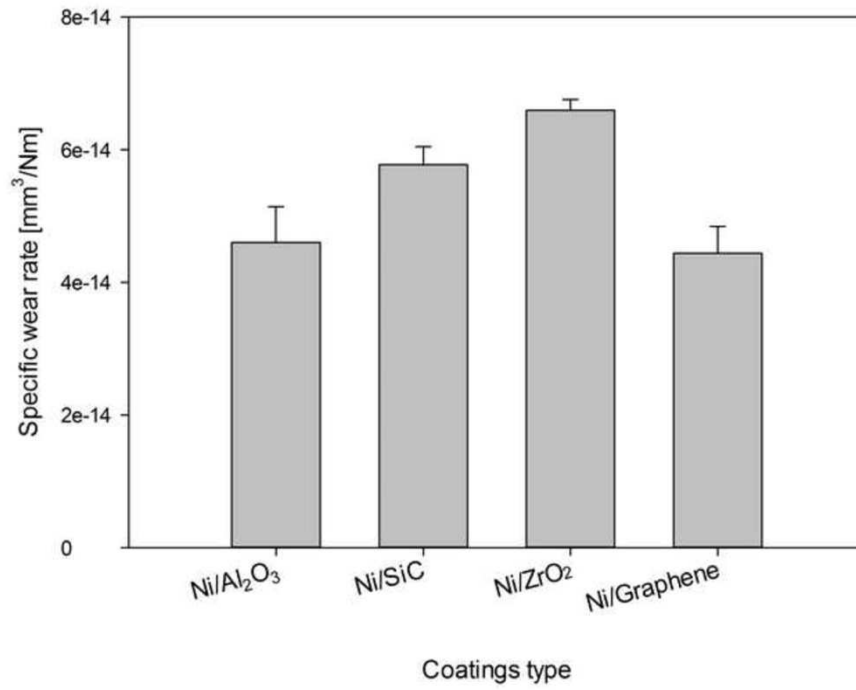
Figure(1)



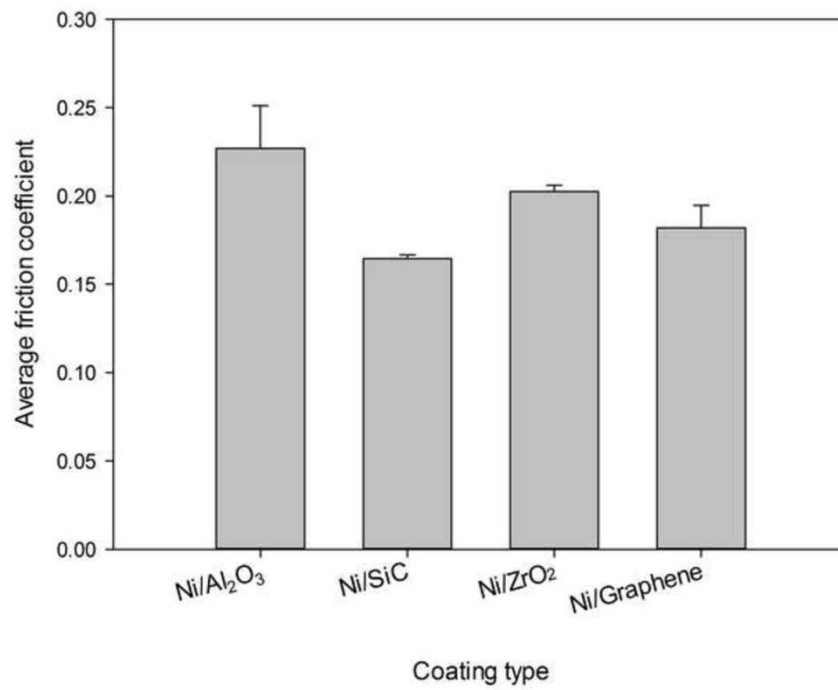
Figure(2)



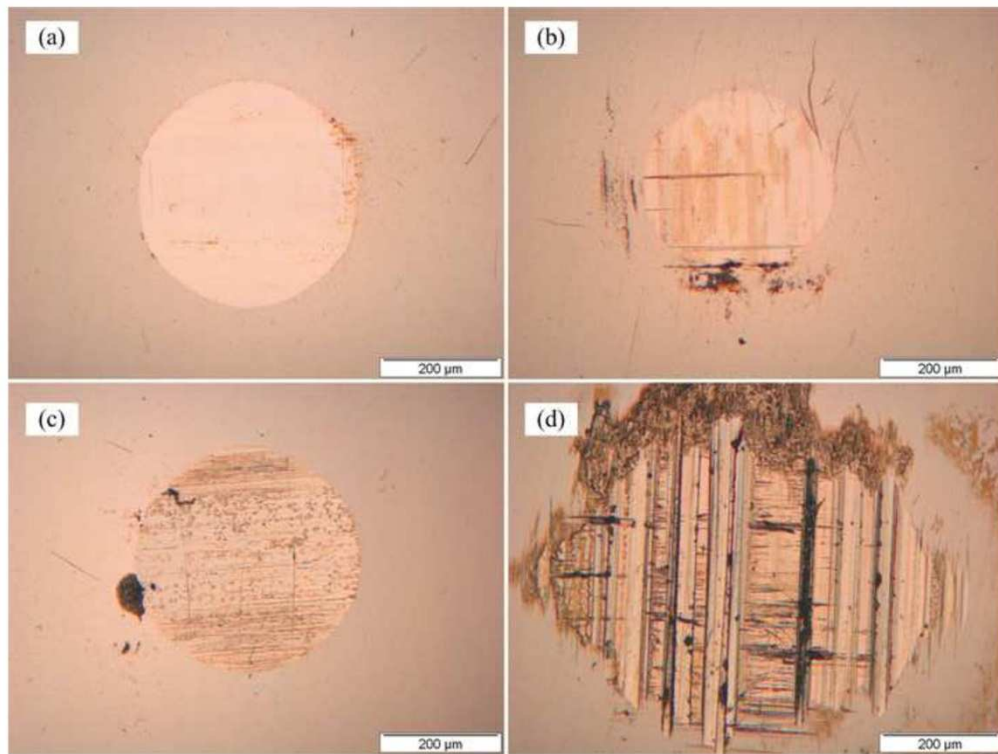
Figure(3)



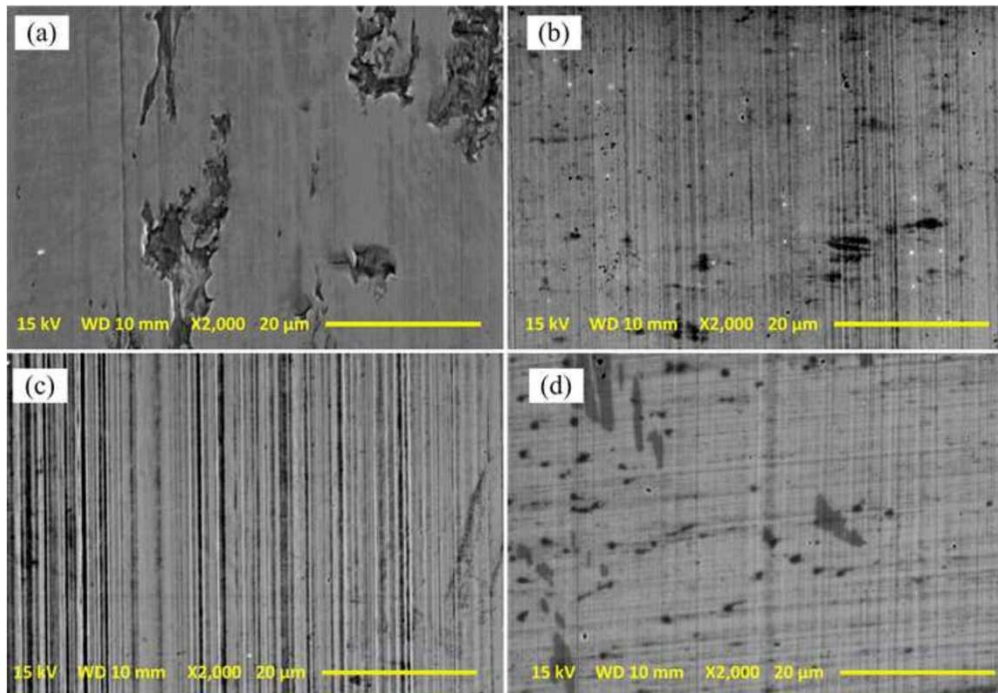
Figure(4)



Figure(5)



Figure(6)



Figure(7)

